INFORMATION TO USERS

This material was produced from a microfilm copy of the original document. While the most advanced technological means to photograph and reproduce this document have been used, the quality is heavily dependent upon the quality of the original submitted.

The following explanation of techniques is provided to help you understand markings or patterns which may appear on this reproduction.

1. The sign or "target" for pages apparently lacking from the document photographed is "Missing Page(s)". If it was possible to obtain the missing page(s) or section, they are spliced into the film along with adjacent pages. This may have necessitated cutting thru an image and duplicating adjacent pages to insure you complete continuity.

2. When an image on the film is obliterated with a large round black mark, it is an indication that the photographer suspected that the copy may have moved during exposure and thus cause a blurred image. You will find a good image of the page in the adjacent frame.

3. When a map, drawing or chart, etc., was part of the material being photographed the photographer followed a definite method in "sectioning" the material. It is customary to begin photoing at the upper left hand corner of a large sheet and to continue photoing from left to right in equal sections with a small overlap. If necessary, sectioning is continued again — beginning below the first row and continuing on until complete.

4. The majority of users indicate that the textual content is of greatest value, however, a somewhat higher quality reproduction could be made from "photographs" if essential to the understanding of the dissertation. Silver prints of "photographs" may be ordered at additional charge by writing the Order Department, giving the catalog number, title, author and specific pages you wish reproduced.

5. PLEASE NOTE: Some pages may have indistinct print. Filmed as received.

Xerox University Microfilms
300 North Zeeb Road
Ann Arbor, Michigan 48106

SEISMOLOGICAL INVESTIGATIONS OF PLATE TECTONICS IN SOUTH CENTRAL ALASKA

A
THESIS

Presented to the Faculty of the
University of Alaska in partial fulfillment
of the Requirements
for the Degree of

DOCTOR OF PHILOSOPHY

by

John Norman Davies, B.A., M.S.

Fairbanks, Alaska

May, 1975

SEISMOLOGICAL INVESTIGATIONS OF PLATE TECTONICS

IN SOUTH-CENTRAL ALASKA

RECOMMENDED:

D. B. Slove

Chairman, Advisory Committee

APPROVED:

Keith B Mather
Director, Geophysical Institute by Paul Davis

May 9, 1975
Date

Vice President for Research

12 May 75
Date

ABSTRACT

Over the past decade the concept of plate tectonics has grown out of the ideas of sea-floor spreading and continental drift and has gained wide acceptance. According to this concept south-central Alaska contains the junction of two major plate boundaries: The Aleutian trench subduction zone and the Queen Charlotte transform fault zone. Several seismological investigations of these boundaries have been carried out to test and clarify the application of plate tectonics to this region. The principle result is the delineation of the Benioff zone which is shown to parallel the volcano trend line in the upper Cook Inlet region, bending thirty degrees to the east at the Yentna lineament then trending N47°E and ending just north of the Alaska Range, about 75 miles south of Fairbanks. This termination is shown to lie on a segment of a small circle about a pole of relative motion for the Pacific and North American plates which is also congruent with the Queen Charlotte transform fault zone and is therefore seen to delineate the northeast corner of the Pacific plate. Just as in the Aleutian Islands, the Benioff zone in south-central Alaska is composed of a number of independent blocks. It also shows increasing distance from the trench axis as one proceeds to the northeast, in contrast to the parallel structure seen in the Aleutian Islands.

ACKNOWLEDGMENTS

This work was supported by Air Force Contract F-44620-71-C-0105, NSF Grant GA-28404 and State of Alaska funds. The cooperation of the Air Force in providing helicopter support and the FAA in making housing available at the Skwentna airstrip contributed greatly to the success of the field portion of this project.

There are many people in all parts of the Geophysical Institute who contributed in numerous ways to the completion of this project and to an atmosphere which made the work very enjoyable. Special contributions were made by Dr. Keith Mather, who provided counsel and encouragement at crucial times; Dr. Eduard Berg, who chaired my M.S. work and the early phases (including the field portion) of this project; Dr. Hans Pulpan, who assumed the role of chairman, midstream; Dr. David Stone, Dr. Niren Biswas, and Dr. Kenelm Philip, who were members of my advisory committee; Dr. Robert Forbes, Dr. Jurgen Kienle, Dr. Lewis Shapiro, Larry Gedney, and Doug VanWormer, who contributed many hours of helpful discussions; Ron Rasmussen, who helped fabricate the field equipment and install it; he also assisted in many hours of tedious calibrations of various components of the seismic network and in troubleshooting all manner of technical problems; Orwin Westwick, who taught me many skills in the care and feeding of electronic equipment; and Karen Brown, who typed the manuscript.

Finally, and with much love, I acknowledge the rough-draft typing, encouragement, moral support, and endurance of my wife, Kathleen.

TABLE OF CONTENTS

	Page
Title Fly	i
Title Page	ii
Abstract	iii
Acknowledgments	iv
Table of Contents	vi
List of Figures	vii
List of Tables	viii
Chapter I, Introduction and Review	1
Statement of the problem	1
Review of previous work	2
Spreading rates	5
Aleutian trench and volcanic arc	11
Gravity anomaly belts	13
Benioff zones	14
Crustal structure	16
Chapter II, Data Acquisition and Reduction	29
Seismograph stations	29
Data reduction	42
Chapter III, Data Analysis and Results	44
Location programs	44
Residual studies	80
Attenuation studies	89
Teleseismic P-phases	99
Focal mechanisms	102
Chapter IV, Discussion and Conclusion	113
Appendix I, Catalog of events located	123
Appendix II, Description of computer programs	144
HYPLOT	144
STARES	144
Appendix III, Calibration of the seismograph systems	158
Literature Cited	187

LIST OF FIGURES

Figure	Subject	Page
1-1	Relative plate motion near San Francisco	9
1-2	Divergence of volcanoes and trench	12
1-3	Alaskan crustal velocity models	21
1-4	Matumoto and Page's velocity model	24
1-5	Velocity histogram for crustal models	26
1-6	Continental and marine crustal models	28
2-1	Seismic station location map.	30
2-2	Seismic station downtimes.	31
2-3	University of Alaska equipment block diagram.	36
2-4	Skwentna equipment block diagram.	39
2-5	Skwentna time corrections.	40
3-1	Rampart earthquake aftershock zone.	50
3-2	Seismicity map, June and July, 1971	51
3-3	Seismicity map, 1972	53
3-4	Seismicity map, June and July, 1971	55
3-5	Seismicity map, 1972-1973	57
3-6	HYPLOT projection geometry	58
3-7	Upper Cook Inlet hypocenter cross sections	59
3-8	Mount McKinley vicinity hypocenter cross sections	60
3-9	Mount McKinley vicinity hypocenter cross sections	61
3-10	Cross section location map	62
3-11	Hypocenter longitudinal sections	64
3-12	Longitudinal section location map	65
3-13	Averaged cross sections	68
3-14	Contour map of the Benioff zone	72
3-15	Contour map of the Beinoff Zone	74
3-16	Envelopes of Benioff zone error bars	75
3-17	HYP071 cross sections	77
3-18	Hypocenter cross section comparisons	78
3-19	Arrival-time residual contour maps	83
3-20	Location of sample earthquakes	90
3-21	Seismograms from sample earthquakes	91
3-22	Possible attenuation of local P-phases	98
3-23	Possible attenuation of teleseismic P-phases	104
3-24	First motions for four sets of events	108
3-25	First motions for four individual events	111
4-1	Map of Benioff zone depth contours	113a
4-2	Map of Benioff zone contours and seismicity	114
4-3	Various Benioff zone cross sections	119

LIST OF TABLES

Table	Subject	Page
1-1	Slip rates near San Francisco.	8
1-2	Alaskan crustal velocity models.	17
2-1	Seismograph station parameters.	32
3-1	Comparison of University of Alaska and NOAA epicenters.	46
3-2	Statistical summary of Table 3-1.	48
3-3	Averaged hypocenter positions.	67
3-4	Attenuation values for local events.	96
3-5	Calibration check using teleseisms.	101
3-6	Attenuation values for teleseisms.	103
3-7	Polarity check using teleseisms.	106

CHAPTER I

INTRODUCTION AND REVIEW

Part 1: Statement of the problem

South-central Alaska has undergone and continues to undergo intensive deformation. The region contains the Alaska Range, the Chugach Mountains, the Aleutian Range, the Talkeetna Mountains and the Wrangell volcanic mountains. Mount McKinley, in the Alaska Range, is the highest mountain on the North American continent. This region is cut by several major fault systems including the Denali and Border Ranges systems. It also contains the eastern terminus of the Aleutian trench, and associated island arc structures, which has been the locus of several major earthquakes including the Great Alaskan Earthquake of March, 1964.

The geological and geophysical problems of south-central Alaska are quite complex and for the most part are in the first approximation stage of solution. However, an exciting theoretical aid to understanding this region has been developed in the context of studies of continental drift and sea-floor spreading. In some respects south-central Alaska can be viewed as a laboratory for the study of plate tectonics. It contains both arc-trench and transform fault systems and in the case of the arc-trench

system this region contains gradational structures from the clsssic oceanic island arc to its terminus in a continental setting.

Seismological techniques have proved to be useful in many studies of plate tectonics. Seismicity studies have helped to delineate the plate boundaries on a world-wide basis and have been applied in this thesis to study in detail the boundary between the northeast corner of the Pacific plate and the North American plate. This boundary falls mainly in south-central Alaska and the interaction between these twoplates is thought to be responsible for the great deformation of this region. Consequently any regional geological or geophysical study in this area needs to begin by recognizing the location of the boundaries of the major tectonic elements. It is the goal of this work to define, seismologically, these boundaries.

Part 2: Review of previous work

Before proceeding with the details of this study it will be useful to review what is already known of the plate tectonics of the northeast Pacific, and the Benioff zone and crustal structure of south-central Alaska.

Plate tectonics

The fundamental postulate of plate tectonics is that sea-floor spreading occurs. That is, mantle material upwells forming

great mountain ranges on the sea floor called mid-ocean ridge systems. As this new material comes to the surface it cools and spreads laterally from the axis of the ridge forming the lithospheric plates which constitute the approximately 100 km thick outer shell of the earth. The chief verification of this postulate comes from the observation that as the new lithospheric material cools through the Curie point it records the direction of the earth's magnetic field at that time and point, and that as the spreading process continues and the earth's field reverses periodically the magnetic record in the lithosphere takes on the form of a series of normally and reversed magnetized stripes parallel to the ridge axis and usually arranged symmetrically on either side. The correlation of this reversal chronology with other geochronologies in the volcanic, sedimentary and fossil records is substantial evidence in support of the sea-floor spreading postulate.

The other two basic assumptions of plate tectonics are (1) that the plates formed in the spreading process are essentially rigid and (2) that the surface area of the earth remains approximately constant. These two assumptions taken along with the spreading postulate above and certain geometrical theorems imply that there must be regions of plate consumption and that plate boundaries which are neither consumptive nor productive (transform boundaries) must follow small circles about a pole of relative motion for

the plates which are separated by the conservative boundary. Support for the rigidity assumption comes from the lack of seismic activity and the preservation of the magnetic lineation within the boundaries of a plate and from correlation of strain release between rising and sinking edges of the plate (Berg and Sutton, 1974). Consumption of lithospheric plates at trenches is indirect support for the constant surface area assumption. The evidence for consumption at a trench will be discussed later in the context of the Aleutian Island arc-trench system.

The Pacific plate is formed at the Pacific-Antarctic, East-Pacific and Juan de Fuca ridge systems and moves approximately northwest with respect to the North American plate. The North American plate is formed at the mid-Atlantic ridge system spreading westward from the ridge axis. The motion of these plates with respect to some "fixed" coordinate system (e.g., a grid of latitude and longitude lines which would rotate about the spin axis of the earth with the average angular velocity of the earth) is not known since the only fixed coordinate direction available presently is that of the spin axis. It was thought that the mantle plumes might be shown to be fixed but, to the contrary, it has been shown (Burke, Kidd and Wilson, 1973) that these plumes move with respect to each other and therefore are not fixed in the mantle. It has been demonstrated however, (McElhinny, 1973) that there is little or no net motion of the

lithosphere with respect to the spin axis; this leaves open to question any rotation as a whole about the spin axis.

Spreading rates

The relative motion of the Pacific and North American plates can be calculated in several ways. All but one of the following calculations depend on Morgan's (1968) method for determining the direction of relative motion between the two plates. Morgan observed that conservative boundaries between plates on a sphere must follow small circles around the pole of relative motion for the pair of plates. The Queen Charlotte and San Andreas fault systems mark the two major conservative boundaries between the Pacific and North American plates. Morgan determined the pole of relative motion by finding the intersection of great circles constructed perpendicular to these fault systems. The coordinates of this pole were given in Morgan's (1968) paper as 53°N and 53°W; however, Le Pichon (1968) reports that Morgan subsequently recalculated this pole using a least-squares procedure giving 53°N and 47°W, which will henceforth be referred to as Morgan's pole.

Le Pichon used this pole and the spreading rate in the Juan de Fuca ridge system during the Plio-Pleistocene ($\sim$1 Myr BP) to obtain the relative angular velocity vector for the Pacific and North American plates. The relative rotation rate for this vector is 0.60 deg/Myr and the slip implied at the location of

the San Andreas system (viz: San Francisco, 37 1/4°N and 122 1/2°W) is 5.4 cm/yr while the convergence rate in the eastern Aleutians (57°N and 150°W) is 5.5 cm/yr.

Atwater and Molnar (1973) used the Pacific-Antarctica-India-Africa-North American spreading rates to compute the Pacific-North American relative motion, which they give as slip rates on the San Andreas system. For the time interval 0-4 Myr BP this rate is 5.5 cm/yr, which implies a rotation rate about Morgan's pole of 0.61 deg/Myr and a convergence rate in the eastern Aleutians of 5.6 cm/yr.

Hamilton and Myers (1966) report that geodetic surveys for coastal California yield a slip rate for the San Andreas system of 6.0 cm/yr. Again using Morgan's pole, this implies a rotation rate of 0.67 deg/Myr and a convergence rate in the eastern Aleutians of 6.1 cm/yr.

Hein (1973) has studied the age and source of the sediments in the Delgada fan off the California coast and computes an offset for the interval 0-4 Myr BP which gives a slip rate of the Pacific floor relative to California of 6.5 cm/yr. This implies a rotation rate about Morgan's pole of 0.72 deg/Myr and a convergence rate in the eastern Aleutians of 6.6 cm/yr.

Stone (1974) uses a method not dependent on Morgan's pole. He assumes that the Hawaiian hot spot and the mid-Atlantic ridge are fixed and uses the Pacific-Hawaiian hot spot and the North

American-Mid Atlantic ridge motions to find the Pacific-North American relative motion. He computes a relative motion vector for the Pacific with respect to Cape Mendocino which has an azimuth of N318°E compared to the azimuth of the tangent to the small circle about Morgan's pole which passes through Cape Mendocino of N320°E. The slip rate at this point is 5.1 cm/yr, which implies a convergence rate of 5.2 cm/yr in the eastern Aleutians.

Minster et al. (1974), using a global inversion of magnetic anomaly rates, fracture-zone directions, and earthquake-slip vectors, obtained about 5.5 cm/yr across the San Andreas transform boundary.

Davies and Brune (1971) obtained 6.7 cm/yr in the eastern Aleutians from earthquake slip vectors.

All of the relative motion data given above are summarized in Table 1-1. Excepting Stone's rate, these data give an average convergence velocity in the eastern Aleutians (57°N and 150°W) of 6.0 cm/yr at N316°E for the Pacific plate relative to North America. It can be argued that one should not average these data, but should take a higher value on two grounds. The first is that, as shown by other data presented in Hamilton and Meyers (1966), Hein (1973) and Atwater and Molnar (1973) and as plotted in Figure 1-1, there has been an increase in the relative

Table 1-1

Slip rates computed for the San Andreas transform fault system near San Francisco by various methods. These rates (except Davies and Brune, see text) are extended to the eastern Aleutians assuming that the relative motion between the North American and Pacific plates is along small circles about Morgan's pole (see text). Rotation rate is about Morgan's pole.

Authors	Method	Time MYR BP	Slip Rate California	cm/yr E. Aleutians	Rotation deg/Myr
Le Pichon (1968)	Juan de Fuca spreading rate adjusted for small motion between Juan de Fuca and North American plates.	1	5.4	5.5	0.60
Hamilton & Myers (1966)	Geodetic survey of coastal California	0	6.0	6.1	0.67
Hein (1973)	Sediment-source offsets for Delgada fan off coast of California.	0-4	6.5	6.6	0.72
Atwater & Molnar (1973)	N. American-African-Indian-Antarctican-Pacific spreading rates.	0-4.5	5.5	5.6	0.61
Stone & Packer (1974)	Fix Hawaiian and Icelandic hot spots and compute N. American and Pacific motions relative to hot spot frame of reference.	0	5.1	5.2	0.57
Davies & Brune (1971)	Sum earthquake moments to obtain slip rate.	0	(1.3)	6.7	0.73

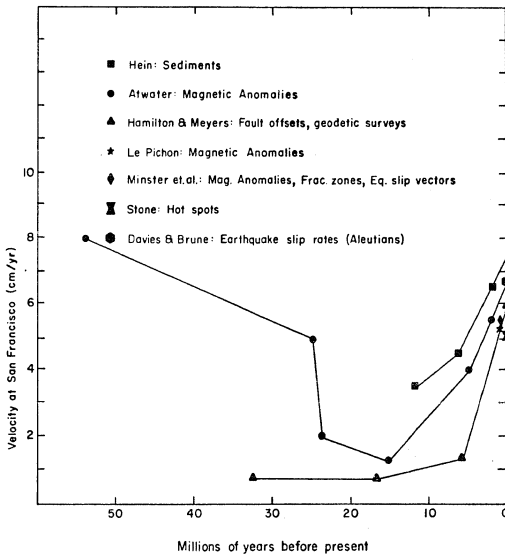

Figure 1-1. Relative motion across the San Andreas transform boundary. Various estimates of the relative motion between the Pacific and North American plates are plotted for the region of the San Andreas transform fault system near San Francisco. Note that for at least the past 10 million years this relative velocity has been increasing. The studies from which these estimates were derived are described in the text and summarized in Table 1-1.

velocity of the Pacific and North American plates for the past 10 Myr. Assuming that this acceleration is still continuing and since the spreading and sedimentation rates are averaged over the last million years, the relative velocity derived from these rates is a little less than the present rate. The only relative velocities which represent present motion are those derived from the geodetic surveys in coastal California. The geodetic and earthquake slip vector values may be low too if some of the relative motion in the crustal blocks is distributed into central California or even into the Basin and Range province. This argument could affect the velocity derived from the sediments depending on how wide the deformation zone is at present.

Extrapolating the data plotted in Figure 1-1 to the present and averaging gives 6.3 cm/yr. Taking the average deviation about this mean yields ±0.5 cm/yr for the 57% confidence interval, assuming that the data are independent and randomly distributed (which they are not). Doubling gives the 80% interval which includes all of the data except one. Therefore 6.3±1.0 cm/yr is adopted as the most reasonable estimate of the present slip rate along the San Andreas transform boundary between the Pacific and North American plates. Assuming Morgan's pole and his estimates of error (53±3°N and 47±5°W) the San Andreas slip rate implies a convergence velocity in the Eastern Aleutians (57°N and 150°W) of 6.4±1.0 cm/yr at N316±6°E. This convergence is responsible

for the formation of the Aleutian island arc-trench system. Convergence on boundaries with other plates has formed the Kurile-Kamchatka, Japan, Mariana and Kermadec-Tonga island arc-trench systems.

The Aleutian Island arc-trench system has all of the classic features (Richter, 1958, p. 413; Sugimura and Uyeda, 1973, p. 3) of a consuming boundary (Isacks, Oliver and Sykes, 1968; Dewey and Bird, 1970): bathy-metric trench, volcanic arc, parallel belts of gravity anomalies and a Benioff zone which attains a depth of about 100 km under the volcanic axis.

Aleutian trench and volcanic arc

The Aleutian trench is well defined by the 6,000 m isobath from south of the Komandorskii Islands to south of the tip of the Alaska Peninsula (King, 1969) and reaches its maximum depth of 7,600 m south of Tanaga Island (Stone, 1968). The trench and the volcanic arc diverge approximately where the trench and the Alaskan continental shelf meet (approximately Akutan Island); the volcanic arc continuing into south-central Alaska and the trench shallowing until it disappears beneath the continental shelf south of Cordova in the Gulf of Alaska. This divergence is illustrated in Fig. 1-2 in which the distances between the trench axis and the Quaternary volcanic centers are plotted. In the pure island arc region of the Aleutian arc this distance is a constant 162±18 km with the volcanic and trench axes following

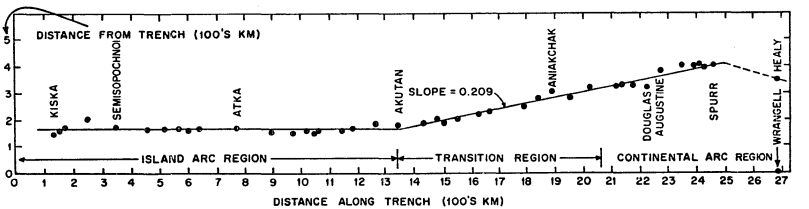

Figure 1-2. Distance between volcanoes and trench for the Aleutian Island arc. The change in slope near Aleutian coincides with the change from oceanic to continental crust in the overthrust plate.

concentric small circles about a center at 61.8°N, 178.0°W and having radii of 10.3° and 11.7°, respectively. In the transition and continental arc region the volcanoes and the trench diverge approximately linearly (±20 km) at a rate of 0.209km/km beginning at a point about 50 km east of Akutan volcano. The volcanoes fall along a small circle centered at 63.8°N, 173.5°W with a radius of 10.3° (the same radius as for the island arc volcanic axis). The trench axis is a small circle about 67.8°N, 172.5°W with a radius of 15.0°.

The scatter in the distribution of the individual volcanic centers about the volcanic axes defined above is non-random. Many sets of three or four volcanoes fall along straight line segments which are in turn arranged in an echelon pattern along the general axis. The significance of this distribution in relation to the morphology of the Benioff zone will be discussed later.

The volcanics have been described by Coats (1962) and Burk (1965). They range in composition from basalts to rhyolites but are predominately andesites. This compositional range is characteristic of the Pacific rim volcanics (Rittman, 1962, pp. 12 and 162) and is genetically related to subduction of an oceanic plate (Dewey and Bird, 1970).

Gravity anomaly belts

Gravity measurements for the Aleutian arc are scattered and uneven. The early results have been reviewed by Stone (1968).

They show the negative isostatic anomaly belt (e.g. Woolard and Strange, 1962) generally associated with trenches (Sugimura and Uyeda, 1973, p. 21). Berg, Kubota, and Kienle (1967) found a negative Bouguer anomaly associated with the Katmai volcanics which was attributed to the presence of shallow magma chambers. Similar anomalies are associated with volcanoes in Japan (Sugimura and Uyeda, 1973, p. 18). Kienle (unpublished map) has extended Barnes' (1967) Bouguer gravity anomaly map for south-central Alaska. This map shows strong negative anomalies in the Cook Inlet and Susitna River regions.

Benioff zones

The idea that island arcs are a result of some kind of megathrust has been around for a long time. Richter (1958, p. 414) points out that "Especially since the time of Suess [E. Suess, Das Antlitz der Erde Vols. 1-4, 1885-1904] geologists have often interpreted the Pacific arcs as the surface traces of great thrusts". Sugimura and Uyeda (1973) note that the geographic coincidence of volcanoes and the 100 km isobath of the Benioff zone was observed in Japan by Honda (1934) and Wadati (1935) in the earty thirties. Benioff (1954) systematically established the general relation of the inclined seismic zone which bears his name to the island arcs.

These ideas were applied to Aleutian-Alaskan tectonics fairly early also. Gutenberg and Richter (1954) noted that the

general trend of earthquake foci dipping to the north under the Aleutian island arc and attaining a depth of 100km under the volcanic axis persisted into the continental region of Alaska. Coats (1962), in an hypothesis which is strikingly similar in many details to present day plate tectonic concepts, postulated that the Aleutian island arc and Benioff zone were due to a megathrust in which the northern plate was being thrust over the southern one. As a result of this thrusting, oceanic trench materials and water were carried to the 100 km depth zone where a granodioritic magma was formed and combined with the ambient basaltic magma which rose to the surface and differentiated along the basalt-andesite-rhyolite line to form the Aleutian volcanics.

That the Benioff zone continued well into south-central Alaska has only recently been confirmed. Suggestions that this was the case were given by Tobin and Sykes (1965), Berg, Kubota and Kienle (1967), Barzangi and Dorman (1969), Tarr (1970), Gedney (1970) and Davies and Berg (1973). Recent advances in computer techniques for locating earthquakes and increased seismograph station densities have allowed more precise definition of the Benioff zone morphology. In other regions, e.g. Fiji-Tonga (Sykes, Isacks and Oliver, 1969), Japan (Ishida, 1970) and the central Aleutians (Engdahl, 1973), it has been shown that the Benioff zone is less than 20 km thick. Similar results have been obtained for the Cook Inlet region by Lahr, Page and Thomas (1974).

Crustal structure

Studies of Alaskan-Aleutian crustal structure have been reviewed by Menard (1967), Berg (1967) and Stone (1968). These reviews are all pre-plate tectonics and many important papers bearing directly and indirectly on Alaskan-Aleutian crustal structure have since been published. An attempt has been made by the author to review the more recent publications relevant to understanding this structure. Some of the pertinent work on the Aleutian arc structure has been discussed earlier. However, in the following summary (and later in Chapter IV) no claim is made that the review on which it is based is exhaustive. In particular, for example, Bowers Ridge will not be discussed since it does not relate directly to the present tectonic boundaries in south-central Alaska.

Seismic velocity models for the crust have been constructed from refraction and microearthquake data. These models have been summarized in Table 1-2.

Berg, Kubota, and Kienle (1967) assumed a two layer crustal model based initially on Jeffreys and Bullen (1958) velocities and Woollard and Strange (1962) thicknesses which they refined in order to obtain a best fit to the observed travel times from microearthquakes in the Kodiak-Katmai region. Depths to the Moho calculated from Bouguer gravity anomalies are in agreement with their model.

Table 1-2a

Alaskan crustal velocity models by various studies. See Figure 1-5 for layer assignments.

Data Source	Berg, Kubota and Kienle; 1967 Microearthquake Data						Hales and Asada; 1966 Reexamination of Tatel and Tuve's (1956) refraction data											
area	Kodiak Island			Katmai			Aishihik Road			Carross-Dawson			Haines Highway			Valdez-Tok		
Code	BKD			BKD			HAR			HCD			HHH			HVT		
Layer	V	T	H	V	T	H	V	T	H	V	T	H	V	T	H	V	T	H
a																		
b				(2.8*)			3.0	0.5	0.5	3.0	0.5	0.5	3.0	0.5	0.5	3.0	3.0	3.0
c																		
d	5.5	12.0	12.0	5.5	15.0	15.0												
e	6.5	20.0	32.0	6.5	23.0	38.0	6.0 6.6	26.2 9.9	26.7 36.6	6.0 6.7	20.6 14.1	21.1 35.2	6.0 6.7	13.7 27.3	14.2 41.5			
f																6.8 7.0	35.1 11.5	38.1 49.6
g	8.1			8.1			8.0			8.0			8.0			8.1		

*Gedney, Matteson and Forbes; 1970

Table 1-2b

Data source	Hanson et al; 1967 Refraction data			Matumoto and Page; 1965 Microearthquakes			Menard; 1967 Review			Peter, Elvers and Yellin; 1965. Aleutian Trench S. of Kodiak Is. Modified from Shor (1962) using gravity measurements											
Area	Healy-College			Kenai Peninsula			Small Ocean Basin			85km NW of trench			20km NW of trench			60km SE of trench			115km SE of trench		
Code	HHC			MKP			MSO			PT1			PT2			PT3			PT4		
Layer	V	T	H	V	T	H	V	T	H	V	T	H	V	T	H	V	T	H	V	T	H
a							2.1	2.0	6.0	1.9	4.5	4.5	1.9	3.0	7.5	1.9	0.5	5.0	1.9	0.5	5.0
b	3.7	2.6	2.6																		
c							3.9	2.0	8.0												
d	5.4	2.3	4,9	5.3	5	5				5.4	5.0	11.5	5.4	2.5	9.0	5.4	3.0	8.0	5.4	2.0	7.0
	5.8	6.8	11.7	5.7	5	10															
e	6.4	20.3	32	6.2	5	15	6.6	10.0	18.0	6.6	12.5	24.0	6.6	5.5	14.5	6.6	4.0	12.0	6.6	4.5	11.5
		36.3	48																		
f				6.9	5	20															
				7.4	5	25															
g	(8.1)			7.7	5	30	8.1			8.1			8.1			8.1			8.1		
				8.2	30	65															

Table 1-2c

Data Source	Shor; 1964 Refraction						Shor; 1962 Refraction											
Area	Bearing Sea Shelf near Pribilof Is.			Aleutian Basin			Aleutian Ridge near Adak Is.			NE of Kodiak			S of Kodiak			Aleutian Trench S of Kodiak/Adak			Abyssal depths NE Pacific		
Code	SBS			SAB			SAR			SKN			SKS			SAT			SAP		
Layer	V	T	H	V	T	H	V	T	H	V	T	H	V	T	H	V	T	H	V	T	H
a	1.7	1.1	1.3	2.2	1.4	5.2				1.7 2.2	0.2 1.0	0.2 1.2	1.8 2.1	0.3 0.7	0.4 1.1	2.0	0.6	7.1	2.1	0.3	4.4
b				2.8	1.2	6.4	3.2	0.2	0.3												
c	3.6	2.0	3.3	3.7	2.8	9.1	3.8	0.5	0.8	4.0	1.7	2.9	4.2	2.3	3.4						
d	5.5	5.4	8.6				5.5	4.7	5.5				5.5	6.3	9.6	5.3	1.9	9.0	5.1	1.1	5.4
e	6.4	20.5	29.1				6.6			6.0	3.1	6.0	6.2	13.2	22.8	6.5	5.2	14.2			
f				6.9	5.5	14.6				7.0									6.8	5.3	10.7
g	8.1			8.0									8.1			7.9			8.3		

Table 1-2d

Data Source	Woollard et al; 1960 Reexamination of Tatel and Tuve's (1956) refraction data											
Area	Homer vicinity			Portage vicinity			Valdez vicinity			Tok vicinity		
Code	WHM			WPT			WVZ			WTK		
Layer	V	T	H	V	T	H	V	T	H	V	T	H
a	2.3	7.0	7.0									
b												
c												
d	5.7	9.1	16.1	5.7	9.1	9.1	5.7	9.4	9.4	5.7	6.1	6.1
e	6.6	14.2	30.3	6.6	15.0	24.1	6.6	3.8	13.2	6.6	10.6	16.7
f	7.3	16.2	46.5	7.3	22.0	46.1	7.3	40.0	53.2	7.3	32.2	48.9
g	8.3			8.3			8.3			8.3		

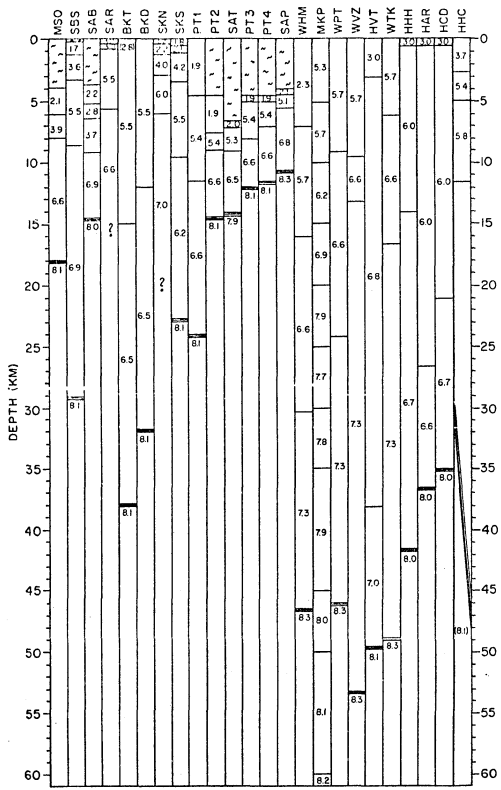

Figure 1-3. Alaskan crustal models. See Table 1-2 for an explanation of the codes.

Hales and Asada (1968) and Woollard et al (1960) have both reexamined Tatel and Tuve's (1956) refraction data from shot points in College Fjord and Skagway. Comparing their results for the Valdez-Tok area one can see vague agreement. Hales and Asada also calculated a model without the sedimentary layer which had layer velocities of 5.8, 6.8, and 7.0 km/sec with the Moho at 53 km depth. This model is in better agreement with Woollard et al's seismic results, but the model with the sedimentary layer better matches the 33-41 km depths to the Moho derived by Woollard et al from gravity data alone, and is presented here to illustrate the effect of introducing a lower velocity layer into the model.

Hanson, Berg, and Gedney (1967) used quarry blasts at the Suntrana coal mine near Healy and a series of seismic stations along the road to College to construct an unreversed refraction profile of a section of interior Alaska crust just north of the Alaska Range. They attributed the high apparent P_n velocity of 8.8 km/sec to a sloping Moho. Under this assumption and that of a normal P_n velocity of 8.1 km/sec they obtain a depth to the Moho under College of 32 km, which is in good agreement with the 33 km gravimetric depth obtained by Woollard et al (1960).

Matumoto and Page (1969) used microearthquakes from the March 1964 Alaska earthquake aftershock series to obtain a mean velocity versus depth relationship from which they calculated

interface velocities for a uniformly layered crust with layer thicknesses of 5 km. It is difficult to assign a depth to the Moho from this model since there is no abrupt transition from crustal to mantle velocities. Velocities of 7.7 km/sec are attained at 30 km and increase relatively smoothly to 8.2 at 65 km. The maximum negative curvature in their velocity versus depth relation is at about 26 km for their model A and about 35 km for their model B (see Fig. 1-4). One might infer that the Moho is between 26 and 35 km deep, significantly shallower than the depths obtained by Woollard et al (1960) and Hales and Asada (1966) from Tatel and Tuve's (1956) refraction data, but in good agreement with the 25 km lower boundary to the 1964 aftershocks (Matumoto and Page, 1969) and Woollard et al's 33-41 km gravimetric depth.

The velocity model given in Table 1-2 for Menard (1967) is a composite of the velocity models reviewed by him for small ocean basins and is presented here for comparison with the Aleutian Basin and northeast Pacific abyssal depths data given by Shor (1962, 1964).

Peter, Elvers, and Yellin (1965) interpolated Shor's (1962, 1964) velocity data to obtain an initial model which they modified using their gravity data by the method of Talwani (1959). Their Moho depths provide a smooth transition from Shor's (1962) northeast Pacific values to Berg, Kubota, and Kienle's (1967) Kodiak and Katmai values.

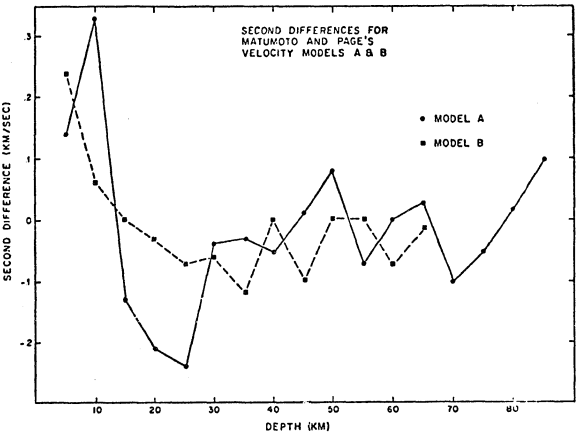

Figure 1-4. Second differences for Matumoto and Page's velocity model. Second differences indicate the rate of change in slope of the velocity versus depth curve. Positive second differences result from curvature toward increasing velocity. The negative minima between 25 and 35 km depth mark points of maximum negative curvature. These points might represent the crust-mantle transition under the Kenai Peninsula.

Shor's (1962, 1964) data were obtained from many marine refraction lines. The Aleutian Basin, Aleutian Trench, and abyssal depths of the northeast Pacific models are averages of several profiles for each area.

In order to make comparisons among these crustal models a frequency of occurrence histogram (Figure 1-5) was constructed from each model which was regarded as semi-independent. For example, Woollard et al's (1960) models each have the same layer velocities: 5.7, 6.6, 7.3 and 8.3 km/sec. These velocities were only entered in the histogram once even though they appear in four models. Also, one set of Hale and Asada's (1966) layer velocities were regarded as independent even though they were derived from the same primary data as Woollard et al. The histogram is somewhat arbitrarily divided into velocity regions or "layers". The layers are lettered a-g and are the "layers" indicated in Table 1-2. The most clear break in the velocity distribution is that between layer c and d velocities. This break is assumed to divide the three "sedimentary layers" a, b, and c from the three "crustal layers" d, e, and f. Layer g is the sub-Moho or uppermost mantle "layer". An interesting distinction between continental and marine velocity models emerges from this layering assignment. The marine models are characterized by the presence of layers a and c and the absence of b, while just the

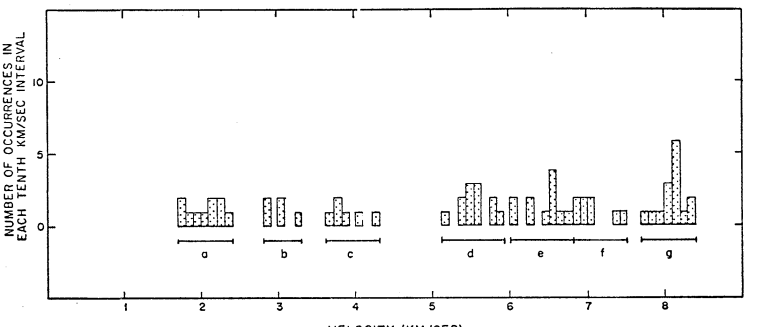

Figure 1-5. Velocity histogram from crustal models given in Table 1-2 and shown in Figure 1-3. The frequency of occurrence in these models of velocities in each one tenth km/sec interval is shown. These velocity intervals are grouped into larger intervals which might represent the range of velocities associated with a generalized crustal layer. These "layers" are labeled a-f. The group labeled "g" consists of sub-moho velocities.

opposite occurs for the continental model. This observation is illustrated in the histogram in Figure 1-6 and is consistent with the generalized model given for small ocean basins from Menard's (1967) review.

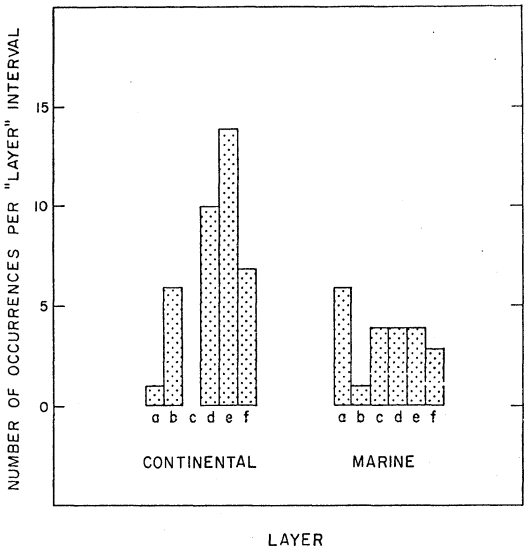

Figure 1-6. "Layer" velocity histograms for continental compared to marine crustal models. Continental models appear to be characterized by the presence of layer b and the absence of layers a and c. Marine models are oppositely characterized by the presence of a and c and the absence of b.

CHAPTER II

DATA ACQUISITION AND REDUCTION

Seismograph stations

The primary data for this study were obtained from four seismographic networks. The stations from these networks which were utilized are shown in Figure 2-1. The stations of the large aperture array of the Geophysical Institute of the University of Alaska are indicated by solid squares. The open squares indicate the temporary stations which augment the geographical distribution of stations in the region of interest. The triangle shows the location of the Augustine volcano research project which is also run by the Geophysical Institute. The stations represented by circles are part of the Tsunami Warning System operated by the Palmer Observatory of the National Oceanic and Atmospheric Administration. The coordinates and some of the parameters of all of these stations are given in Table 2-1. Appendix III gives the data used in calculating the magnifications in this table.

Figure 2-2 summarizes the time periods during which each of the stations was operational. The solid bars indicate operational status. Open bars mean that data were not available from that station during that time interval. This

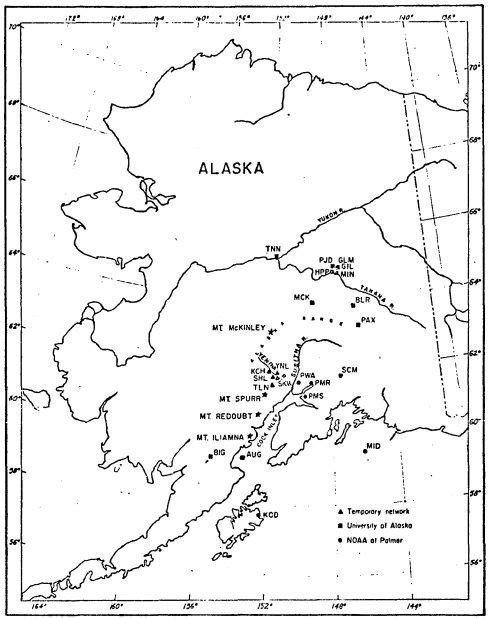

Figure 2-1. Seismograph stations used in this study. The triangles represent temporary stations operated during June and July 1971. They were VHF telemetered to Skwentna and recorded on magnetic tape. Stations marked by squares are part of the large aperature array of the University of Alaska. AUG monitors the volcanic activity of Mount Augustine and is recorded in Homer. Stations of the Tsunami Warning System are shown by circles. They are recorded at NOAA's Palmer Observatory.

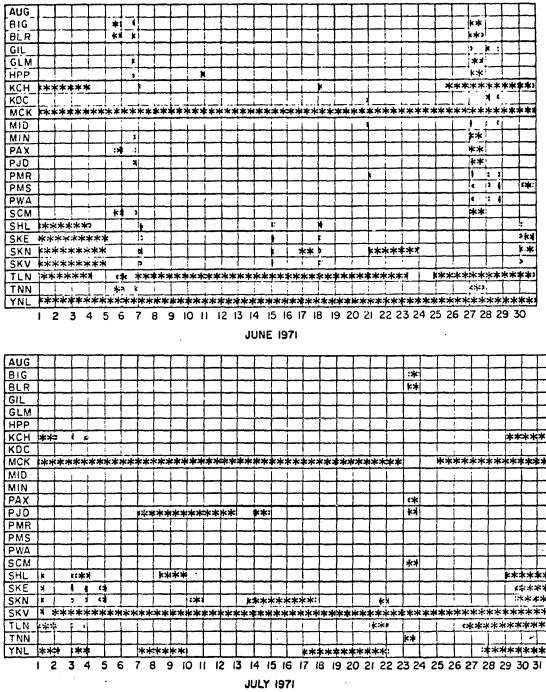

Figure 2-2 Operational status of seismic stations used in this study. Downtime is shown by the asterisks.

Table 2-1

Seismograph station parameters for July, 1971

Code	Location	Component	Latitude (North)	Longitude (West)	Elev (Km)	Magnification 1 Hz	Magnification 5 Hz	Seismometer	Amplifier	Operator	Notes
AUG	Augustine Island	SPZ	59.380	153.420	0.6	17 K	100K	Mark L-4	Develco 6202-02	U of A	a,c,v
BIG	Big Mountain	SPZ	59.389	155.216	0.6	50	300	Geotech S-13	Electro-Tech SPA	U of A	m,o
BLR	Black Rapids	SPZ	63.502	145.845	0.8	1500	7000	Geotech S-13	Electro-Tech SPA	U of A	m,o
GIL	Gilmore Creek	SPZ	64.975	147.495	0.4	200	1000	Geotech S-13	Geotech 12613 PTA	NOAA	m
GLM	Gilmore Creek	SPZ	64,987	147.389	0.8	1600	8000	Ranger SD-215	Sandia N89653	U of A	b,p
HPP	Judge Hepp's House	SPZ	64,791	147.959	0.2	150	900	Johnson-Math.	Geotech 4300 PTA	U of A	v
KCH	Kichatna River	SPZ	62.100	152.022	0.6	710	2950	Geotech S-13	Electro-Tech SPA-1	U of A	s, v
KDC	Kodiak	SPZ	57,748	152.492	0.0	50	300	Geotech 4681A	Geotech 12613 PTA	NOAA	m
MCK	McKinley Hotel	SPZ	63.732	148.935	0.6			Ranger SD-215	Sandia N89653	U of A	b,v
MID	Middleton Island	SPZ	59.428	146.339	0.0	6	35	Geotech 4681A	Geotech 12613 PTA	NOAA	m
MIN	Minitrack Site	SPZ	64,872	147.828	0.2	170	1000	Geotech S-13	Electro-Tech SPA-1	U of A	c,p
PAX	Paxson	SPZ	62,971	145.469	1.1	350	1700	Ranger SD-215	Sandia N89653	U of A	b,m
PJD	Pedro Dome	SPZ	65.034	147.509	0.7	150	1000	Geotech S-13	Electro-Tech SPA-1	U of A	m,t
PNR	Palmer	SPZ	61.592	149.131	0.1	100	600	Geotech 4681A	Geotech AS-330	NOAA	n,p
PMS	Arctic Valley	SPZ	61.245	149.561	0.7	100	600	Geotech S-13	Geotech 12613 PTA	NOAA	p
PWA	Houston	SPZ	61.650	149.879	0.1	100	600	Geotech S-13	Geotech 12613 PTA	NOAA	p
SCM	Sheep Mountain	SPZ	61.833	147.328	1.0	250	1000	Geotech S-13	Electro-Tech SPA-1	U of A	m
SHL	Shell Hill	SPZ	61.979	151.525	0.5	360	1480	Geotech S-13	Electro-Tech SPA-1	U of A	s,v
SKE	Skwentna	SPH	61.968	151.222	0.0	45	190	Ranger SD-215	Electro-Tech SPA-1	U of A	d,s
SKN	Skwentna	SPH	61.968	151.222	0.0	45	190	Ranger SD-215	Electro-Tech SPA-1	U of A	d,s
SKV	Skwentna	SPZ	61.972	151.223	0.0	45	190	Geotech S-13	Electro-Tech SPA-1	U of A	d, e, s
TLN	Talachulitna River	SPZ	61,748	151.530	0.5	710	2950	Geotech S-13	Electro-Tech SPA-1	U of A	s, v
TNN	Tanana	SPZ	65.257	151.912	0.5	300	1200	Geotech S-13	Electro-Tech SPA-1	U of A	m
YNL	Yenlo Mountain	SPZ	62.038	151.200	0.4	45	190	Geotech S-13	Electro-Tech SPA-1	U of A	e, s, v

NOTES FOR TABLE 2-1

*) The magnification is the ratio of the display amplitude in mm to the ground amplitude in mm. All of the stations except those in the Skwentna network (note s) are recorded on a Geotech Develocorder and displayed on a Geotech 6585 FilmViewer. This recorder-display system has an approximate 100 mm/v response at 1 and 5 Hz. The Skwentna stations were recorded on FM tape and displayed on an 8 channel Sanborn chart recorder. This system has an approximate 6 mm/v response at 1 and 5 Hz.

#) See Appendix III for frequency response of these components.

a) Augustine Project: Volcanic tremor monitoring station operated by J. Kienle, University of Alaska.

b) Borehole Installation: These stations have SPZ, SPH, LPZ and LPH components at approximately 6-10 m depth. The LP components are recorded in a tilt-meter mode.

c) Code Change: Aug is now AG1 and MIN is now MIK.

d) Direct Hookup: Seismometer and amplifier are connected directly into the recorder.

e) Exchange: On July 1, SKV was moved to Yenly Mountain becoming YNL.

m) Microwave: The White Alice microwave/troposcatter system is part of the data link.

n) NOAA HQ: At NOAA's Palmer Observatory there are also SPH and LPZ components.

o) Operator Change: BIG is now operated by R. Page of the USGS at Menlo Park and BLR by NOAA, at Palmer.

p) Phone Line: A VCO-phone line-discriminator combination is part of the data link.

s) Skwentna: This station is part of the temporary Skwentna network.

t) Terminated: This station is no longer in operation.

v) VHF: A VHF transmitter and receiver are part of the data link.

lack of data may be due to a variety of causes, e.g.: (1) a failure at the station, (2) failure of one of the data links between the station and the recorder, (3) failure of the recorder or (4) failure of the timing system. Operationally, for June and July, 1973, AUG was the most reliable station, having recorded zero percent downtime. Next, in order of descending reliability, were the Palmer stations with an average per station downtime of 0.73 percent. There was only one station failure for this network (PMS) and the few additional hours of downtime were due to failure of the White Alice system, working on the Develocorder, etc. The University of Alaska stations averaged 6.4 per cent downtime. This network suffered two individual station failures (HPP and PJD) and a few more hours of White Alice system and

Develocorder downtime than did the Palmer network. Not surprisingly, the temporary VHF network at Skwentna had by far the worst downtime recorded at 22 per cent. Most of this time is due to an intermittent failure in the transmitter at TLN. The second largest cause of downtime was loss of power at YNL and KCH due to rearrangement of the stations by bears. The next most significant problem was the uneven settling of the horizontal seismometers at Skwentna which caused the transducer to tilt enough to pin the mass against one end of its cage. Another common problem was the sporadic failure of the time code generator which necessitated making frequent checks of the timing system in order to lose as little data as possible before resetting the generator. The most reliable stations in this network were KCH, SHL and SKE.

The large aperture array of the University of Alaska has been described in detail by Berg, Sperlich, and Feetham (1967) and by Berg (1970 and 1971). The network consists of two parts: (1) the basic array of short period vertical (SPZ) seismometers and (2) the tripartite borehole installation. Each borehole package contains orthogonal sets of short and long period transducers. In this study only the SPZ mode was utilized. An updated version of the block diagram of typical station configuration of the University of Alaska array is given in Figure 2-3. Stations BIG, BLR, PAX, PJD, and TNN transmit their signal over a telephone channel of the White Alice microwave/troposcatter system which

REMOTE STATION CONFIGURATION FOR U. OF A. ARRAY

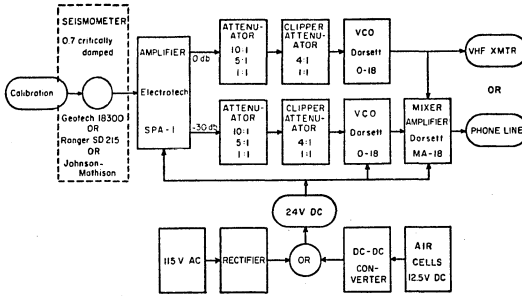

UNIVERSITY OF ALASKA, GEOPHYSICAL INSTITUTE RECEIVING AND RECORDING SYSTEM

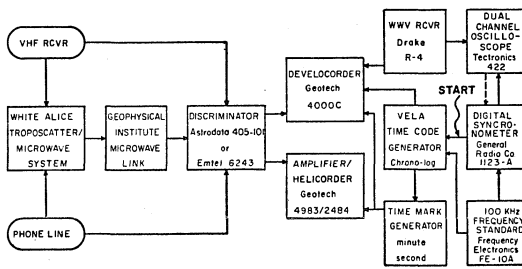

Figure 2-3. Seismographic equipment configuration for the large aperature array of the University of Alaska.

is now operated by RCA. The Geophysical Institute maintains a microwave communications system between the White Alice repeater station at Pedro Dome and the Institute itself. GLM and MIN transmit over the local Municipal Utilities System lines directly into the Intitute building. HPP is broadcast on a VHF carrier directly to the Institute. These stations are all recorded on a Geotech Develocorder and displayed on a Geotech FilmViewer. GLM is also recorded on a Geotech Helicorder which provides a real-time monitor and a means of easily determining the approximate arrival times of earthquakes to be read in detail from the Develocorder film, obviating tedious scanning of the film record. The time standard for this system is a 1MHz crystal oscillator which controls a VELA time code generator and a digital syncronometer. The 1 PPS output of the syncronometer can be compared with and matched to the second pulses of WWV by dialing in microsecond delays. This output pulse is also used to start the time code generator. The drift of the time standard is monitored with precision of better than 1 millisecond and is never allowed to exceed 50 milliseconds.

The temporary stations were operated during June and July, 1971 in the vicinity of Skwentna, Alaska. The base for the operation was a house trailer rented from the FAA at the Skwentna emergency airfield. This trailer housed the timing, recording

and receiving equipment and the operator. Figure 2-4 is a block diagram of the Skwentna network. The remote stations KCH, SHL, TLN and YNL were transmitted on a VHF carrier to the FAA site where they were recorded on a seven-channel tape recorder along with the local stations SKE, SKN and SKV. Note that YNL replaced SKV on July 2. The time standard for this system was a portable crystal clock whose 100 KHz output provided the control frequency for a VELA time code generator. The drift of this timing system was monitored by comparing the 1 PPS output of the time code generator with the second pulses of WWV on a dual channel oscilloscope. This drift is shown in Figure 2-5. It was noted that corrections taken in the morning hours (local time) were systemmatically about 4 milliseconds larger than those taken in the evening; for this reason just the evening observations were used. The slope of a straight line ("Evening Line" in Figure 2-5) fit to these data yields a drift rate of 0.77 milliseconds per day. This line was then translated -17 milliseconds to correct for the travel time of the WWV signal from Honolulu to Skwentna; the resultant time correction is shown to be less than ±25 milliseconds for the duration of the Skwentna network.

The Tsunami Warning System has been described by Butler (1971) and additional information is available from the Palmer Observatory, Palmer, Alaska. In principle a block diagram of this system is quite similar to Figure 2-3 for the University of

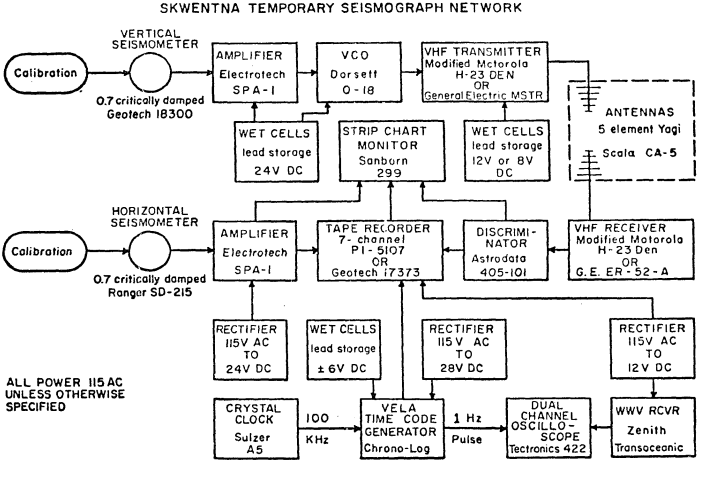

Figure 2-4. Seismographic equipment configuration for the temporary network at Skwentna.

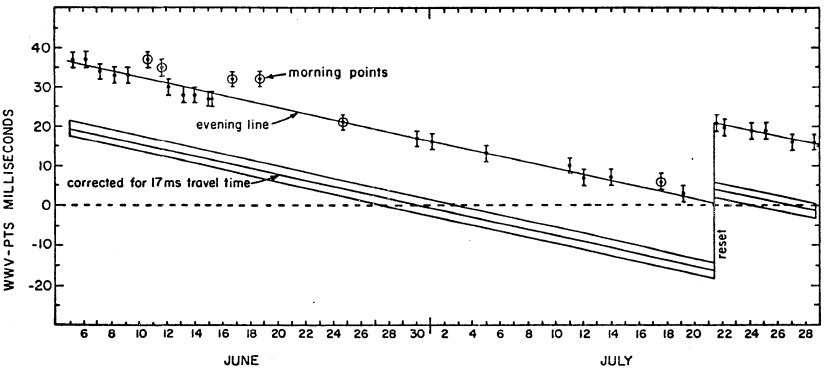

Figure 2-5 Time corrections for Skwentna network. The time corrections were obtained by comparing the one-second pulses of the portable time standard (PTS) to WWV using a dual-trace oscilloscope. Positive time correction means that the PTS was leading WWV. A correction for the travel time of the WWV signal from Honolulu to Skwentna is also shown.

Alaska's system. Also, curves of system magnification versus frequency for the two systems are almost congruent (see Appendix III). Stations GIL, GMA, KDC, and MID are transmitted over the White Alice system while PMS and PWA utilize the Matanuska Valley Telephone Co. lines. All of the stations are recorded in the Palmer Observatory on a Geotech Develocorder and displayed on a Geotech FilmViewer. The observatory time standard is maintained within one millisecond of the WWV time signal.

The seismic monitoring system of the Augustine volcano research project broadcasts its data over a VHF carrier from the remote, air cell powered stations on Augustine Island to a recording base in Homer. This base consists of a Geotech Develocorder, a crystal controlled time code generator and a WWV receiver. Timing precision is a few milliseconds. Through fortuitous circumstances an electronics technician who used to run the equipment of the University of Alaska seismology laboratory is available to operate the recording base in Homer. The data films are mailed to the Geophysical Institute in Fairbanks where they are displayed on a Geotech FilmViewer. During June and July, 1971, only the one station, AUG, had been installed.

From the foregoing network descriptions it can be seen that these four networks are quite compatible for the purpose of accurately locating hypocenters within their combined perimeter.

All of the seismometers used have approximately 1 second natural periods and the timing accuracy at each recording base is better than ±50 milliseconds. The major problems associated with accurate hypocenter location do not come from equipment or operational considerations, but from the complexity and unknown crustal and tectonic structure of the region, about which more will be said later.

Data reduction

In the following, "reading records" means scaling the arrival times and amplitudes of various seismic body wave phases recorded by each of the stations for a given event. For each station the year, month, day, hour, minute, second and tenth of second (GMT) are recorded for each phase. In general, only the largest phase at a given station was scaled for amplitude. Second and third P and S phases were not always read unless they were exceptionally clear. Copies of the Develocorder film records for June and July, 1971, from the Palmer Observatory were made by the Geophysical Institute photographic services department. These records were scanned on the FilmViewer and all events of interest with clear arrivals at any of the Palmer stations, PMR, PMS, or PWA, were read. The tape recordings from the Skwentna network were scanned by increasing the playback speed so that the seismic signals were in the audio range and could be heard as a sharp noise like that of two wooden blocks

being clapped together. Whenever an earthquake was heard in this manner the tape recorder foot-meter was noted to facilitate later playback of each event at 10 times the recording speed and display of the event on an eight channel strip-chart recorder. The additional channel on the strip-chart recorder over the seven of the tape recorder allowed the time code to be displayed on the two outside channels so that the events could be read more accurately. All events with clear arrivals at KCH, SHL or TLN were read.

Data from events read at four or more stations and at least one station each from the Palmer and Skwentna networks were keypunched onto IBM cards and augmented by data for these events, if any, from the University of Alaska and Augustine networks. This restricted set of data for the two months June and July, 1971, comprises the special observations made for this study. Some analysis was also done of the events located by the University of Alaska in 1972-1973. These two data sets will be referred to as the Skwentna and the University of Alaska data sets and contain about 500 and 5000 events, respectively.

CHAPTER III

DATA ANALYSIS AND RESULTS

Location programs

The preliminary location of the events in the two data sets described in Chapter II was carried out using a computer program in routine use at the Geophysical Institute, University of Alaska (Gedney, personal communication). This program, EPICENTR-II, is based on Geiger's iterative, least-squares procedure for finding a hypocenter which minimizes the arrival time residuals at the observing stations and uses Herin's (1968) velocity structure.

A restriction of this type of program is that for common station distributions there are often large areas within the network in which depth control is not very good. This condition occurs when the distance to the nearest station is greater than one or two times the depth to the hypocenter. Under this circumstance the minimization procedure is not very sensitive to depth. The reason for this is that the derivatives of the travel time with respect to depth become very nearly the same for all of the stations, and the system of equations for the corrections to position and origin time for the trial hypocenter ceases to be linearly independent (Eaton, 1970). EPICENTR-II attempts to circumvent this depth control problem by assuming a series of

depths, finding the best-fit epicenter for each of them and picking the epicenter and depth that had the smallest root-mean-square arrival time residual. This procedure apparently works quite well under a wide variety of circumstances, but also breaks down when the equations are not "linerarly-independent-enough".

The major drawback to EPICENTR-II is that it does not have any provision in it to detect when it has lost depth control. Another problem is that as presently written the program outputs only discrete depths; viz., those used in the Herin tables. Both of these failings could be rectified and probably should be, so that the program can be utilized with more confidence for its advantages, the chief one of which is that it is relatively fast due to its simplicity.

In order to obtain an estimate of the relative precision of locations made using EPICENTR-II and those computed by the Earthquake Research Laboratory of the National Oceanic and Atmospheric Administration, locations for forty-eight events were compared. The event parameters are given and compared in Tables 3-1 and 3-2. On the average the EPICENTR-II locations were 0.6 km north and 3.9 km west of the NOAA epicenters. The root-mean-square deviations of the individual differences about the average was 8.2 km and 9.0 km in the north-south and east-west directions, respectively. As one would expect, the origin

Table 3-1

Comparison of NOAA epicenter locations to University of Alaska locations.

		NOAA Parameters						$\Delta X = X_{NOAA} - X_{U\ of\ A}$			
Day	Hour Min	Sec	θ(Lat) North	ϕ(Lon) West	H Depth	Std. Dev. Sec	Number of Stations	ΔT Sec	Δθ Deg	Δϕ Deg	ΔH Km
January 1972											
1	1845	20.7	62.3	151.2	96	0.6	10	-1.7	-.03	-.05	+21
1	1920	31.0	60.3	153.3	139	0.7	11	-2.8	-.04	+.03	+39
1	2002	54.7	58.7	153.5	60	0.9	12	+ .2	+.02	+.03	+60
2	0906	16.5	60.1	152.8	143	0.7	8	-2.7	-.03	-.28	+68
5	0804	12.0	60.0	153.1	128	0.7	9	-2.5	0	-.09	+28
9	0606	19.4	60.5	152.4	103	0.5	9	-2.0	+.05	+.04	+28
10	0217	49.8	62.0	151.0	18	0.5	8	-1.4	-.02	+.11	+ 3
11	0039	19.0	61.7	150.1	38	0.7	12	-1.5	-.19	+.47	+38
11	0546	04.5	61.4	147.0	57	1.0	13	-2.5	-.06	-.06	+17
11	0703	47.8	61.2	147.2	71	1.1	14	+ .2	-.02	+.36	+56
14	0021	29.2	64.7	147.6	12	1.6	8	+ .3	-.24	+.39	-28
14	1737	37.4	63.1	151.0	129	0.4	11	-1.6	+.02	-.05	+29
15	0935	44.8	63.2	150.0	91	0.8	9	-1.2	0	+.23	- 9
20	0924	23.2	60.7	153.2	138	0.7	36	-4.0	+.02	+.51	+38
20	1507	06.9	62.0	148.8	76	0.7	15	-2.1	-.02	-.03	+36
20	1700	45.9	63.1	150.7	104	0.8	15	-1.6	+.02	+.22	+ 4
23	0853	22.2	58.3	151.7	34	1.0	27	+ .5	+.07	+.28	+34
24	1904	55.9	59.6	151.4	83	0.6	10	+1.7	0	-.06	+83
26	1613	07.6	59.7	152.6	119	0.6	16	-2.8	-.04	-.01	+69
26	1747	57.7	63.5	151.2	N	1.0	14	+1.1	-.05	+.08	+18
28	1250	54.4	60.4	153.5	N	1.2	9	-2.4	+.10	+.25	-77
28	1319	24.3	61.6	147.6	19	1.4	14	- .8	-.04	+.11	+ 4
29	2006	55.4	61.4	151.8	118	0.8	10	-2.0	+.06	+.09	+18
30	2141	17.2	63.3	150.9	N	0.9	13	+2.6	0	+.04	+33
31	2231	44.3	62.1	150.5	74	1.0	20	-1.9	+.04	+.02	+34

Table 3-1, continued

Day	Hour Min	NOAA Parameters Sec	θ(Lat) North	φ(Lon) West	H Depth	Std. Dev. Sec	Number of Stations	ΔX = $X_{NOAA} - X_{U\ of\ A}$ ΔT Sec	Δθ Deg	Δφ Deg	ΔH Km
February 1972											
3	0416	04.6	63.1	149.3	88	0.4	14	-1.2	+.04	+.05	+13
8	2330	01.2	60.0	148.0	N	0.5	8	+ .1	+.05	+.21	+33
12	2153	01.6	64.6	147.0	36	0.5	9	+ .8	+.09	-.05	+21
12	2214	37.3	59.9	148.6	50	0.8	10	-2.0	-.01	-.19	+50
13	2240	16.2	59.9	154.2	153	0.9	58	-3.5	-.04	+.04	+53
15	1433	22.0	65.5	147.9	8	1.1	8	- .5	-.02	-.09	- 7
16	1657	13.0	5[illegible].5	152.9	112	0.7	14	-2.7	+.03	+.05	+37
19	1923	15.9	[illegible].0	152.4	102	0.4	13	-2.4	+.04	+.04	+52
25	0926	59.0	6[illegible].2	149.4	45	0.9	14	-2.6	-.11	+.21	+30
27	1349	15.5	5[illegible].2	151.6	50	0.9	26	+1.4	+.11	+.22	+50
29	0732	45.6	63.2	150.5	118	0.4	13	-1.4	-.02	-.06	+18
29	2015	02.0	60.4	150.9	75	0.5	13	+ .1	-.01	+.04	+60
March 1972											
1	1152	23.3	61.1	148.2	16	0.6	13	- .8	-.04	+.05	+16
12	0908	58.1	61.2	147.2	29	0.7	15	-1.2	-.11	-.27	+14
14	0516	49.8	60.0	147.7	34	0.9	27	+1.4	-.02	+.10	+34
14	0543	29.4	63.1	149.4	94	0.3	16	- .6	-.02	+.05	- 6
15	0645	33.4	65.6	149.9	19	0.6	12	+1.2	-.07	-.03	+14
19	0624	09.3	62.4	150.6	25	1.0	15	+ .4	-.06	+.12	+25
21	1548	29.1	60.3	150.9	84	0.4	14	+ .9	+.23	+.56	+84
23	0807	33.0	59.6	153.0	143	0.6	15	-2.6	-.06	-.21	+43
24	0642	22.2	59.5	150.1	34	0.4	9	+1.8	+.12	+.07	+34
28	1013	53.3	64.7	150.2	48	1.0	11	- .1	0	+.05	+ 8
28	1311	17.0	63.6	148.9	119	0.4	13	-1.8	-.02	+.14	+19

Table 3-2

Statistical summary of comparison of epicenter locations given in Table 3-1.

$\Delta X = X_{NOAA} - X_{U \text{ of } A}$	$\Delta\theta$ (deg)	$\Delta\epsilon$ (deg)	ΔT (sec)	ΔH (km)	ΔY (km)	ΔX (km)
$\overline{\Delta X} = \Sigma \Delta X / N$	-0.0058	+0.0777	-1.0	+27.7	-0.64	-3.92
$\sigma = \frac{1}{N}(\overline{\Delta X} - X)^2$	0.074	0.179	1.56	27.4	8.22	9.03

times and depths show larger variations. EPICENTR-II solutions tend, on the average, to be one second later and 28 km deeper than those of NOAA. The root-mean-square deviations about the average were 1.6 seconds in origin time and 27 km in depth.

The clustering of events located by EPICENTR-II into linear groups apparently related to faults provides a means to estimate empirically the accuracy of the locations. Figure 3-1 shows the Rampart fault and events apparently associated with it. If one assumes that all of the earthquakes in the cluster occured on a vertical plane through the fault then the width of the cluster provides an estimate of the precision of the locations, and the position of the cluster with respect to the fault indicates the accuracy of the locations. On this basis one can say that EPICENTR-II has a precision of ±5 km and an eastward bias of about 5 km for the Rampart aftershocks. This is a reasonable estimate for shallow events anywhere inside the perimeter of the network of stations used.

EPICENTR-II was used to make preliminary locations of the earthquakes in the Skwentna data set. Epicenters for these events (recorded during June and July, 1971) are plotted in Figure 3-2. Due to the selection criteria discussed in Chapter II this seismicity map is complete down to magnitude 2, from the Alaska Range in the north to the upper Cook Inlet area in the south. However, no selection of data has been made for this map

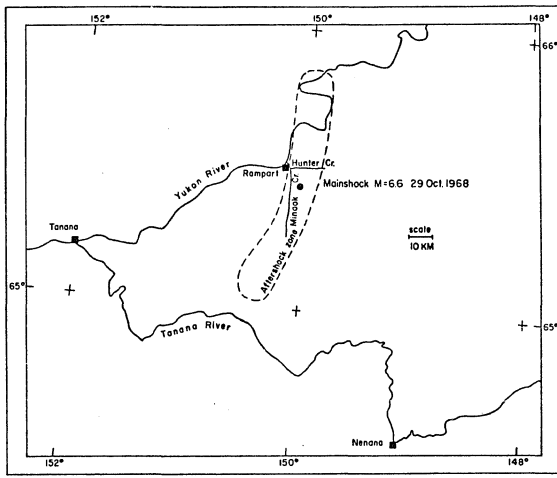

Figure 3-1. Epicenter and aftershock zone of the Rampart earthquake of 29 October 1968, m_b=6.6. The Minook Creek Valley shows as a strong linear feature in the ERTS imagery. The proximity of the elongated afterschock zone, landslides, and hot springs to this valley support the interpretation that it is the surface expression of an active fault.

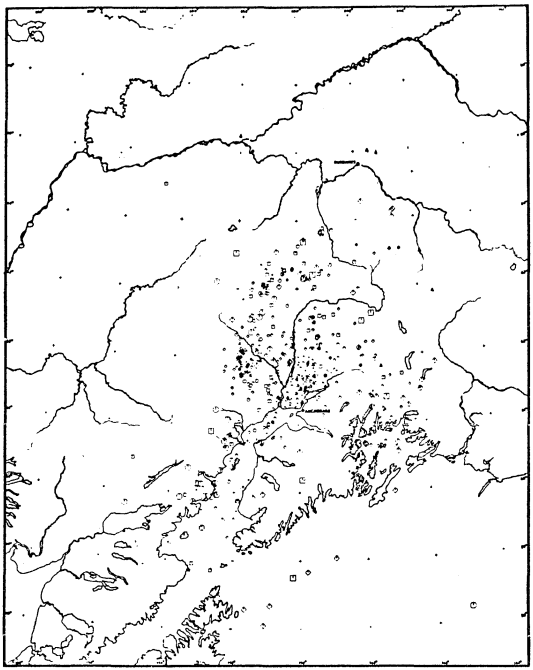

Figure 3-2. South-Central Alaska seismicity, June and July, 1971. See Figure 3-3 for an explanation of the symbols. These hypocenters were computed with EPICENTR-II using the Skwentna data set.

so apparent concentrations of events are seen in the Skwentna and Palmer vicinities which reflect the concentrations of seismograph stations there.

The Skwentna seismicity map may be compared with the central Alaska seismicity map for 1972 (VanWormer, Davies and Gedney, 1973) shown in Figure 3-3. The latter map has been limited to those events of magnitude 3 or greater. By comparison it can be seen that the concentrations of events in the Skwentna and Palmer areas on the Skwentna seismicity maps are in fact due to station distribution in these areas. Both maps show the rather abrupt cessation of seismicity to the west. Figure 3-3 shows that the band of deeper events along the west side of the Cook Inlet - Susitna River topographic low ceases approximately at latitude 63°N. This feature will be discussed in more detail later.

Some of the above events were relocated by a slightly modified version of the program HYPO71 (Lee and Lahr, 1971). This program is also based on Geiger's method but is considerably more sophisticated than EPICENTR-II. The most important feature of HYPO71 is an attempt to solve the depth control problem. The travel time derivatives are continually monitored and if the system of equations for the trial hypocenter corrections ceases to be linearly independent, the depth of the trial hypocenter is fixed until the epicenter is refined enough to again allow the

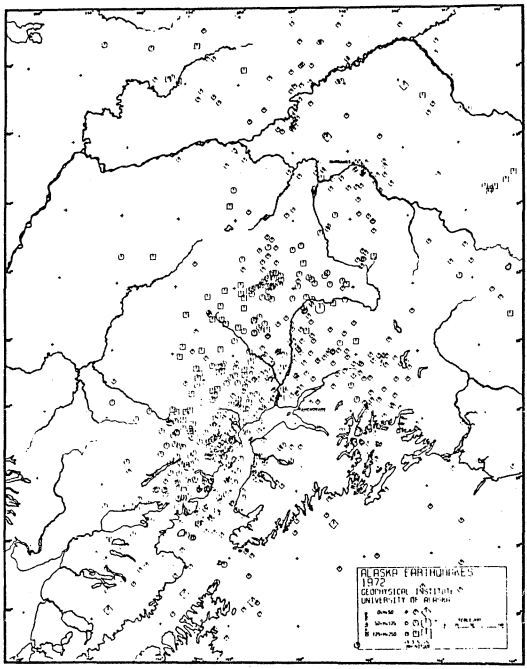

Figure 3-3. Southcentral Alaska seismicity, 1972. These hypocenters were computed with EPICENTR-II using events larger than m_b=3.0 from the University of Alaska data set.

depth to vary, if ever. Fixed depth solutions are flagged so that it is known if depth control has been lost for a given event. This is obviously a desirable procedure, but care must be taken not to make it too restrictive or useful information will be lost.

Other features of HYPO71 are (1) a user specified velocity model, (2) the possible incorporation of S-wave arrival time information and (3) the calculation of distance, travel time and angles of azimuth and incidence to each of the observing stations used in locating a given hypocenter. An obvious problem is that all of these features come at the expense of larger core-space requirements and more computing time per event.

HYPO71 was used to relocate 186 events from the Skwentna data set. These events were selected on the basis of the following criteria: (1) latitude between 61° and 68°N, (2) number of observing stations greater than four and (3) root-mean-square arrival time residual less than or equal to one second. These epicenters are plotted in Figure 3-4. The general trend of deeper events to the northwest can be seen more clearly on this map.

HYPO71 was also used to relocate 744 events from the University of Alaska data set for 1972 and 1973. These events were selected on the basis of the following criteria: (1) latitude between 59° and 66°N, (2) longitude between 144° and 156°W, (3) number

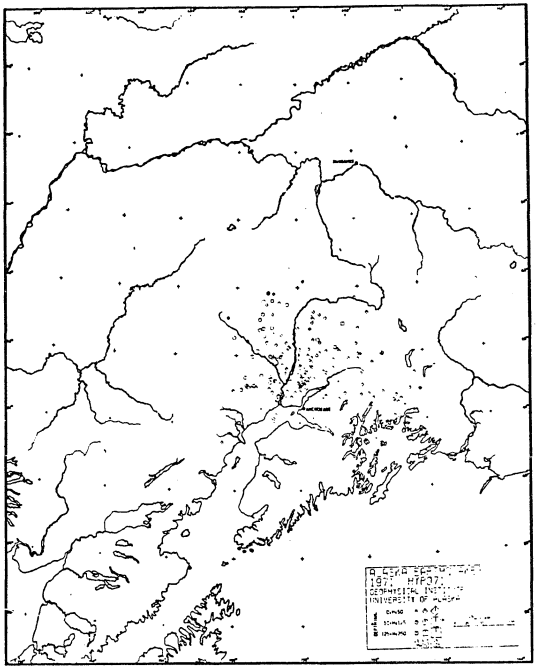

Figure 3-4. Southcentral Alaska seismicity, June and July, 1971. These hypocenters were computed with HYPO71 using 186 events selected from the Skwentna data set.

of observing stations greater than four, (4) root-mean-square arrival time residual less than one second and (5) magnitude greater than three. In spite of these initial restrictions HYP071 froze the depth on about two thirds of these events. The remaining 236 events are plotted in Figure 3-5.

The seismicity indicated in this figure should be complete down to magnitude 2 for the boundaries indicated above. Many of the features noted above can be seen on this map: The abrupt westward boundary, the cessation of the deeper events just north of the 63rd parallel, and the general trend below this parallel for the hypocenters to deepen to the northwest. Shallow clusters of events in the Rampart and Fairbanks areas are also seen. Finally one can note the hiatus of events along a NW-SE line at about latitude 62°N. Many of these features will be examined in more detail in cross-sections presented below.

In order to delineate the Benioff zone a computer program called HYPLOT (see Appendix II) was written to make vertical cross-sections of the hypocenters represented in the above seismicity maps. These cross-sections are made by projecting the hypocenters contained within a thin rectilinear volume, see Figure 3-6, onto a vertical plane normal to the projection or look azimuth. Figures 3-7 through 3-9 show cross sections plotted by HYPLOT.

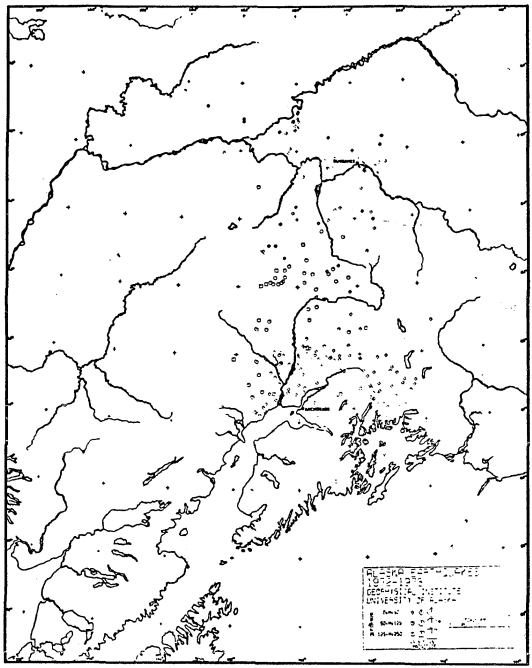

Figure 3-5. Southcentral Alaska seismicity, 1972 and 1973. These hypo_enters were computed with HYPO71 using 236 events selected from the University of Alaska data set.

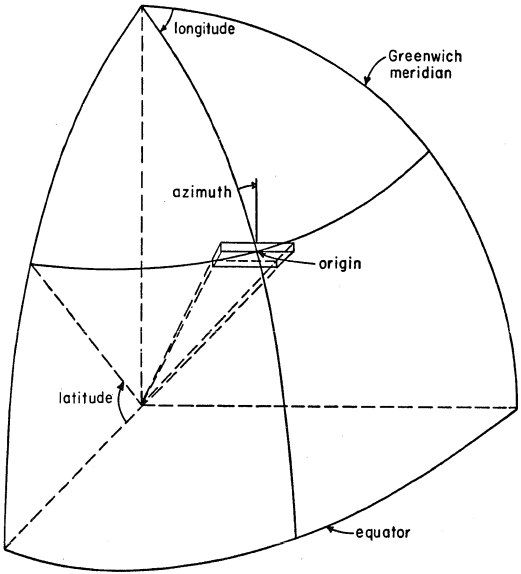

Figure 3-6. HYPLOT projection volume geometry. Hypocenters contained within a thin rectilinear volume are projected onto a plane nomal to the azimuthal direction.

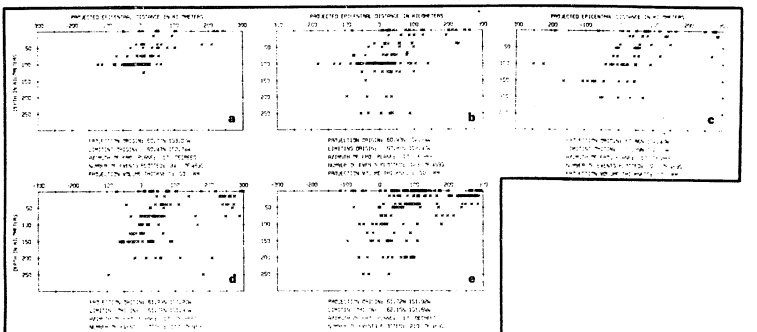

Figure 3-7. Upper Cook Inlet hypocenter cross sections. A location map is shown in Figure 3-10. The projection azimuth is aligned with the volcanic axis, N17°E, so left is approximately west-northwest. The projection volumes are 50 km thick.

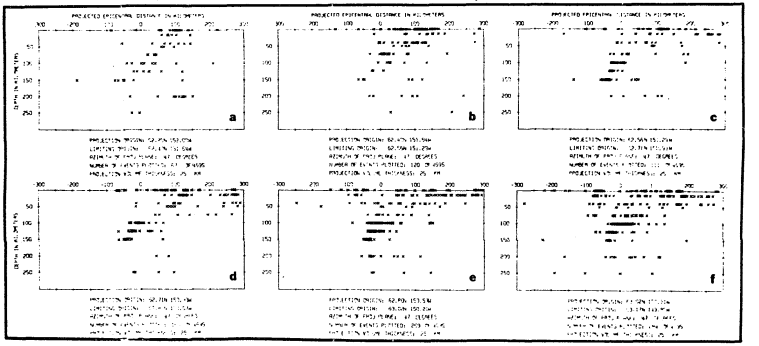

Figure 3-8. Mount McKinley vicinity hypocenter cross sections, part one. A location map is shown in Figure 3-10. The projection azimuth is N47°E so left is approximately northwest. The projection volumes are 25 km thick.

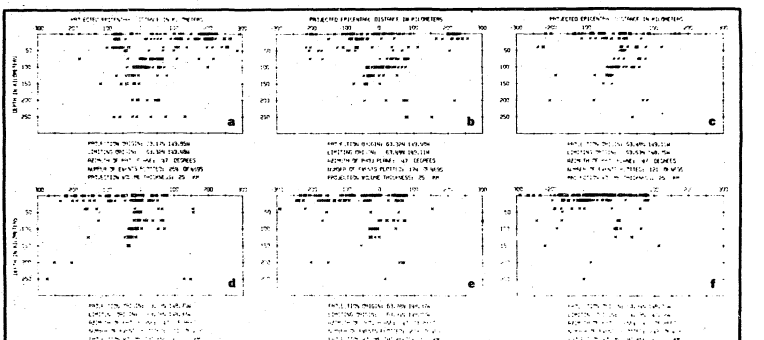

Figure 3-9. Mount McKinley vicinity hypocenter cross sections, part two. A location map is shown in Figure 3-10. The projection azimuth is N47°E so left is approximately northwest. The projection volumes are 25 km thick.

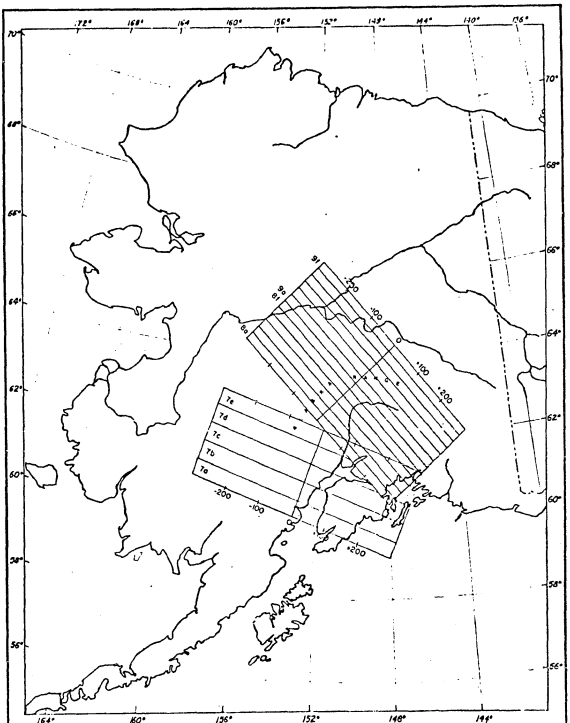

Figure 3-10. Location map for upper Cook Inlet and Mount McKinley vicinity hypocenter cross sections. Sections 7a-7e refer to Figure 3-7, 8a-8f to 3-8 and 9a-9f to 3-9.

Figure 3-7 shows a series of cross sections (7a-7e) in the upper Cook Inlet region with the look azimuth aligned with the volcanic axis (N17°E). Figures 3-8 and 3-9 show a second series (8a-8f, 9a-9f) in the vicinity of Mount McKinley with the look azimuth generally paralleling the Alaska Range (N47°E). A location map for these two series of cross sections is shown in Figure 3-10. Figure 3-11 shows three 100 km thick cross sections (a-c) perpendicular to those in 3-7 and three (d-f) perpendicular to those in 3-8 and 3-9. The maps in Figure 3-12 give the locations of these perpendicular cross sections. The hypocenters shown were located with EPICENTR-II and were selected from the 1972-1973 University of Alaska data set with the following criteria: (1) number of recording stations greater than or equal to five and (2) root-mean-square travel time residual less than or equal to two seconds. This data subset consists of 4,695 events.

There is a good deal of scatter among the hypocenters shown in these cross sections, but in the first two series of cross sections (7a-7f and 8a-9f) there is a strong suggestion of a Benioff zone dipping to the northwest. In order to examine this suggestion in an unbiased way, a straight line was least-square fit through the hypocenters in the following manner: For each cross-section a rectangular region containing the suggested Benioff zone was defined by the 40 and 150 km depth levels and

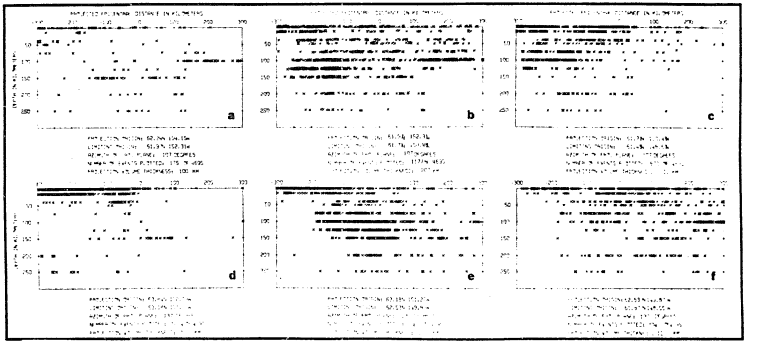

Figure 3-11. Hypocenter longitudinal sections. A location map is shown in Figure 3-12. Sections a-c are perpendicular to the upper Cook Inlet cross sections. Their projection azimuth is E17°S so left is approximately north-northeast. Sections d-f are perpendicular to the Mount McKinley vicinity cross sections. Their projection azimuth is E47°S so left is approximately northeast. All of these projection volumes are 100 km thick.

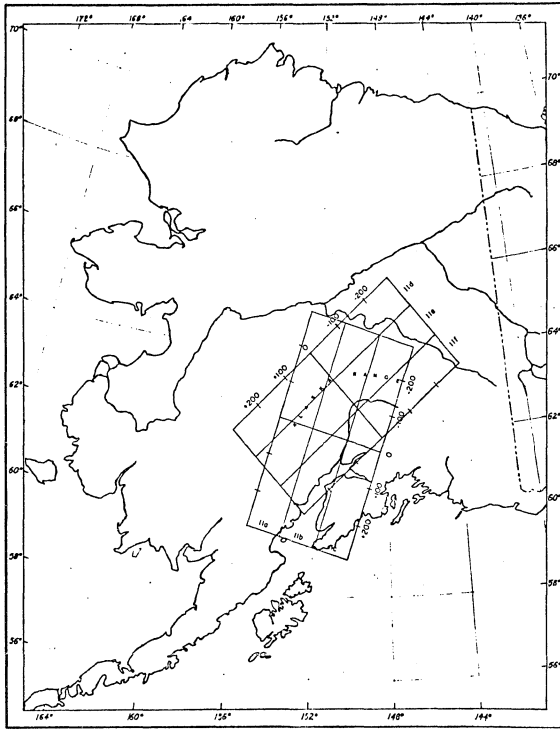

Figure 3-12. Location map for upper Cook Inlet and Mount McKinley vicinity. Hypocenter longitudinal-sections section lettering refers to Figure 3-11.

by extending the vertical boundaries 50 km to either side of the concentration of events which defined the suggested dipping zone. Then the positions of the events within this rectangle were averaged for each depth level (viz: 40, 75, 100, 125, and 150 km) and the standard deviation about this average position was found. The number of events was divided by the standard deviation (km) to obtain the simplest weighting factor for each position. These average positions, standard deviations, numbers of events used in calculating each position, and weighting factors are given in Table 3-3. Finally, for each cross section a weighted-least-square-fit line was drawn through the averaged positions as shown in Figure 3-13. Also shown in this figure (lower right, 13a) is a composite cross section made up of all of the least-square lines from the 8a-9f series. This composite cross section shows that while there is some variation in the slopes of these least-square lines they generally indicate a Benioff zone dipping to the northwest at about 45 degrees. Most remarkable is the convergence of these lines at about 125 kilometers depth, indicating the consistency of the location of the deeper portion of the Benioff zone and that the variation in slope is primarily due to the poor locations of the shallow averaged positions. This is consistent with the generally lower weights assigned to these positions (Table 3-3), which is, in turn, due to fewer events and contamination with events which are related to crustal deformation.

Table 3-3

Averaged hypocenter positions. The cross-section numbers refer to Figures 7, 8 and 9. $\bar{X}$ is the average position (km) of all of the hypocenters at each depth in a given cross-section. The standard deviation, σ, is given in kilometers. The number of events, N, averaged at each depth is divided by σ to obtain a weighting factor, W, for the averaged position.

DEPTH	40 km				50 km				75km				100 km				125 km				150 km			
X-SECT.	$\bar{X}$	σ	N	W	$\bar{X}$	σ	N	W	$\bar{X}$	σ	N	W	$\bar{X}$	σ	N	W	$\bar{X}$	σ	N	W	$\bar{X}$	σ	N	W
7a	19	29	6	.21	42	43	7	.16	2	35	11	.31	-12	32	52	1.63	-	-	-	-	-	-	-	-
7b	35	33	9	.27	32	53	4	.08	9	50	12	.24	0	46	56	1.22	-26	41	10	.24	-	-	-	-
7c	72	61	4	.07	26	32	5	.16	37	54	5	.09	10	36	12	.33	-	-	-	-	-46	70	10	.14
7d	69	22	7	.32	39	22	3	.14	24	24	17	.71	11	17	10	.59	-14	15	7	.47	-18	33	18	.55
7e	80	26	19	.69	46	33	11	.33	14	10	6	.60	7	50	10	.20	-30	13	2	.15	14	56	10	.18
8a	93	41	6	.10	73	20	3	.15	34	9	5	.53	15	48	7	.13	20	46	8	.18	-58	20	5	.25
8b	69	46	21	.45	62	20	4	.20	18	27	16	.59	25	27	5	.18	-15	18	3	.16	-56	9	3	.33
8c	39	43	9	.21	90	5	3	.57	0	20	8	.40	-13	13	14	1.08	-25	13	8	.62	-42	12	15	1.25
8d	102	8	6	.80	87	10	4	.39	47	8	2	.24	-7	23	25	1.07	-26	5	23	4.67	-43	9	12	1.31
8e	54	75	21	.28	3	4	2	.68	38	52	14	.27	-5	28	37	1.33	-17	17	34	1.95	-37	6	19	3.18
8f	85	67	21	.31	46	86	7	.08	14	51	23	.45	7	28	49	1.78	-25	24	27	1.13	-33	6	10	1.58
9a	105	29	4	.14	63	37	3	.08	33	30	22	.73	5	23	41	1.76	-32	18	9	.50	-30	20	6	.31
9b	77	38	3	.08	51	18	2	.11	53	24	17	.71	5	31	29	.94	-20	25	14	.56	-40	22	7	.31
9c	38	37	11	.30	8	5	61	.19	34	35	7	.20	-1	27	19	.71	-32	4	12	2.67	-36	17	2	.12
9d	-	-	-	-	-8	8	6	.74	11	29	12	.42	-14	11	15	1.42	-30	9	12	1.37	-31	3	4	1.40
9e	-	-	-	-	14	57	2	.04	34	26	10	.39	-18	9	8	.86	-22	11	6	.57	-	-	-	-
9f	17	57	2	.04	-	-	-	-	-4	3	3	.00	-9	7	5	.76	11	33	2	.06	-	-	-	-

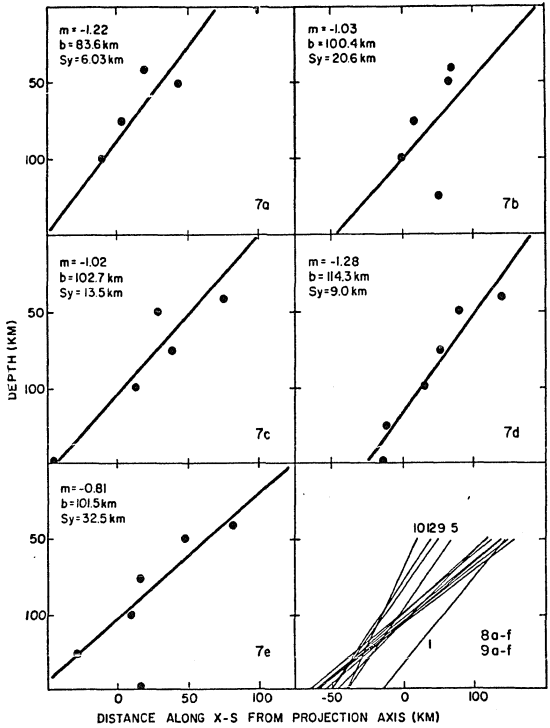

Figure 3-13a. Caption following part c.

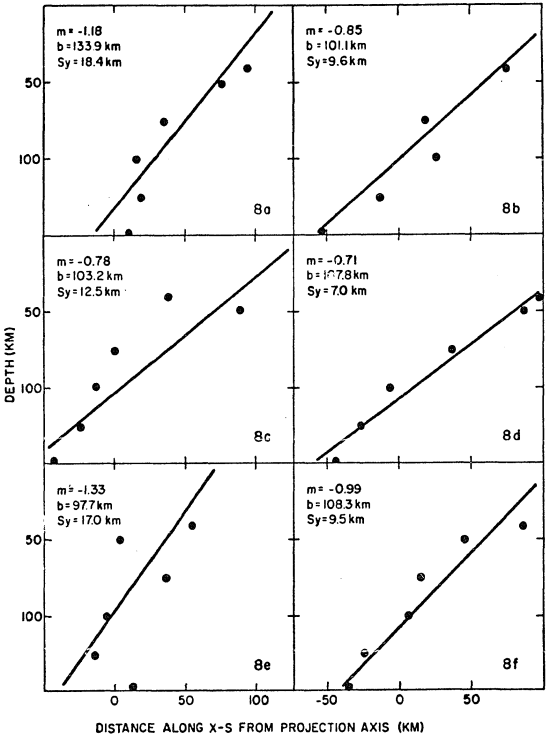

Figure 3-13b. Caption following part c.

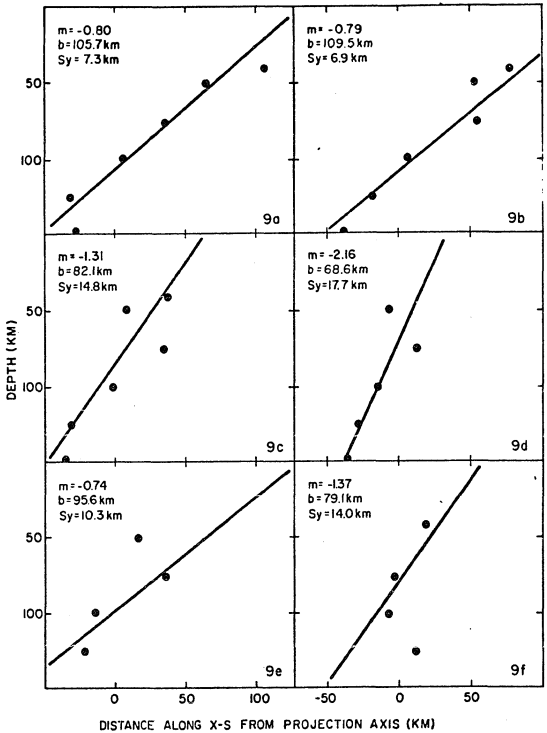

Figure 3-13c. Caption following part c.

Figure 3-13. Averaged hypocenter positions. The solid circles mark the average position of the hypocenters at each depth level in the cross sections shown in Figures 3-7, 8, and 9 (the codes 7a, 7b, etc. refer to these figures). A first-order representation of the intersection of the Benioff zone with each cross section is given by the straight lines which were fit through the averaged hypocenter positions using a weighted (see text) least square procedure. The slope, depth intercept, and standard estimate of goodness-of-fit in the vertical direction are given by the values of m, b, and Sy, respectively. The lower right plate in part "a" is a composite of these lines from parts b and c. The congruency of these lines illustrates how planar is this representation of the Benioff zone.

This increase in consistency of these least-square cross-section lines with depth is also illustrated in Figure 3-14, which shows depth contours constructed from the intersections of the least-square lines and a given depth. This figure is presented to show in map view the overall consistency of the averaged positions with the interpretation that they represent a Benioff zone. This interpretation is examined in more detail in the following analysis.

In order to obtain a better estimate of the shape of the Benioff zone, the averaged positions for each depth were contoured

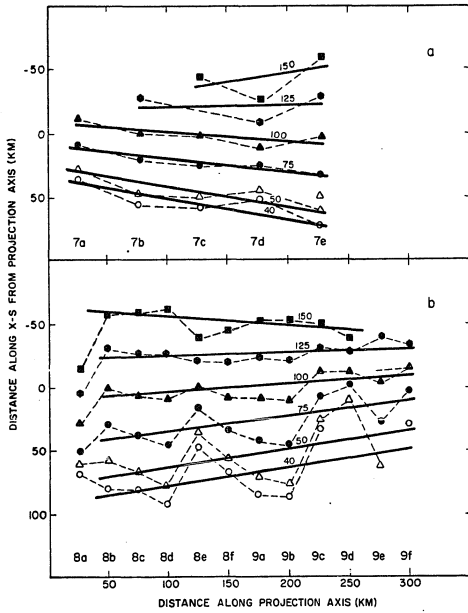

Figure 3-14. Contour map of the Benioff zone. The various symbols connected by dashed lines and marked 40, 50, 75, 100, 125, and 150 represent the depth to the Benioff zone in kilometers as determined by the least square fit straight lines for each cross section shown in Figure 3-13. The straight lines were fit by eye. The convergence of these lines in the lower half of this figure indicates a steepening of the Benioff zone at its northern terminus (see Figures 3-10 and 4-1 for location maps). The codes 7a, 7b, etc. correspond to the cross sections shown in Figures 3-7, 8 and 9.

by fitting a straight, weighted-least-square line through them as shown in Figure 3-15. The lines representing 40, 75, 100 and 150 kilometers depth form an internally consistent set of contours, and are subparallel to the contours given in Figure 3-14, while those for 50 and 125 kilometers cross other contours and are not consistent with those in Figure 3-14 and will therefore be ignored in the following description. The consistent set of contours indicates that the Benioff zone is convex upwards and that the dip increases along the strike of the zone to the northeast. The convexness is illustrated in Figure 3-16 which shows a cross section at 8e of the contour lines presented in Figure 3-15. This cross section was chosen because it happened that in this section both the 50 and 125 kilometer depth contours lie approximately midway between their respective adjacent contours. The length of the bar representing the location of each contour is twice the standard estimate of goodness-of-fit for that contour. The 50 and 125 kilometer depth bars are included in this figure to show the progression of this estimate.

An impression of the accuracy of the position and, to a lesser extent, the shape of the Benioff zone defined by the consistent set of contours in Figure 3-15 can be obtained by comparing the cross section given in Figure 3-16 with cross sections of events located (presumably more accurately) with HYP071. Figure 3-17 shows six such cross sections. The locations

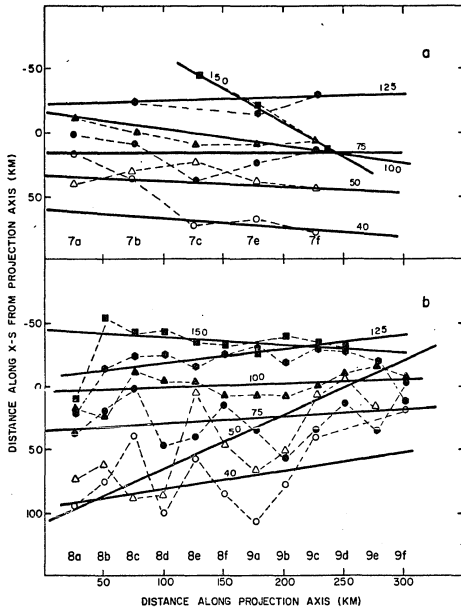

Figure 3-15. Contour map of the Benioff zone. The symbols are the same as in Figure 3-14, except that they represent the average hypocenter position for each depth rather than the intercept with each depth level of the straight line which was fit to the average positions for each vertical cross section. The straight lines in this figure were fit through the symbols for each depth level using a weighted (same as those for Figure 3-13) least square procedure. Again, the cross-section codes 7a, 7b, etc. correspond to those in Figures 3-7, 8, and 9.

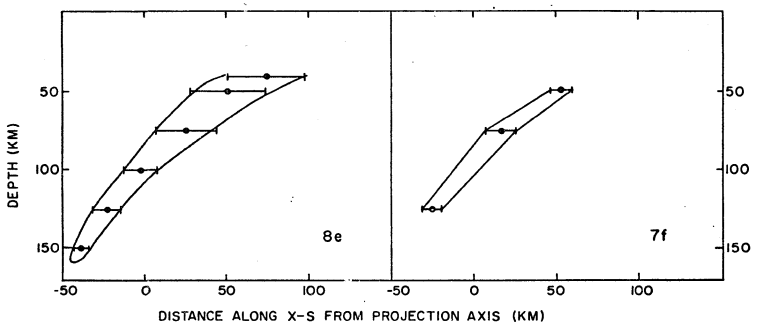

Figure 3-16. Envelopes of error bars for the Benioff zone depth contours in the previous figure. The error bars represent the standard estimate of goodness-of-fit in the horizontal direction transverse to the strike of the Benioff zone. The envelopes are drawn for cross-section 8e and 7f (see Figures 3-15, 3-8, and 3-7). Note that both envelopes suggest that the Benioff zone is convex, upwards.

of these cross sections are shown by the dashed lines in Figure 3-10. The envelope of the 8e cross-section bars from Figure 3-16 is drawn on the HYPO71 section 17d and is shown in Figure 3-18. It coincides remarkably well with the events between 100 and 150 kilometers depth; however, there is so much scatter among the events between 50 and 100 kilometers depth that no comparison can be made except that there is a suggestion in Figure 3-18B that the dip of the Benioff zone might be shallower than indicated by the envelope for this depth range.

It is also interesting to compare the shape of this envelope with a cross section of hypocenters in the upper Cook Inlet region. The envelope and a cross section of events located by HYPO71 from data given in Figure 3-4 are shown in Figure 3-18A. This section is from the Skwentna data set. It compares quite well with the envelope from the McKinley region data in shape and orientation, but it was necessary to translate horizontally the envelope origin about 20 kilometers to the southeast to fit the Skwentna data. There is no a priori reason to assume that the McKinley and upper Cook Inlet region Benioff zones should have the same shape and orientation relative to their 100 kilometer depth contours except that they are adjacent and that their depth contours are close to being continuous with each other. In fact, there are several morphologic and tectonic reasons why it might be expected that these zones are somewhat independent (which will be discussed below).

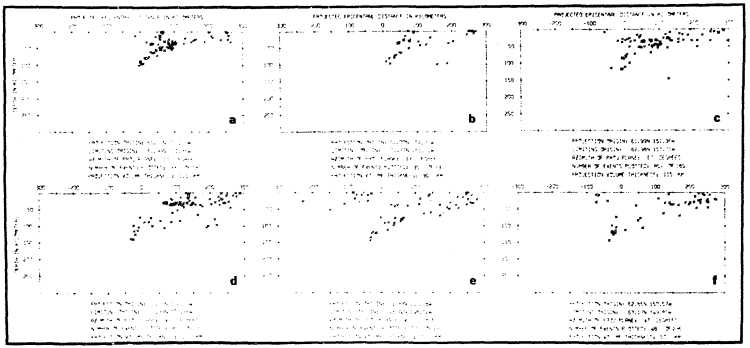

Figure 3-17. Cross sections of hypocenters located using HYPO71. See dashed lines in Figure 3-10 for location of cross sections. Plates a and c show adjacent 115 km thick sections through the Skwentna data set. Plate b shows a 90 km section through the University of Alaska data set which is about congruent with a. Plates d and e show adjacent 120 km thick sections through the University of Alaska data set in the vicinity of Mt. McKinley. Plate f shows a 50 km section which straddles the boundary between the sections shown in d and e.

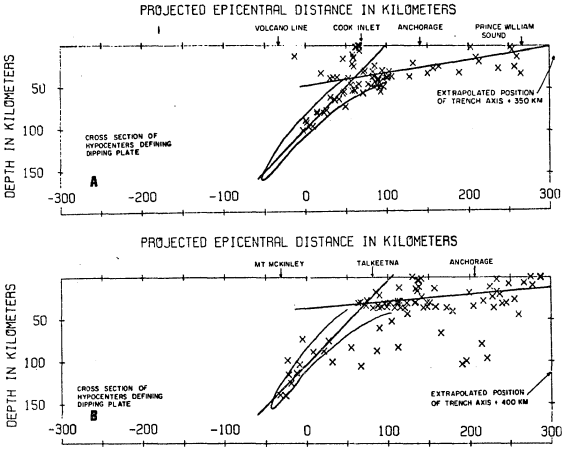

Figure 3-18. Hypocenter cross sections with superimposed error bar envelope. Plate A shows the fit with the Skwentna data; B shows the fit with the McKinley data, both as shown in the previous figure.

An envelope of contour error bars for cross sections 7a-7e data is also given in Figure 3-16. This envelope was constructed in the same manner as was the envelope for the 8a-9f series except that the inconsistent contours were omitted. This envelope is displaced about 15 kilometers to the west compared to the 17a cross section of the Skwentna data. This is qualitatively what one would expect since the envelope location was determined from the University of Alaska data set whose stations were mostly to the east of the Benioff zone.

The above data are summarized in a contour map of the Benioff zone as shown in Figure 4-1. The positions of these lines are taken from a generalization of Figure 3-15. The horizontal extent of the contours is taken from consideration of the perpendicular sections shown in Figure 3-11. The southern termination of the depth contours is arbitrarily taken at the southern edge of section 11b and merely represents the boundary of the region under consideration and is not intended to represent a real boundary in the Benioff zone. The data for the 150 kilometer depth contour, however, based on section 9a show an abrupt cessation of events deeper than 100 kilometers to the south of +125 kilometers along the section. The break in the contours in the Yentna vicinity is a reminder that the two sets of contours were constructed independently. However, there is a suggestion in the data that there is a hiatus in the seismicity

(Figure 3-5) along the Yentna lineament. This hiatus can be seen in the perpendicular sections also. The northern termination of the contours is based on the abrupt cessation of all events deeper than 15 kilometers north of -185 kilometers in sections 11e and 11f. This contour map shows that the Aleutian arc Benioff zone continues into interior Alaska and terminates about 75 kilometers south of Fairbanks, slightly north of the Alaska Range and the Denali fault.

Residual Studies The arrival-time residual at a given station, R, (neglecting explicit station and path corrections) is defined by the equation:

$$R = T_a - T_c$$

where T_a = the observed arrival time at a station

and $T_c = T_o + T_t$ = the calculated arrival time

with T_o = the origin time of the event

and T_t = the model travel time from the hypocenter to the station (a function of the assumed velocity structure).

The arrival-time residual distribution at a set of stations due to a single event contains information about the velocity structure of the region traversed by the seismic waves. This distribution has been used by seismologists to examine the gross structure of the subducted lithospheric plate in the Aleutian arc (e.g.: Jacob, 1972, and Biswas, 1973).

Several years ago the author considered another travel time residual distribution: The residuals at a single station due to a set of earthquakes plotted at their respective epicenters. This distribution was examined for several of the University of Alaska large aperture network stations (Berg, 1966) using data from June, July and August, 1970, which were calculated by EPICENTR-I. EPICENTR-I was based on a single-layer-over-a-half-space velocity model and the network was widely spaced so that the accuracy of locations and especially of depths of the events used in this study is problematic. Another major consideration is that the nature of a least-squares solution is to minimize the residuals by the successive adjustment of the trial hypocenters so that any structural information may be averaged out of this distribution in the location process. However, when several of these distributions were plotted it was found that there was a consistent pattern for each station so that relatively simple contours could be fit to the data with no exceptions. Further, there was a general north-south elongation of the contour patterns for each station which suggested that it might be structurally controlled. It also might be due to the north-south elongation of the station distribution if the residual pattern represents in some way the relative accuracy of the location of the events as a function of their positions within the network (Peters, 1972).

In any case these distributions were enticing and it was thought that with better location programs and more information on the tectonic structure of south-central Alaska the question of whether or not this kind of residual distribution contains structural information could be answered. Figure 3-19 shows six such distributions. The events used in constructing these travel-time residual distributions were located using HYPO71 and were restricted to those in the Skwentna-Palmer vicinity which were deeper than 50 kilometers in an attempt to obtain an accurately located set of events which would be likely to have ray paths which traversed the Benioff zone and the inferred dipping lithospheric plate. HYPO71 heavily weights the closer stations where the effect of the inferred structure would be, in general, the least, so that residuals at more distant stations might contain structural information. The residuals contoured in Figure 3-19 were calculated with a computer program called STARES (see Appendix II) which uses HYPO71 locations and the Herin (1968) velocity model and gives residuals plotted at epicenter positions on a cartesian grid centered at 62.5°N and 149.5°W such that the resulting distribution is a Lambert conformal mapping at a scale of one to a million.

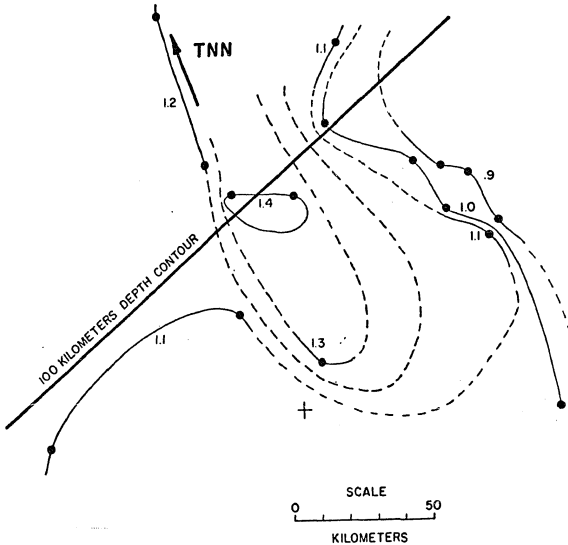

Figure 3-19. Arrival-time residual contour maps. Arrival-time residuals (in seconds) to the indicated station are plotted at their respective epicenter (solid circles). Extrapolated contours are dashed. The heavy line is the 100 km depth contour of the Benioff zone as shown in Figure 3-14b. The cross marks the point at 62.5°N and 149.5°W.

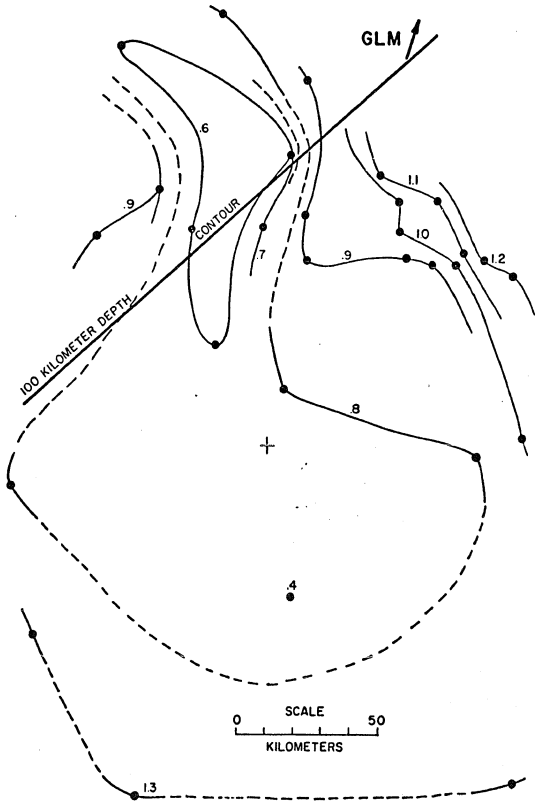

Figure 3-19 B.

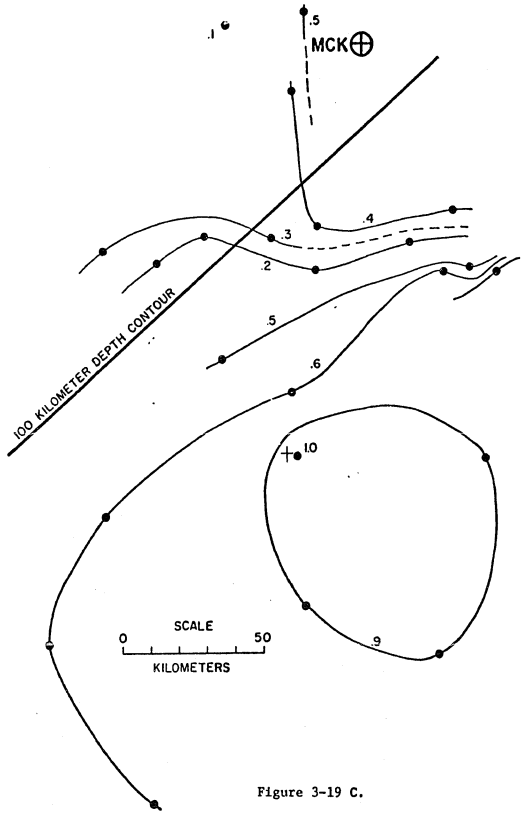

Figure 3-19 C.

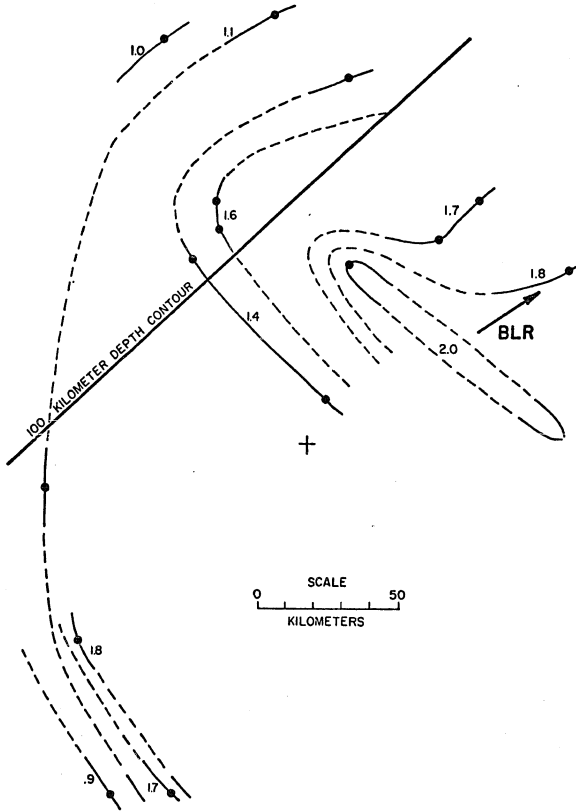

Figure 3-19 D.

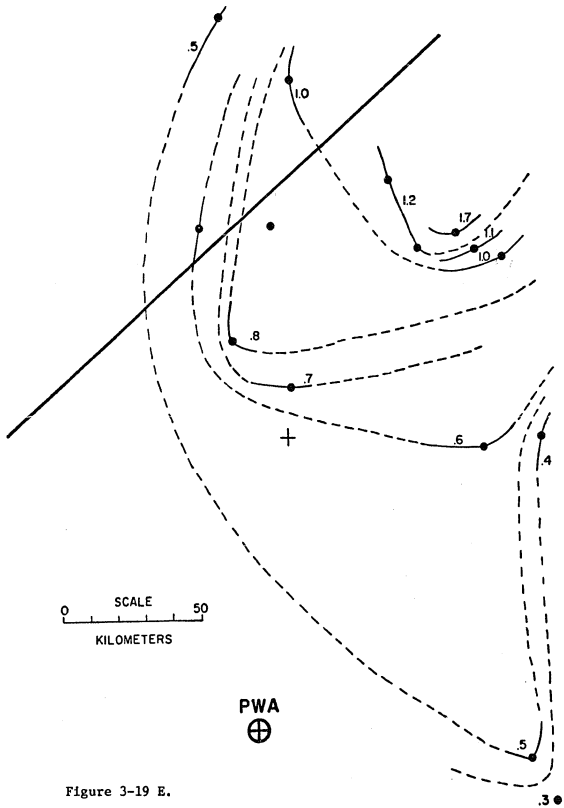

Figure 3-19 E.

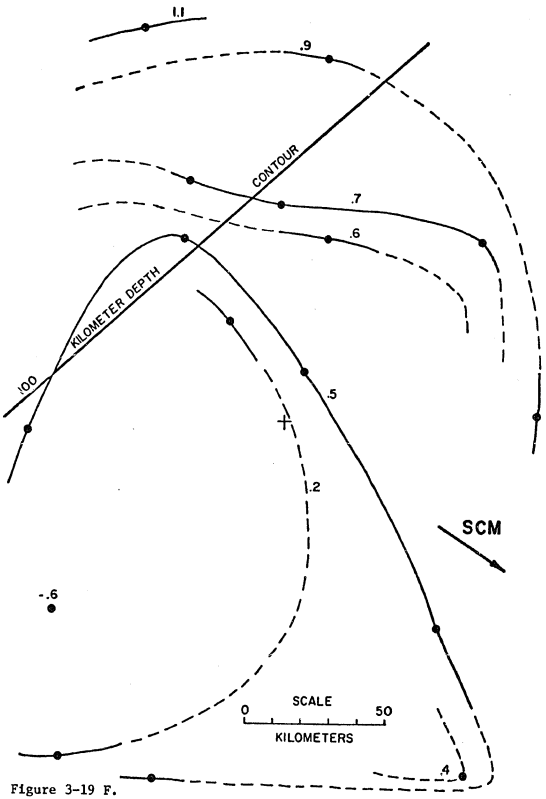

Figure 3-19 F.

The maps in Figure 3-19 are presented to illustrate what is concluded to be a null result. That is, these maps do not show features which might be thought to be related to a dipping slab of higher velocity material. The gradient direction is in most cases perpendicular to the expected direction and in some cases is opposite to the direction expected. Also the patterns are of too small a scale to be explained by a dipping plate.

Attenuation studies

One of the general features of a subduction zone is the low Q region under the volcanic arc and above the underthrusting plate. It is of interest to examine the subduction zone in the vicinity of Skwentna because this is the transition area just beyond the end of the active volcanic arc. Three methods were employed in this investigation.

First, the waveforms of the S-phase arriving at the horizontal seismometers at Skwentna were examined for several events which had ray paths traversing different regions of the subduction zone. This type of analysis has shown in other regions a marked reduction in the envelope area for the S-phase for events with ray paths through the low Q region below the volcanic arc. At Skwentna no such reduction was observed. Figure 3-20 gives in cross section the location and ray paths from several events to the Skwentna horizontal seismometers, and Figure 3-21 shows

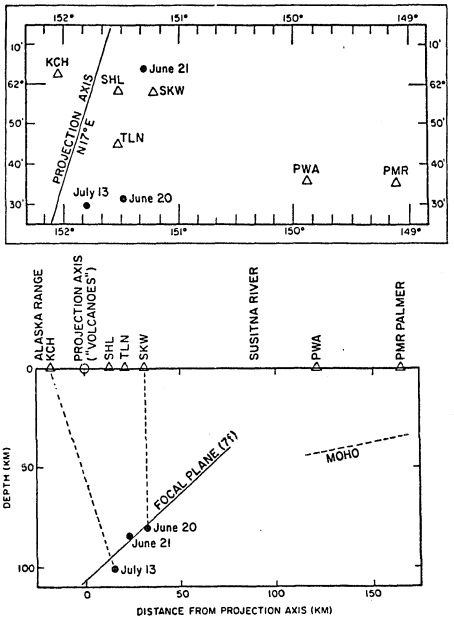

Figure 3-20. Location map (a) and cross-sectional view (b) of three deep earthquakes near Skwentna showing ray-path region to Skwentna network. The projection axis is the zero line for the upper Cook Inlet cross sections 7a-e as shown in Figure 3-10. The cross section shown in part b is a projection onto a plane normal to the projection axis. The focal plane is taken from Figure 3-13a. The moho depths under the Palmer stations PWA and PMR are taken from Davies and Berg (1973).

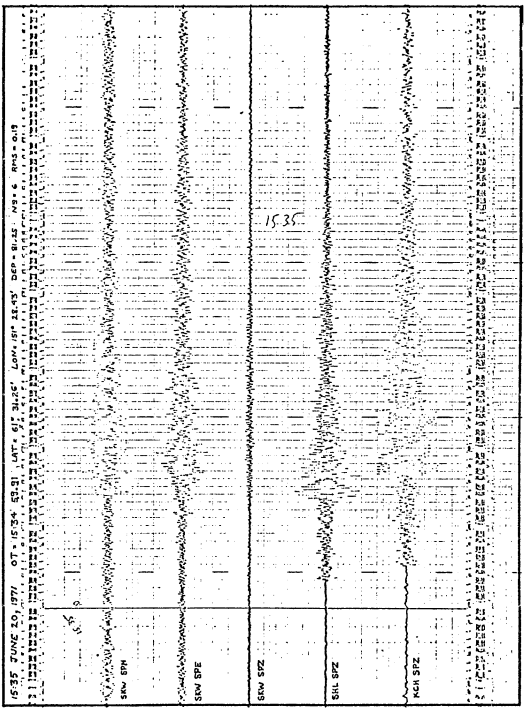

Figure 3-21 A. Caption following C.

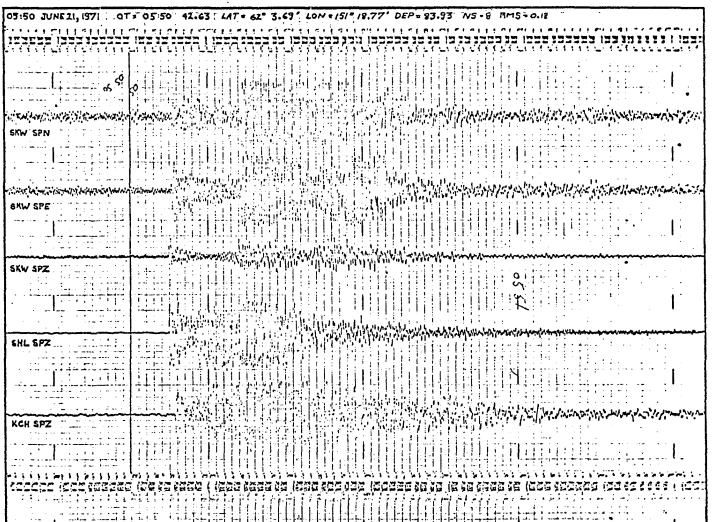

Figure 3-21 B. Caption following C.

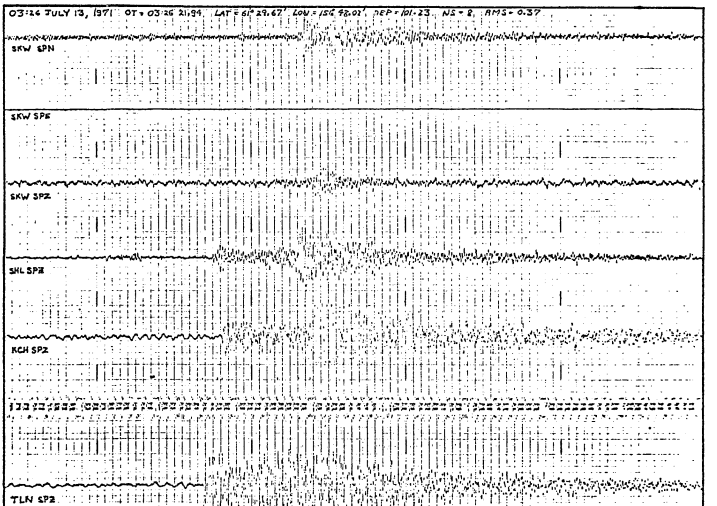

Figure 3-21 C. Caption following.

where we have assumed σ to be a constant of the medium which may then be given as

$$\sigma_{12} = \frac{\ln(r_1A_1/r_2A_2)}{r_1-r_2}$$

Of course we propose to examine the variation of the parameter σ_{ni} as a function of position to examine the attenuation properties of the Skwentna region and therefore the assumption that σ is a constant is violated; if, however, σ_{ni} doesn't vary too much this can be tolerated. Another assumption we have made is that the ray paths are straight lines. This is also not strictly true but the events have been chosen so that the error introduced by this assumption is small.

The parameters from six earthquakes used in calculating the σ_{ni}'s are given in Table 3-4. These earthquakes cluster into two groups of three, one about 40 kilometers under PMW and the other about 90 kilometers under SHL, as illustrated in Figure 3-22, which also shows a plot of the σ_{ni}'s associated with the i-th station. Note than n was always taken to represent SCM so that the ray path from the hypocenter to SCM is the reference path in each case. Figure 3-22 shows that most of the σ_{ni}'s are negative, which is to be expected since this represents an attenuating medium, that is, one in which energy is lost to dispersion and internal friction as the wave propagates. Some of the σ_{ni}'s in the Skwentna region are positive which indicates

Figure 3-21. Seismograms from the Skwentna network for the three events shown in the previous figure. The strong S phases and high-frequency content seen in these records preclude high attenuation due to a low Q region in the magmagenic region above the Benioff zone as might be expected from the absence of quaternary volcanics near Skwentna.

copies of the recorded waveforms. This implies that there is probably no significant (in terms of seismic wave propagation) partial melting above the subducted plate in the Skwentna vicinity and is consistent with the lack of active volcanics.

The second method used was an analysis of the attenuation of P-phase amplitudes from local events. A harmonic wave amplitude can be written in the form:

$$A(r_1 t) = \frac{Ao}{r} e^{\pm\sigma r} e^{-i(kr-wt)}$$

where r = the radius from the hypocenter to the observing station,

t = the time,

A_o = the initial or source amplitude,

σ = the attenuation factor,

w = the circular frequency of the wave, and

k = the wave number.

Note that negative σ corresponds to attenuation. The ratio of the maximum amplitude at two observing stations will then be:

$$\frac{A_1}{A_2} = \frac{r_2}{r_1} e^{\sigma(r_1-r_2)}$$

where we have assumed σ to be a constant of the medium which may then be given as

$$\sigma_{12} = \frac{\ln(r_1 A_1 / r_2 A_2)}{r_1 - r_2}$$

Of course we propose to examine the variation of the parameter σ_{ni} as a function of position to examine the attenuation properties of the Skwentna region and therefore the assumption that σ is a constant is violated; if, however, σ_{ni} doesn't vary too much this can be tolerated. Another assumption we have made is that the ray paths are straight lines. This is also not strictly true but the events have been chosen so that the error introduced by this assumption is small.

The parameters from six earthquakes used in calculating the σ_{ni}'s are given in Table 3-4. These earthquakes cluster into two groups of three, one about 40 kilometers under PMW and the other about 90 kilometers under SHL, as illustrated in Figure 3-22, which also shows a plot of the σ_{ni}'s associated with the i-th station. Note than n was always taken to represent SCM so that the ray path from the hypocenter to SCM is the reference path in each case. Figure 3-22 shows that most of the σ_{ni}'s are negative, which is to be expected since this represents an attenuating medium, that is, one in which energy is lost to dispersion and internal friction as the wave propagates. Some of the σ_{ni}'s in the Skwentna region are positive which indicates

Table 3-4a

Calculation of attenuation values plotted in Figure 3-22. Column headings: STA, station designator code; Δ, epicentral distance; P, peak-to-peak trace amplitude; r, radial hypocentral distance; A, peak-to-peak ground displacement in nanometers; σ_{ni}, attenuation factor from equation 3-2, n corresponds to reference station SCM except for event 71-06-12 where PMR is the reference station, i refers to the station numbers in the first column. The brackets denote average values: $\langle\sigma_{ni}\rangle$ is the average σ_{ni} for each event; $\langle\sigma_{ni} - \langle\sigma_{ni}\rangle\rangle$ is the average deviation for the i^{th} station over the three events in either Table 4a or 4b.

i	STA	Δ(km)	P(mm)	r(km)	A(nm)	$\sigma_{ni}(km^{-1})$	$\sigma_{ni} - \langle\sigma_{ni}\rangle$	$\langle\sigma_{ni} - \langle\sigma_{ni}\rangle\rangle$
71-06-12	1301	41.41						
1	KCH	14	124.9	131.6	3.94	+.02093	+.02705	-.08613
2	SHL	7	95.5	104.1	3.89	+.00822	+.01434	+.03048
3	SKW	3	81.3	91.2	13.3	-.01512	-.00900	+.00412
4	PWA	15	11.6	43.0	15.0	-.00935	-.01547	+.01486
5	PMS	22	40.2	57.7	22.0	-.01509	-.02121	+.00946
6	PMR	57	43.9	60.3	57.0	-.02634	-.03246	
7								
71-06-19	1511	38.29						
1	KCH	21	132.0	137.4	5.92	-.16485	-.11532	
2	SHL	10	102.5	109.4	5.56	-.00785	+.04168	
3	SKW	12	87.9	95.9	53.3	-.05760	-.00807	
4	PWA	10	10.7	39.8	10.0	-.00825	+.04128	
5	PMS	68	37.5	53.6	68.0	-.03198	+.01755	
6	PMR	45	35.3	52.1	45.0	-.02669	+.02284	
7	SCM	11	133.8	139.2	4.40			
71-07-25	0602	38.26						
1	KCH	20	134.6	139.9	5.63	-.19505	-.17012	
2	SHL	30	105.6	112.3	16.7	+.01050	+.03543	
3	TLN	34	98.7	105.7	9.58	+.02819	+.03512	
4	SKW	4	(91.0)	98.7	17.8	+.00451	+.02944	
5	PWA	37	11.4	39.9	37	-.00617	+.01876	
6	PMS	52	40.3	55.6	52	-.01181	+.01312	
7	PMR	31	29.7	48.4	31	-.00471	+.02022	
8	SCM	(52)	127.6	133.2	20.8			

Table 3-4b

i	STA	Δ(km)	P(mm)	r(km)	A(nm)	$\sigma_{ni}(km^{-1})$	$\sigma_{ni} - \langle\sigma_{ni}\rangle$	$\langle\sigma_{ni} - \langle\sigma_{ni}\rangle\rangle$
71-06-20	1534	81.25						
1	SHL	51.1	13	96.0	8.3	+.00042	+.00765	+.00325
2	KCH	70.7	14	167.7	4.5	+.00974	+.01697	+.00718
3	PWA	85.9	38	118.2	38	-.01237	-.00514	-.00635
4	PMS	106.7	32	134.1	32	-.01261	-.00538	-.00161
5	PMR	124.6	33	148.8	33	-.01507	-.00784	-.00197
6	SCM	222.1	22	236.5	8.8			+.00105
71-06-21	0550	83.73						
1	SKW	11.5	27	82.1	137.2	-.01418	-.00695	
2	SHL	14.4	40	82.5	25.4	-.00731	-.00008	
3	KCH	37.3	31	89.4	21.4	-.00682	+.00041	
4	PWA	88.2	89	119.9	89.0	-.01467	-.00744	
5	PMR	126.4	13	150.3	13.0	-.00636	+.00067	
6	PMS	129.9	7	153.2	7.0	-.00292	+.00431	
7	SCM	211.0	27	226.1	10.8	-.00927	-.00204	
8	PAX	317.8	15	328.0	4.2			
71-07-13	0326	101.23						
1	TLN	31.7	(38)	87.2	12.3	-.00511	+.00212	
2	SHL	55.9	18	98.6	11.4	-.00504	+.00219	
3	KCH	68.5	20	106.3	6.4	-.00305	+.00418	
4	PWA	103.5	81	131.6	81.0	-.03710	-.00648	
5	PMS	122.8	35	147.2	35.0	-.01099	-.00376	
6	PMR	142.6	10	164.1	10.0	-.00598	+.00125	
7	SCM	239.7	9	253.1	3.6	-.00203	+.00520	
8	PAX	368.3	10	377.1	2.8			

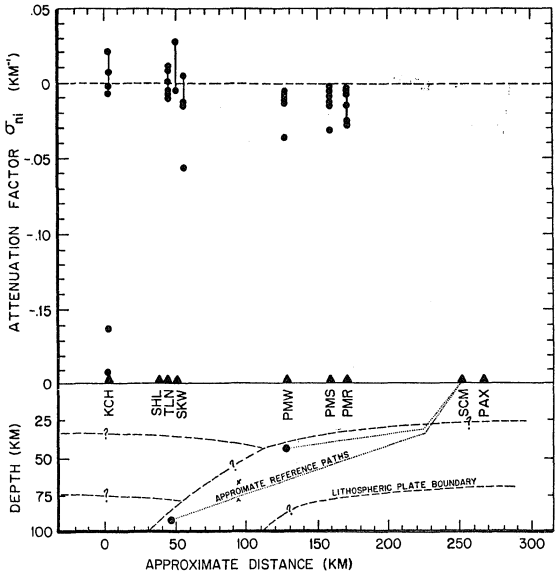

Figure 3-22. Possible attenuation of local P phases. See text for a description of the attenuation factors plotted in the upper portion of this figure. The solid circles in the lower portion mark the approximate location of the two groups of three hypocenters used in the computation of the attenuation factors. This cross section is oriented ENE-WSW as was the one shown in Figure 3-20b.

either anomalous attenuation along the paths to the Skwentna stations or magnification along the reference path to SCM. Because most of the other σ_{ni}'s indicate that the reference path is in an attenuating medium the positive σ_{ni}'s in the Skwentna region might be argued to represent anomalous attenuation along the ray paths to stations in this region. However, the scatter in the data is so large and the number of events suitable for this analysis so small that it is questionable at best to attach significance to the apparent trend toward more positive σ_{ni}'s in the Skwentna region.

Teleseismic P-phases

The third method used was to study the attenuation of teleseismic P-phases. Since this method is critically dependent on the magnification assumed for each station, a rather extensive check of the calibration of each station was made. This calibration analysis is presented in Appendix III. The fortuitous circumstance that the three different kinds of seismograph systems calibrated had representative stations operating in close proximity during part of 1971 provided the opportunity to make a direct comparison of derived teleseismic ground amplitudes for these different systems. This situation allows the ultimate test of the calibration process. The three stations were PJD, GLM and GIL (see Table 2-1). PJD represents the standard University of Alaska station:

Geotech 18300 seismometer and Electrotech amplifier. GLM is a borehole station: Ranger SD-215 seismometer and Sandia amplifier. GIL is a standard NOAA station: Geotech 18300 seismometer and Geotech amplifier. These stations are all located on Birch Creek schist within a circle of radius 7 kilometers.

Trace amplitudes and periods were scaled from the Develocorder records for three well recorded teleseisms which occurred during June and July, 1971. Each of these events was about 90 degrees distant so the rays arrived almost vertically. The periods were converted to frequency and averaged for each event. The harmonic system magnification for each station at this average frequency was used to reduce the trace amplitudes to ground amplitudes. The average frequency was used since the periods were determined only for the half cycle for each event from which the amplitude was read and therefore were subject to some variation. Because the stations were so similarly situated and within a few wavelengths of each other, it was regarded as a reasonable assumption that the period of the teleseismic wave should be the same at each station.

These calculations are summarized in Table 3-5. In the worst case the standard deviation about the average ground amplitude for a given event is 14 percent of the average value. This is good agreement and indicates that the station calibrations are reliable enough to proceed with this investigation.

Table 3-5

Check of system calibration using teleseisms. Column headings: STA, station designator code, H stands for high gain trace; T, peak-to-peak trace amplitude; P, period; f, frequency; M($\bar{f}$), system magnification at $\bar{f}$; A(nm), peak-to-peak ground displacement in nanometers; R, ratio of max. A to min. A; D, deviation expressed as percentage of <A>.

STA	T(mm)	P(s)	f(5')	M($\bar{f}$)	A(nm)	R	D
71-06-19 1734							
GIL	22	.90	1.11	560	39.3		
GLM-H	75	.90	1.11	1900	39.4		
PJD-H	37	.70	1.43	950	38.9		
			<1.22>		39.22 ± .2	1.01	.51%
71-06-22 1135							
GIL	41	.76	1.32	560	73.2		
GLM-H	115	.84	1.19	1900	60.5		
PJD-H	60	.90	1.11	950	63.2		
			<1.21>		<65.63>± 5.5	1.21	8.5%
71-07-19 1500							
GIL	44	.68	1.47	860	51.2		
GLM-H	115	.60	1.67	2850	40.4		
PJD-H	85	.64	1.56	1500	56.7		
			<1.57>		<49.43>± 6.8	1.40	14%

Table 3-6 expands the data in 3-5 to other stations. The average ground amplitude over all of the stations for each event was used to normalize the amplitudes to the 71-06-22 event. Then these normalized amplitudes were averaged by region, viz: Skwentna, Palmer and Gilmore. These averages show that the Skwentna region is characterized by lower amplitudes than Gilmore and that Palmer has higher amplitudes. These relationships are illustrated in Figure 3-23 and are interpreted by regarding the Gilmore region as typical of an average continental crust-mantle structure whereas Skwentna is considered to be above a low Q region with incipient partial melting but not enough to attenuate the S-phase relative to the P-phase, and Palmer is thought to be above the zone where the dipping slab predominates and the rays travel through a region of higher-than-average Q.

Focal mechanisms

An attempt was made to study the relationship of focal mechanisms to source region using small earthquakes and local stations. This attempt failed because no reliable solutions for focal mechanism were obtained. For the record, a brief description of the procedure used follows.

First a polarity check was made to determine whether or not all of the stations were set up so that compressional (dilatational) waves gave upward (downward) first motion on the Develocorder

Table 3-6

Attenuation of teleseismic P-waves. Column headings: STA, station designator code; Mag., system magnification at 1Hz; Av, peak-to-peak trace amplitude on viewer; Ag, peak-to-peak ground displacement in nanometer; <Ag>, average Ag over stations in the Skwenta (KCH, SHL), Palmer (PWA, PMS, PMR) and Gilmore (GIL, GLM, PJD) regions respectively.

STA	Mag.	71-06-19 1734		71-06-22 1135		71-07-19 1500	
	1Hz	Av(mm)	Ag(nm)	Av(mm)	Ag(nm)	Av(mm)	Ag(nm)
KCH	225	7	31	11.5	51	18	80
SHL	115	9	78	5.2	45	8	70
PWA	200	22	110	23	115	20	100
PMS	200	14	70	22	110	---	---
PMR	200	13	65	20	100	23	115
GIL	400	22	55	41	103	44	110
GLM	1340	75	56	115	86	115	86
PJD	686	37	54	60	87	85	124
			<64.9>		<87.1>		<97.9>
		<Ag>		<Ag>		<Ag>	
SKWENTNA		54.5 ± 23.5		48.0 ± 3.0		75.0 ± 5	
PALMER		81.7 ± 20.1		108.3 ± 6.2		107.5 ± 7.5	
GILMORE		55.0 ± 0.8		92.0 ± 7.8		106.6 ± 15.7	

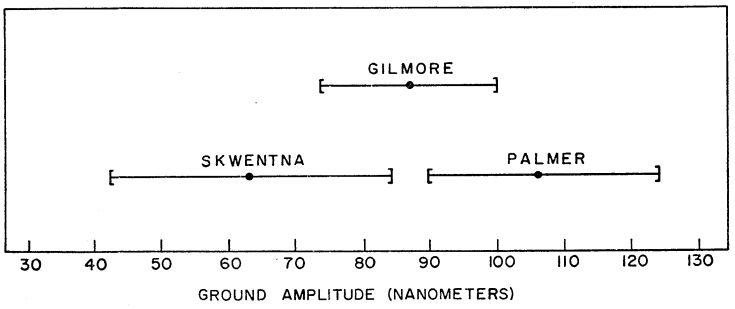

Figure 3-23. Possible attenuation of teleseismic P phases. Shown are the normalized regional average ground amplitudes for the Skwentna, Palmer, and Gilmore regions. The events averaged were all approximately 90° distant.

screen. This check is summarized in Table 3-7 which gives first motion readings for the 9 teleseims which were assigned at least three impulsive arrivals on either the Skwentna or Palmer reading sheets for June, 1971. All emergent readings were omitted from this table. For all 9 events there is a clear consensus in the first motion readings. For six of the events there are no exceptions to the consensus. For the worst case (event # 6) there are two exceptions out of seven readings. The consensus motion may therefore be assumed to represent the actual ground motion and any readings in disagreement with the consensus assumed in error. Since no station listed in Table 3-7 is seen to yield consistently erroneous readings it may be concluded that none of them had reversed polarity during June, 1971. However, for the six stations listed in Table 3-7 which are in the Skwentna-Palmer vicinity four out of 34 of the readings are in error, about 12%. This error rate (which is likely to be higher for local events) is too high for good focal mechanism solutions. The possible reasons for the erroneous readings in descending order of probability are thought to be: (1) weak arrival causing first motion to be lost in the noise, (2) phase reversal during reflection, (3) mistaken reading and (4) station across quadrant boundary.

Two kinds of solution were attempted: (1) group solutions where many events occurred in a small volume and (2) individual

Table 3-7

Analysis of first-motion picks on seismograms from nine teleseisms. Stations ADK, GIL, GMA, KDC, NIK, PMR, PMS, PWA, SIT and SMY were recorded by NOAA in Palmer; KCH, SHL and SKW were recorded by the University of Alaska in Skwentna. Compressions (up on record) are denoted by C and dilatations (down) by D. The asterisks mark picks which disagreed with the majority for a given event.

Event			Station and First Motion												Totals
#	Date	Time	ADK	GIL	GMA	KCH	KDC	NIK	PMR	PMS	PWA	SHL	SIT	SKW	SMY	
1	71-06-11	1307		D	D	D						D		D		5/0
2	71-06-11	1403				C						C		C	C	4/0
3	71-06-12	2251	D	D	D		D	D	D	D	D					8/0
4	71-06-15	2216		C	C		C		C	C	C	D*				6/1
5	71-06-19	1734		C	C	C	C		C		C	C				7/0
6	71-06-22	1135		C	C	D*			C	C	C	D*				5/2
7	71-06-24	1403		C	C		C		C	C	C	C	C	D*		8/1
8	71-06-27	1435		C	C		C		C	C	C	C				7/0
9	71-06-27	1803		C	C				C	C	C					5/0
agree/disagree			1/0	8/0	8/0	3/1	5/0	1/0	7/0	6/0	7/0	5/2	1/0	2/1	1/0	55/4

solutions where one event was well recorded by many stations. In all cases first motion data were restricted to those determined to be from impulsive arrivals. The azimuth and dip angle for the ray at the focal sphere were calculated using HYPO71. The parameters of the events used in the analysis are given in Table 3-8. These events, all from HYPO71 Skwentna data set, were divided into 5 classes based on location (last column, Table 3-8): The corresponding focal sphere projections are shown in Figures 3-24 and 3-25.

The first class (Figure 3-24a) consists of six shallow events in the Palmer vicinity selected by the following criteria: (1) depth between 35 and 50 kilometers, (2) latitude between 61°31' and 61°45'N, (3) longitude between 149° and 150°W and (4) quality rating (Q in HYPO71) equal to "C". There is a strong tendency for the dilatational rays to plot toward the center of the projection, however, this distribution can be interpreted as either dip-slip on one of a complementary set of planes striking N12°E or right-lateral strike-slip along N45°W. The three-dimensional pattern of seismicity from which these events were selected mildly suggests that the solution implying dip-slip to the west at 50° along a plane striking at N12°E is preferred. This kind of fault might be explained in the way Kanamori (1971) argues for tensional normal faults at the sharp bend of the subducted plate as a result of gravity induced "slumping" of the

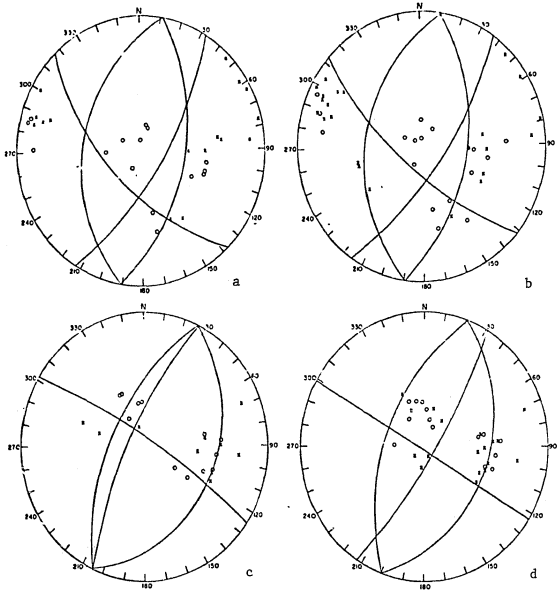

Figure 3-24. Composite upper hemispheric projections of first motions at local stations from four sets of earthquakes. See text for descriptions of these events. Crosses represent compressions and circles, dilatations.

leading edge. If this kind of faulting is indeed occurring its spatial relationship to the Cook Inlet graben is suggestive of cause and effect.

The second class of events (Figure 3-24b) was selected exactly as was the first except that the quality rating criterion was changed to the requirement that the ratio of impulsive arrivals to total arrivals be at least six sevenths and that the number of stations recording the events ("NS", column 8, Table 3-8) be at least seven. There is no essential change from the pattern shown in Figure 3-24a. The ratio of compressional to dilatational points in the western portion of the projection is strengthened but this does not enhance any of the possible interpretations.

The third class (Figure 3-24c) consisted of deeper events in the Skwentna vicinity selected by the following criteria: (1) depth between 70 and 85 kilometers, (2) latitude between 61°30' and 62°N and (3) longitude between 150°30' and 151°30'W. This selection volume is approximately 55 kilometers square and 15 kilometers deep. The projection could be interpreted in the dip-slip sense as before except that the dip angle would be about 30 degrees and is too shallow to represent normal faulting. It is, of course, tempting, at this depth, to begin to think about underthrusting, but the relative motion implied in this figure is in the wrong direction. An interesting possibility is

right-lateral strike-slip along an almost vertical plane at N60°W. This would be consistent with relative motion between the Kenai and McKinley blocks along the Yentna lineament in which the Kenai block moves with the Pacific plate and the McKinley block remains relatively fixed to the North American plate.

The fourth class (Figure 3-24d) contains events in the same vicinity as the third, but which are deeper. They were picked by the following criteria: (1) depth between 80 and 102 kilometers, (2) latitude between 61°21' and 62°05'N and (3) longitude between 151°10' and 151°50'W. This class can be interpreted in the same manner as was the third class: Right-lateral strike-slip along a vertical plane at N60°W, consistent with relative motion between the Kenai and McKinley blocks. This solution is less satisfactory than the last since the percentage of rays plotted in exception to the inferred motion increased from 25 to 34.

The four individual solutions which make up the fifth class of solutions are shown in Figure 3-25. In general there are fewer projected ray paths on which to base these solutions so they are even more speculative than were those in Figure 3-24. The June 17 event was 48 kilometers deep on the Yentna lineament and its solution (Figure 3-25a) is consistent with the focal mechanism inferred above for the third and fourth classes of events. The July 27 event was 77 kilometers deep and also on

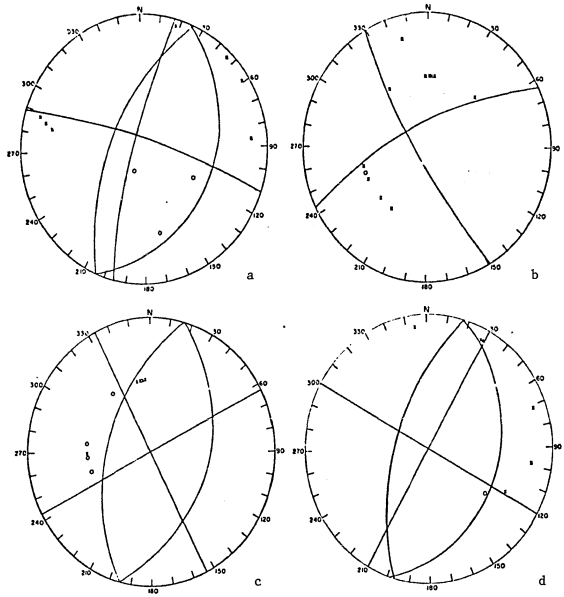

Figure 3-25. Focal sphere projections of first motions at local stations for four individual earthquakes. See text for descriptions of these events. Figures 25 a and d are upper-hemisphere projections, while b and c are lower-hemisphere projections. Symbols are the same as the previous figure.

the Yentna lineament. Its solution (Figure 3-25d), while very weak, is also consistent with right-lateral motion along the lineament.

CHAPTER IV

DISCUSSION AND CONCLUSION

The principle result of this study is the delineation of the Benioff zone in the upper Cook Inlet-Mount McKinley region of Alaska. The contours in Figure 4-1 for this region represent the depth in kilometers to the Benioff zone as determined in Chapter III. The other information in the figure is given for comparison with this determination of the Benioff zone geometry.

One of the major features of the contours in Figure 4-1 is their abrupt termination just south of Fairbanks. The heavy line marking this boundary and trending out of the figure to the southeast, subparallel to the Alaska panhandle coastline, is a segment of a small circle about a pole at 51.5°N and 49.0°W. This pole is well within the error circle about Morgan's pole (see page 5) for the relative motion between the Pacific and North American plates. The NOAA seismicity data in Figure 4-2 shows that this line generally marks the seismic zone which parallels the southeast Alaska coast and also marks the northeast end of the Aleutian arc seismic zone. It is therefore a reasonably good representation of the Pacific-North American plate boundary. One can conclude then, that the termination of the Benioff zone just south of Fairbanks delineates the northeast corner of the Pacific plate.

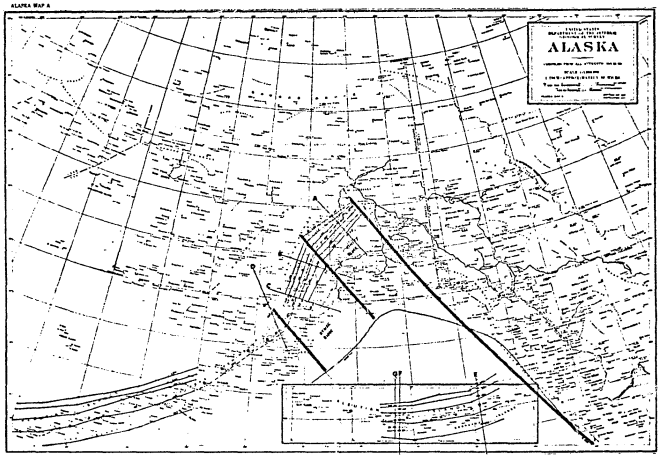

Figure 4-1. Benioff zone depth contours. The contours in the Cook Inlet--Mt. McKinley region are from Figure 3-14, those in the Aleutians are from Jacob (1972). The heavy black lines are segments of a small circle about Morgan's pole as discussed in the text. The lines labeled A,B, etc. show the location of the corresponding cross sections given

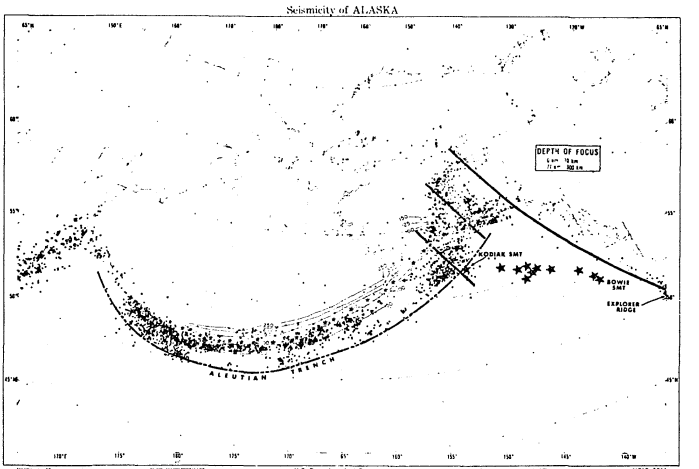

Figure 4-2. Benioff zone depth contours and seismicity of Alaska as determined by the NEIC. Contours and heavy black lines are shown in Figure 4-1.

It might be argued that one should have used a more recent determination of the relative motion pole, e.g.: Minster et al's (1974) pole at 50.9°N, 66.3°W. This pole was considered and it was found that small circles about it did not match the San Andreas and Queen Charlotte transform boundaries as well as did those about Morgan's pole. This is perhaps not too surprising since Morgan's pole was determined from a least-squares fit to these particular boundaries, while Minster et al's was derived from a global best fit.

Another striking feature of these contours is the thirty degree bend which occurs approximately along the Yentna River valley. This valley almost transects the Alaska Range and shows prominently on Earth Resources Technology Satellite (ERTS) imagery of the region and is therefore referred to as the Yentna lineament. The heavy line segment which marks the bend in the contours in Figure 4-1 was constructed along the Yentna lineament and parallel to the heavy line marking the plate boundaries and delineates the McKinley block. This line is also shown on Figure 4-2. The McKinley block region is seen to contain the Prince William Sound aftershock zone of the March 1964 Great Alaska Earthquake.

A second heavy line segment is shown parallel to the first. It is constructed through the forty degree bend in the volcano trend at Cape Douglas and it is speculated that the Benioff zone

contours undergo a similar bend along this line. The region of the Pacific Plate delineated by these two line segments is called the Kenai Block. The Benioff zone contours in this region are subparallel to the volcano trend line which approximates the 115 kilometer depth contour (when this set of contours is slightly adjusted to match cross-section B as discussed below).

The other contour lines shown in Figure 4-1 and in the insert are from Jacob (1972) who determined them primarily from NOAA data. Also shown in this figure are several cross-section lines labeled A through G. See Figure 4-3 for cross-sections C through G. In every case except A (no volcanoes) and D (offset due to projection used) the 100 kilometer depth contour is determined to lie along or slightly south of the volcano trend line. For this reason Jacob's 100 kilometer depth contour was speculatively extended subparallel to the volcano trend line and through the 100 kilometer depth marks at sections C, B and A. This line is dashed in Figure 4-1. Based on the consistency of the relationship of the 100 kilometer depth contour to the volcano trend line and on the greater reliability of the data used in constructing cross-sections A and B (Figures 3-15 and 3-16) at this depth it is suggested that the contour lines in the McKinley and Kenai regions should be shifted about 20 kilometers to the southeast so that the 100 kilometer depth contour is congruent with the dashed line in these regions. This argument

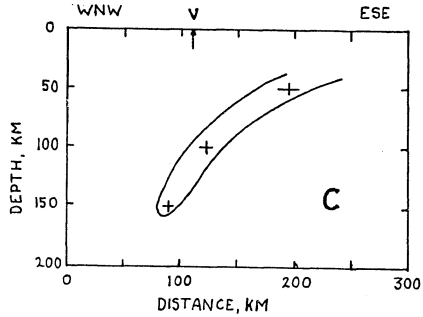

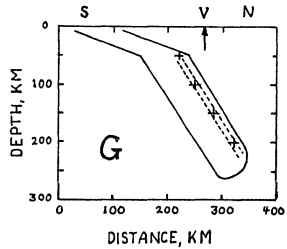

Figure 4-3 C&G. Caption following.

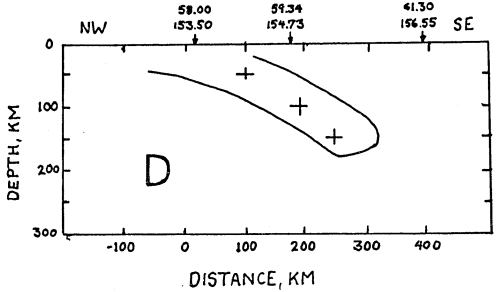

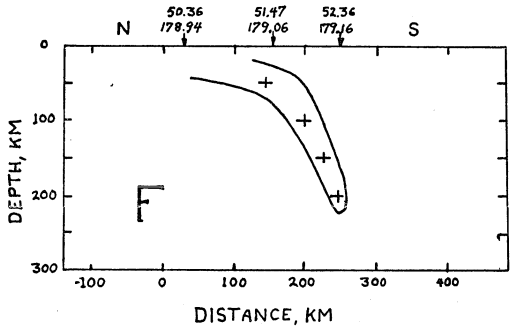

Figure 4-3 D&F. Caption following.

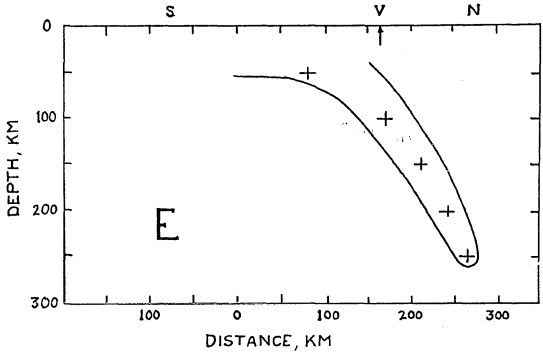

Figure 4-3. Various cross sections through the Aleutian-Alaskan Benioff zone. The crosses inside the Benioff zone envelopes mark the contour locations picked for Figure 4-1.

A--see Figure 3-17e, this study

B--see Figure 3-17a, this study

C--from Figure 8, Lahr and Page (1972)

D--from Figure 7, Willis, et al. (1972)

F--from Figure 8, Willis, et al. (1972)

E--from Figure 82, LePichon, Francheteau, and Bonnin (1973) (after Grow (1972))

G--from Figure 2, Engdahl (1973)

applies less strongly in the McKinley region since the A section is less well defined than the B section and since the 150 and 125 kilometer depth contours match section A quite well. The consequence of shifting the Kenai contours and not the McKinley contours is to exaggerate the apparent mismatch of the contours at the Yentna lineament. This, in turn, would suggest that the McKinley and Kenai blocks are indeed independent as indicated by two of the possible focal mechanisms for the two events on the Yentna lineament discussed in Chapter III.

The last and perhaps most interesting feature of the contours shown in Figure 4-1 is the lack of volcanoes along the McKinley contours. The Skwentna network was situated beyond the end of the volcano line, just north of Mount Spurr. The attenuation of teleseismic P-waves at this network coupled with the lack of a relative attenuation of S-waves with respect to P-waves suggests that this region is marginal in the development of a volcanogenic zone at about the 115 kilometer depth level. A tentative explanation for the fading of the volcanogenic zone at this point along the arc-trench system might lie in the geometry revealed in Figure 1-2 This figure shows that at this point the divergence of the volcano trend line and the trench approaches 400 kilometers. If the suggestions of Davies and Berg (1973) and Plafker (1969) are correct, then for about 300 kilometers of this distance the plate plunges at a very shallow angle attaining

the more typical Benioff dip angle in the vicinity of the 40 kilometer depth contour. Perhaps the trench sediments and water are scraped off, never attaining the 100 kilometer depths required to form the andecitic magma.

Though the Benioff zone seismicity has been the main focus of this study it should be noted in closing that there are other interesting features of the seismicity of south-central Alaska shown in the cross-sections given in Chapter III. For example the Prince William Sound earthquakes can be seen in sections 7d, 7e and 8d; the Castle Mountain earthquakes in 9a and 9b; and the Kantishna earthquakes in 8e, 8f, 9a, and 9b. The latter cross-sections show that the Kantishna events probably occur on a nearly vertical plane striking approximately N45°E which attains at least 20 kilometers depth and 100 kilometers length. It would be quite interesting to detail the relationship of this group of earthquakes to the plate geometry determined in this study.

In conclusion it has been shown that the Pacific-North American plate boundary, the Queen Charlotte transform, continues into interior Alaska to a point about 75 kilometers south of Fairbanks; that the Pacific plate begins a relatively shallow plunge under the crustal material of south-central Alaska at the Aleutian trench but does not begin the more typical Benioff zone dip angle of about 45 degrees until it has moved about 400

kilometers northwest into the vicinity of the Cook Inlet-Susitna River lowlands; that there is a thirty degree bend in the Benioff zone depth contours at the Yentna lineament which may mark the boundary between the McKinley and Kenai blocks of the Pacific plate; and that these blocks may move independently of one another.

APPENDIX I

Following is a chronological listing of the earthquakes located during the course of this study. The data is given in the order: Year, month, day, hour, minute, seconds, rms residual arrival time, number of stations used in location, lattitude (N), longitude (W), and depth (km). The first list gives the events from the Skwentna data set located by EPICENTR-II. The second gives those located by HYPO71. The third list gives events from the University of Alaska data set located by HYPO71.

71	6	4	04747.1	0.6	8	62.10	148.03	15
71	6	4	34821.1	1.1	13	59.93	153.45	100
71	6	4	52926.3	0.3	7	62.16	150.17	15
71	6	4	71148.4	0.6	8	61.70	149.65	50
71	6	4	9 354.4	0.2	7	61.17	147.29	15
71	6	4	1325 4.1	0.9	16	60.93	151.00	0
71	6	4	161614.9	0.2	6	60.47	152.06	250
71	6	4	1648 5.7	0.3	5	60.15	152.12	125
71	6	4	203747.4	0.5	9	61.56	150.85	50
71	6	5	045 8.9	0.2	6	60.80	150.80	40
71	6	5	13720.0	0.5	10	61.58	150.92	50
71	6	5	143 1.9	0.4	10	63.07	151.48	0
71	6	5	34138.1	0.9	10	64.61	145.93	0
71	6	5	63934.8	0.6	13	61.64	151.31	75
71	6	5	811 5.4	0.2	8	62.34	150.49	15
71	6	5	84545.5	0.1	5	61.92	151.44	75
71	6	5	133448.9	0.5	10	61.44	147.64	15
71	6	5	152223.6	0.6	6	60.72	151.76	100
71	6	5	212434.7	0.1	4	62.12	150.20	0
71	6	6	121722.1	0.5	7	61.00	150.92	0
71	6	6	1355 0.8	2.8	6	64.48	154.62	150
71	6	6	14 210.0	0.5	5	61.21	151.22	200
71	6	6	144345.2	0.5	17	59.69	152.54	100
71	6	6	15 433.4	0.0	3	61.36	149.75	0
71	6	6	152341.1	0.5	12	59.58	152.28	15
71	6	6	16 2 1.3	0.6	10	61.05	147.55	15
71	6	6	1620 1.7	0.5	13	62.12	149.52	15
71	6	7	04246.1	0.0	3	62.42	151.81	0
71	6	7	52157.8	0.4	9	59.76	155.28	75
71	6	7	62650.4	0.3	8	62.46	148.14	15
71	6	7	74957.6	0.4	12	62.57	149.49	15
71	6	7	91515.4	0.6	12	60.54	151.90	50
71	6	7	135434.9	0.8	6	60.62	147.49	0
71	6	7	163632.0	0.9	11	60.70	146.92	0
71	6	7	18 148.3	0.5	16	62.15	149.38	15
71	6	7	234635.4	0.6	11	62.38	149.65	200
71	6	8	04856.1	0.0	3	61.71	149.49	0
71	6	8	5 0 1.1	0.6	11	60.12	152.54	75
71	6	8	73224.2	0.0	3	61.33	149.89	0
71	6	8	74820.9	0.0	3	61.27	150.24	15
71	6	8	75258.8	0.6	8	61.14	149.23	15
71	6	8	144838.0	0.3	5	61.44	152.07	0
71	6	8	155232.2	0.8	8	59.74	153.08	15
71	6	9	04542.9	2.0	8	63.19	149.50	150
71	6	9	2 934.8	0.4	9	62.53	149.92	15
71	6	9	45628.0	0.0	3	61.64	149.74	15
71	6	9	5 546.2	0.0	3	61.52	149.79	0
71	6	9	53628.0	0.0	3	61.57	150.18	0
71	6	9	81159.2	0.7	13	62.02	151.02	75
71	6	9	191015.3	0.3	6	62.12	149.32	15

71	6	10	4	141.9	0.0	3	61.51	149.91	15
71	6	10	54227.7		0.5	10	58.46	152.36	0
71	6	10	91752.8		0.0	3	61.71	149.67	0
71	6	10	1159	3.0	0.4	7	61.95	148.00	0
71	6	10	134437.3		0.3	7	61.78	149.76	40
71	6	10	1458	5.0	0.7	12	59.34	152.21	100
71	6	10	16	048.9	0.5	7	61.47	149.74	250
71	6	10	164518.1		0.4	12	62.56	149.58	200
71	6	10	165516.0		0.4	12	62.59	151.49	100
71	6	10	17	419.7	0.4	7	62.28	149.40	15
71	6	10	23	746.4	0.0	3	62.29	151.62	0
71	6	11	8	128.3	0.4	9	59.98	147.08	0
71	6	11	115431.0		0.2	6	61.71	149.14	15
71	6	11	164213.1		0.3	7	60.32	150.76	40
71	6	11	17	816.7	0.3	6	61.39	150.05	40
71	6	11	171211.0		0.2	6	61.41	150.64	40
71	6	11	233650.9		0.0	4	62.10	149.32	0
71	6	12	05115.0		0.4	6	62.35	150.45	0
71	6	12	35610.5		0.5	15	60.73	151.57	50
71	6	12	540	2.5	0.4	10	61.46	146.11	15
71	6	12	81627.1		0.6	13	62.89	151.19	100
71	6	12	111823.1		0.6	15	59.95	152.48	75
71	6	12	13	156.8	0.5	7	61.54	149.91	40
71	6	12	183610.8		0.4	5	61.64	149.61	40
71	6	12	194542.1		0.5	7	61.04	150.82	0
71	6	12	2320	8.9	0.5	9	61.48	146.13	15
71	6	13	05640.8		0.4	6	60.89	148.01	0
71	6	13	327	9.6	0.6	9	61.66	150.15	40
71	6	13	449	7.9	0.3	5	60.27	148.45	0
71	6	13	45549.0		0.5	11	60.05	151.68	15
71	6	13	122958.6		0.9	9	60.73	151.14	0
71	6	13	194044.4		0.1	4	61.25	150.42	50
71	6	13	2350	8.4	0.1	4	61.46	150.94	15
71	6	14	219	0.2	0.6	9	61.63	151.70	75
71	6	14	3	225.8	0.6	8	61.06	147.09	15
71	6	14	32752.9		0.5	5	61.70	149.74	40
71	6	14	454	9.4	0.5	7	61.17	150.72	0
71	6	14	7	631.8	0.3	5	61.88	149.53	40
71	6	14	16	231.5	0.6	14	60.06	152.58	75
71	6	14	185130.9		1.4	8	60.75	151.28	0
71	6	14	202827.8		0.3	6	60.91	151.35	75
71	6	14	213354.1		0.4	9	62.40	151.38	100
71	6	15	44144.2		0.4	11	62.91	148.16	40
71	6	15	62013.1		0.0	4	61.34	150.39	40
71	6	15	8	5 8.9	0.5	11	61.53	146.46	15
71	6	15	92545.9		0.6	11	65.15	156.83	100
71	6	15	155234.5		0.2	6	61.90	149.97	40
71	6	16	22649.5		0.2	6	61.97	149.64	40
71	6	16	332	2.8	0.6	6	61.47	150.34	15
71	6	16	61635.8		0.5	7	61.86	149.53	15

71	6	16	62344.6	0.5	11	61.20	152.59	125
71	6	16	1033	8.4	0.3	14	62.54	151.16	75
71	6	16	1041	7.8	0.8	8	61.54	149.80	15
71	6	16	124123.8		0.2	7	60.09	147.14	15
71	6	16	162219.0		0.2	5	61.62	150.72	50
71	6	16	182122.6		2.1	13	62.53	152.14	15
71	6	16	1843	6.6	0.8	8	61.54	149.98	40
71	6	17	33020.5		0.0	5	61.04	148.83	0
71	6	17	35816.6		0.6	10	61.06	152.21	100
71	6	17	42642.8		0.3	6	60.78	148.13	0
71	6	17	82431.7		0.7	12	59.84	153.21	100
71	6	17	84634.9		0.3	6	61.53	151.52	75
71	6	17	165140.7		0.3	7	61.62	149.78	50
71	6	17	21 041.1		1.1	17	61.90	149.65	15
71	6	17	225949.4		0.5	15	60.02	152.89	100
71	6	17	23 656.0		0.7	12	63.20	151.01	150
71	6	18	84421.6		0.8	11	59.46	152.90	15
71	6	18	95023.2		0.1	5	63.11	150.60	125
71	6	18	125148.7		0.8	12	63.53	146.89	0
71	6	18	1954	3.6	0.8	12	63.53	146.89	0
71	6	19	23918.0		0.2	5	60.81	150.54	15
71	6	19	101228.6		0.4	8	61.39	148.69	15
71	6	19	151026.9		0.6	7	61.53	149.76	250
71	6	19	171749.6		0.2	10	60.88	151.52	50
71	6	19	22 141.1		0.4	10	61.37	147.66	15
71	6	19	232841.9		0.8	4	58.75	150.16	200
71	6	20	22438.7		0.9	10	63.53	146.98	0
71	6	20	453	2.3	0.8	8	61.37	147.21	250
71	6	20	112545.7		0.2	6	61.78	149.09	15
71	6	20	1535	2.2	0.4	7	61.47	151.44	50
71	6	20	154726.5		0.5	11	60.15	151.52	15
71	6	20	163254.3		0.6	13	59.86	151.84	50
71	6	21	21751.9		0.4	12	63.77	149.18	100
71	6	21	536	5.4	0.3	6	61.93	150.66	50
71	6	21	55043.7		0.2	8	62.07	151.31	75
71	6	21	104331.1		0.8	19	60.04	152.08	100
71	6	21	11 622.6		0.5	10	63.20	150.51	125
71	6	21	1226	4.0	0.0	3	61.48	149.83	0
71	6	22	23740.7		0.5	7	60.99	150.94	0
71	6	22	42554.3		0.4	8	59.46	152.90	125
71	6	22	62057.6		0.2	4	64.20	149.85	150
71	6	22	131748.7		0.3	9	63.67	149.81	150
71	6	22	214231.6		0.9	8	61.53	150.39	40
71	6	22	231426.2		0.5	7	61.61	150.33	40
71	6	22	232717.3		0.6	14	65.76	150.01	40
71	6	23	22235.7		1.0	16	58.29	151.99	15
71	6	23	72031.1		0.6	11	59.69	151.88	50
71	6	23	93546.2		0.2	4	61.92	151.29	0
71	6	23	121119.8		0.3	4	61.71	149.51	15
71	6	24	41956.3		0.2	12	63.13	149.80	100

71	6	24	63425.3	C.1	5	60.67	147.76	15
71	6	24	121715.6	C.5	11	59.93	142.42	15
71	6	24	134024.9	C.3	9	64.25	147.80	0
71	6	24	161720.5	C.3	7	63.02	151.15	150
71	6	24	175048.5	0.5	11	63.12	149.59	0
71	6	25	353 8.3	C.6	6	61.63	149.57	250
71	6	25	42121.5	C.1	5	60.77	152.27	0
71	6	25	42654.2	C.4	6	61.57	151.02	200
71	6	25	5 738.1	C.5	7	61.49	149.93	250
71	6	25	55532.9	C.9	9	61.43	150.02	40
71	6	25	102342.4	C.4	7	61.41	147.75	0
71	6	25	103039.7	0.0	3	62.58	150.82	0
71	6	25	12 216.0	0.8	7	59.95	152.53	15
71	6	25	124348.0	C.4	8	64.11	146.69	0
71	6	25	15 320.6	C.1	4	62.75	150.87	150
71	6	25	171413.9	0.4	5	64.29	146.74	0
71	6	25	1912 1.3	0.1	3	61.48	149.71	0
71	6	25	21 0 4.7	C.6	13	62.35	151.51	100
71	6	26	02427.0	0.2	5	58.34	150.86	0
71	6	26	35538.4	C.0	3	61.77	148.77	0
71	6	26	73635.9	C.4	6	60.80	152.12	0
71	6	26	836 3.4	C.1	5	63.00	151.08	150
71	6	26	11 226.4	C.3	6	62.09	151.34	100
71	6	26	1358 2.4	1.2	5	63.36	148.10	150
71	6	26	20 431.6	C.8	17	60.31	152.39	75
71	6	26	222723.5	C.5	7	61.72	149.14	15
71	6	26	234940.9	C.5	9	63.12	150.33	0
71	6	27	03750.4	C.7	18	60.10	152.98	100
71	6	27	10 022.1	C.1	4	61.42	149.74	200
71	6	27	102936.6	0.0	4	64.58	148.98	50
71	6	27	123133.3	C.6	4	61.39	150.33	0
71	6	27	124549.2	0.2	4	63.61	149.93	125
71	6	27	145248.9	0.2	6	58.93	153.17	200
71	6	28	1639 6.8	4.5	17	61.32	149.41	100
71	6	28	193542.7	2.0	6	61.80	148.84	15
71	6	28	232516.6	C.1	5	61.26	149.17	0
71	6	29	14139.2	C.3	5	61.40	149.35	15
71	6	29	2323C.6	C.3	4	61.66	149.52	15
71	6	29	3 727.6	C.7	8	61.84	145.61	40
71	6	29	52638.6	1.3	6	61.40	149.56	15
71	6	29	52638.2	C.7	5	61.48	149.66	15
71	6	29	71033.5	C.0	3	61.25	150.07	15
71	6	29	152234.2	C.0	4	61.71	149.42	200
71	6	29	155424.0	3.6	10	60.18	149.88	200
71	6	29	184820.5	5.5	14	62.50	147.92	200
71	6	29	2230 5.4	1.1	9	61.86	151.22	50
71	6	30	54417.7	C.5	7	61.22	147.63	0
71	6	30	620 3.5	1.1	13	62.86	156.51	75
71	6	30	155939.7	C.5	9	63.31	151.23	15
71	6	30	234513.5	0.4	10	62.57	149.15	200

71	7	1	9 836.7	C.1	6	64.00	146.74	40
71	7	1	14849.5	1.3	7	63.27	151.07	0
71	7	1	21958.7	C.C	4	61.62	150.53	40
71	7	1	6 619.9	0.4	9	62.87	151.54	150
71	7	1	61517.8	C.C	3	61.53	149.68	0
71	7	1	620 6.8	0.C	3	61.97	148.97	0
71	7	1	7 338.3	C.2	4	61.57	148.72	0
71	7	1	83920.2	C.8	8	62.21	151.24	75
71	7	1	101450.1	0.1	4	60.76	148.63	15
71	7	1	104819.3	0.2	6	62.32	150.86	40
71	7	1	111028.7	C.1	5	62.60	148.84	150
71	7	1	112257.7	0.3	8	63.47	147.41	15
71	7	1	131945.2	0.7	10	62.39	149.51	15
71	7	1	135351.3	0.C	3	61.61	148.79	0
71	7	1	1532 6.4	0.4	7	61.96	150.77	50
71	7	1	162052.9	0.4	5	61.53	149.93	40
71	7	1	19 246.8	0.C	3	62.57	149.52	0
71	7	1	194434.3	0.C	3	61.30	150.01	0
71	7	1	211851.9	0.3	10	63.21	150.51	125
71	7	1	233721.C	C.5	6	58.93	149.74	0
71	7	2	13753.7	0.4	10	59.16	154.85	75
71	7	2	2 9 4.9	C.C	3	61.76	149.47	0
71	7	2	41531.8	1.2	8	60.62	146.96	0
71	7	2	6 219.1	0.7	6	61.56	149.62	250
71	7	2	91223.3	0.4	7	62.50	149.48	75
71	7	2	103116.1	C.C	4	61.68	147.07	15
71	7	2	111300.8	C.2	7	62.17	148.71	15
71	7	2	111926.3	C.C	3	58.84	152.61	200
71	7	2	1145 1.8	0.9	4	61.40	150.32	0
71	7	2	1237 1.5	C.2	6	62.97	151.52	100
71	7	2	125810.4	0.8	8	61.60	150.80	15
71	7	2	152813.9	0.0	3	61.86	150.29	0
71	7	2	234914.8	0.C	3	61.89	149.46	0
71	7	3	25657.7	C.3	6	62.54	151.56	100
71	7	3	5 523.2	0.5	9	61.83	149.92	40
71	7	3	82320.3	0.C	3	61.42	149.88	0
71	7	3	84819.9	C.0	3	61.59	149.69	0
71	7	3	95141.0	C.4	9	63.08	150.97	150
71	7	3	121343.3	0.C	3	61.50	149.77	0
71	7	3	145631.1	C.9	5	61.70	146.69	250
71	7	3	1559 7.8	0.0	3	61.67	149.70	0
71	7	3	23 742.4	C.4	6	61.70	150.87	200
71	7	4	1 5 7.4	0.0	3	61.56	149.61	0
71	7	4	254 7.0	C.C	3	61.68	149.49	0
71	7	4	41554.6	1.2	14	60.33	153.39	100
71	7	4	51449.2	0.0	4	62.30	149.34	15
71	7	4	54215.3	1.2	8	61.00	146.34	0
71	7	4	6 734.4	0.3	14	62.84	150.78	100
71	7	4	82536.6	0.2	5	61.65	150.32	40
71	7	4	91832.8	0.3	10	63.51	150.06	150

71	7	4	933	3.9	0.2	8	63.53	146.56	15
71	7	4	112014.4		0.4	7	62.19	147.57	15
71	7	4	113339.0		0.2	4	61.90	150.27	0
71	7	4	153020.8		0.1	4	60.60	148.39	15
71	7	4	1635	2.8	0.7	9	63.28	150.17	0
71	7	4	201330.0		0.6	10	62.35	150.50	40
71	7	4	215229.7		0.1	5	61.31	150.24	0
71	7	4	2355	4.1	0.1	4	61.87	150.26	0
71	7	5	228	2.9	0.0	3	61.48	149.80	0
71	7	5	25049.9		0.7	21	61.38	147.54	15
71	7	5	3 912.7		0.5	9	62.35	150.11	0
71	7	5	42944.3		0.4	6	60.66	152.26	40
71	7	5	64038.0		0.1	4	60.26	147.51	40
71	7	5	811	0.3	0.0	3	61.29	148.44	0
71	7	5	10 050.7		0.0	3	61.70	149.68	15
71	7	5	113511.3		0.0	4	61.40	147.69	0
71	7	5	1538	0.1	0.5	7	61.70	149.87	40
71	7	5	214728.7		0.6	11	61.06	146.65	0
71	7	5	231218.4		0.5	16	59.74	151.18	40
71	7	6	22751.0		0.6	6	60.06	151.06	50
71	7	7	63248.9		1.0	14	57.37	153.65	15
71	7	6	10 045.0		0.0	4	61.95	150.16	15
71	7	6	1110	9.5	0.4	8	62.31	151.29	0
71	7	6	1622	0.4	0.4	6	60.67	150.41	15
71	7	6	225817.9		0.3	6	61.13	151.00	50
71	7	7	010	0.6	0.3	6	62.18	149.27	40
71	7	7	14943.8		0.0	3	61.94	151.86	0
71	7	7	35017.3		0.0	3	61.76	151.70	0
71	7	7	6 5	3.2	0.0	4	62.11	149.75	0
71	7	7	111633.9		0.0	3	62.03	151.76	15
71	7	7	124831.5		0.3	7	61.43	150.86	50
71	7	7	125815.9		0.5	12	60.36	152.01	75
71	7	7	14 955.4		0.6	12	60.98	148.18	15
71	7	7	161426.7		0.2	7	61.57	150.00	40
71	7	7	163837.2		0.5	9	61.53	147.33	15
71	7	7	165443.8		0.1	4	61.91	149.83	40
71	7	7	194341.4		0.0	3	61.83	151.66	0
71	7	7	1945	8.1	0.2	7	62.27	150.19	40
71	7	8	22544.9		0.1	4	62.24	149.75	40
71	7	8	32732.8		0.4	9	62.59	149.29	200
71	7	8	42325.2		0.1	4	60.56	146.91	40
71	7	8	443	6.7	0.1	4	60.65	147.54	15
71	7	8	742	4.3	0.1	4	60.72	147.30	15
71	7	8	832	4.4	0.7	9	62.14	151.24	75
71	7	8	92029.4		0.6	12	63.26	150.18	0
71	7	8	11 356.6		0.0	3	61.40	149.49	0
71	7	8	1111	0.0	0.3	6	61.93	150.84	250
71	7	8	143815.3		0.2	11	63.20	149.29	250
71	7	8	1442	7.6	0.4	11	62.57	151.25	75
71	7	8	153430.2		0.4	13	62.28	149.36	50

71	7	8	155356.3	1.7	12	63.50	152.07	150
71	7	9	114721.9	0.3	7	61.95	147.92	15
71	7	9	136355.1	C.C	3	61.56	149.73	0
71	7	9	141611.3	C.6	9	59.88	152.81	75
71	7	9	192556.9	0.5	9	62.11	140.04	15
71	7	10	21534.2	0.5	12	59.92	152.88	100
71	7	10	5 418.4	C.7	12	63.12	150.86	150
71	7	10	91523.3	0.5	10	60.74	152.29	75
71	7	10	1040 7.2	C.C	3	61.50	149.57	0
71	7	10	123718.5	0.C	3	61.37	150.02	0
71	7	10	131531.5	0.5	13	61.90	150.28	0
71	7	10	15 338.1	C.6	7	61.04	150.81	0
71	7	10	181026.9	0.6	9	61.33	146.69	15
71	7	10	232923.3	0.6	10	61.22	150.80	40
71	7	11	011 2.5	0.C	4	61.84	149.70	15
71	7	11	11056.8	0.6	14	61.91	153.24	0
71	7	11	11830.3	C.C	3	61.87	151.61	0
71	7	11	35626.7	0.8	7	61.10	150.74	0
71	7	11	638 4.C	1.C	13	59.90	153.61	100
71	7	11	105319.9	0.0	3	61.74	151.81	0
71	7	11	132153.6	0.C	3	62.11	151.83	0
71	7	11	134018.5	0.2	5	62.74	150.33	75
71	7	11	1448 2.2	0.3	8	61.94	149.54	15
71	7	11	1516 1.8	0.C	3	62.07	151.83	0
71	7	11	16 052.6	C.4	7	61.72	149.99	40
71	7	11	224731.6	0.5	11	60.64	152.23	75
71	7	11	2340 3.9	0.1	3	61.97	151.86	0
71	7	12	04918.5	0.3	8	63.36	150.97	150
71	7	12	9 235.5	C.2	16	63.15	149.78	100
71	7	12	05712.7	0.2	8	62.12	149.58	40
71	7	12	13015.8	0.C	3	61.84	151.63	0
71	7	12	34236.C	0.3	7	61.58	149.84	40
71	7	12	84355.4	C.0	3	62.25	151.88	0
71	7	12	9 236.9	1.8	19	63.21	149.90	40
71	7	12	10 955.9	C.3	7	61.60	151.43	75
71	7	12	11234C.9	0.0	3	62.06	151.77	0
71	7	12	113157.0	0.C	3	61.94	151.91	15
71	7	12	112859.C	1.1	16	60.25	153.05	100
71	7	12	13 825.1	C.8	15	58.84	154.61	100
71	7	12	14 142.5	0.6	7	61.52	149.89	40
71	7	12	141050.5	C.4	7	61.66	149.86	40
71	7	12	141410.1	1.0	12	63.53	150.73	0
71	7	12	15 658.9	C.2	12	62.70	149.43	15
71	7	12	16 118.9	C.C	3	61.98	151.90	0
71	7	13	32625.5	0.4	9	61.59	151.58	75
71	7	13	41958.7	C.3	6	60.94	152.10	100
71	7	13	61313.5	0.C	4	61.69	150.17	15
71	7	13	63012.9	C.6	9	61.99	149.81	15
71	7	13	957 3.8	0.3	11	62.68	149.08	15
71	7	13	142244.7	C.3	8	59.60	151.96	40

71	7	13	145448.7	C.C	3	61.33	149.85	C
71	7	13	153541.2	0.4	10	60.44	151.91	50
71	7	14	81130.3	0.C	3	61.66	151.81	0
71	7	14	102758.1	C.4	12	59.28	151.93	40
71	7	14	1049 1.8	0.4	6	61.36	150.29	40
71	7	14	111345.2	0.2	9	62.31	150.96	50
71	7	14	1241 5.8	C.2	6	59.33	152.12	15
71	7	14	141446.8	0.4	11	59.94	152.78	100
71	7	14	154050.6	0.5	19	59.92	152.62	75
71	7	14	154744.2	0.C	3	62.06	151.66	0
71	7	14	171354.2	C.C	3	62.04	151.75	15
71	7	14	1839 0.1	0.C	3	61.84	152.31	0
71	7	14	20 924.3	0.5	8	61.39	150.61	40
71	7	15	53615.8	1.C	18	60.11	153.13	100
71	7	15	15 618.C	1.4	6	58.20	144.99	100
71	7	15	113351.3	0.1	6	62.05	149.09	15
71	7	15	15 7 1.3	2.7	7	61.15	147.76	40
71	7	15	151837.9	2.5	7	58.05	151.03	40
71	7	15	16 651.5	0.C	3	62.05	151.79	15
71	7	15	162917.8	0.C	4	60.45	148.26	15
71	7	15	181414.8	C.C	3	61.83	151.82	0
71	7	15	22 434.9	C.C	3	62.07	151.80	0
71	7	15	225720.6	C.3	6	61.03	151.86	100
71	7	16	01433.8	C.6	10	62.11	148.51	40
71	7	16	01749.5	2.5	4	60.06	157.92	100
71	7	16	04818.3	0.0	3	61.87	151.58	C
71	7	16	12259.3	C.C	4	61.35	150.91	250
71	7	16	43128.8	1.C	14	59.20	153.88	0
71	7	16	71729.2	C.C	3	61.75	151.53	0
71	7	16	72012.1	0.2	8	63.33	148.93	125
71	7	16	111323.4	C.0	3	61.99	151.83	15
71	7	16	122212.3	C.1	9	63.81	149.18	125
71	7	16	1254 4.5	0.0	3	61.89	151.88	0
71	7	16	19 215.4	C.C	3	61.70	151.80	0
71	7	17	51957.2	C.2	5	61.57	151.51	75
71	7	17	74237.9	0.3	5	62.68	148.66	15
71	7	17	12 3 3.0	0.C	3	61.98	151.83	0
71	7	17	164312.3	C.C	3	61.98	151.89	0
71	7	17	1720 7.1	C.C	3	61.97	151.89	C
71	7	17	192745.9	C.C	3	62.09	152.37	C
71	7	17	224437.1	C.6	9	63.08	152.69	75
71	7	17	232935.5	C.C	3	61.76	151.64	0
71	7	17	233625.9	C.C	3	61.96	151.88	15
71	7	18	45548.7	0.C	3	61.72	151.81	0
71	7	18	522 5.3	C.8	6	61.58	146.06	15
71	7	18	53546.5	C.1	4	61.74	148.55	C
71	7	18	7 926.7	0.4	11	63.36	149.79	200
71	7	18	75458.7	C.C	3	61.81	151.87	C
71	7	18	930 8.4	C.4	6	63.26	150.45	150
71	7	18	94854.8	0.0	3	61.72	151.74	0

71	7	18	114255.7	C.C	3	61.91	151.86	0
71	7	18	13 018.C	C.0	3	61.90	152.04	0
71	7	18	133529.9	C.5	6	61.02	150.94	0
71	7	18	15 717.4	C.7	7	61.98	147.51	15
71	7	18	152616.4	C.2	5	61.51	150.95	250
71	7	18	173911.3	C.3	6	61.86	149.99	50
71	7	18	191740.C	0.3	9	62.31	148.87	15
71	7	19	02526.3	7.8	8	62.60	162.79	100
71	7	19	64719.3	C.2	8	63.61	148.00	50
71	7	19	75914.6	0.0	3	61.72	151.79	0
71	7	19	91148.9	C.C	3	62.02	151.94	0
71	7	19	1129 7.1	C.4	12	62.92	150.99	100
71	7	19	162142.9	0.0	3	62.05	151.80	15
71	7	19	172740.3	0.0	3	61.77	151.61	15
71	7	19	1914 1.8	C.C	3	61.91	151.85	15
71	7	19	191716.6	C.1	5	61.45	148.07	50
71	7	19	195251.1	C.6	15	61.93	150.25	C
71	7	19	222756.1	C.2	7	61.97	150.57	15
71	7	19	225226.4	C.4	15	62.60	147.60	200
71	7	20	6 615.5	C.3	10	63.22	150.44	200
71	7	20	8 229.2	0.3	9	63.87	149.17	150
71	7	20	101427.3	C.6	11	62.03	150.42	50
71	7	20	1237 2.C	C.2	9	62.96	149.50	C
71	7	20	141E29.9	0.0	3	61.90	151.65	C
71	7	20	145052.9	0.3	7	62.52	151.42	125
71	7	20	174558.4	4.6	10	62.08	156.10	100
71	7	21	2 921.8	C.3	7	61.36	151.57	75
71	7	21	25E37.3	C.0	3	61.89	149.68	0
71	7	21	33960.C	C.C	3	61.90	149.66	0
71	7	21	41458.7	C.C	3	62.30	150.50	15
71	7	21	113613.0	1.5	19	60.60	149.95	0
71	7	21	115748.9	1.C	9	63.17	150.85	C
71	7	21	13 231.8	0.7	12	59.97	151.09	40
71	7	21	132457.7	0.0	3	62.07	151.84	0
71	7	21	145637.0	0.6	7	62.17	150.27	40
71	7	21	1843 1.3	C.5	10	61.92	150.24	0
71	7	21	202210.5	C.3	9	63.00	151.00	150
71	7	22	32121.4	0.2	6	61.93	147.55	75
71	7	22	44547.8	C.2	6	61.19	147.34	50
71	7	22	14 324.8	C.2	5	61.72	149.63	50
71	7	22	1414 1.3	0.0	3	62.09	151.71	15
71	7	22	1515 2.6	0.3	8	61.53	149.78	40
71	7	22	17 44C.1	C.5	6	61.34	148.00	15
71	7	22	204414.1	C.0	3	61.70	151.82	0
71	7	23	038 5.5	C.C	3	61.94	151.48	0
71	7	23	24340.0	C.C	3	61.85	151.63	C
71	7	23	34247.4	0.0	3	61.53	152.09	0
71	7	23	43E56.6	0.4	6	60.86	150.58	15
71	7	23	51449.1	C.C	4	61.67	149.82	C
71	7	23	53749.2	C.5	5	61.65	147.28	250

71	7	23	753	7.5	0.5	8	61.00	150.77	0
71	7	23	11 658.1		0.5	13	60.10	153.06	100
71	7	23	113539.2		0.2	5	62.31	151.59	100
71	7	23	14 146.2		0.4	8	60.97	150.94	0
71	7	23	163040.2		0.2	6	62.19	147.81	0
71	7	23	1659 5.7		0.0	3	61.80	151.87	0
71	7	23	174144.5		0.3	6	61.62	150.21	50
71	7	24	01833.9		0.0	3	61.73	151.84	0
71	7	24	05324.7		0.3	7	63.02	150.62	40
71	7	24	333 6.6		0.0	3	61.55	149.74	0
71	7	24	5 535.7		0.1	5	59.76	152.50	0
71	7	24	93143.6		0.0	4	61.78	150.67	250
71	7	24	103918.8		0.4	12	62.92	151.23	100
71	7	24	12 544.6		0.3	12	62.93	151.04	125
71	7	24	123624.2		0.5	7	60.70	152.06	250
71	7	24	1548 2.1		0.4	11	63.18	148.97	0
71	7	24	162159.9		0.2	9	63.01	149.44	200
71	7	24	173022.0		0.3	3	61.95	151.96	0
71	7	24	231152.3		0.0	3	61.67	152.05	0
71	7	24	231523.9		0.4	10	62.12	150.91	40
71	7	24	232136.9		0.9	10	61.33	150.68	15
71	7	25	1 317.9		0.0	3	62.06	151.89	0
71	7	25	5 3 3.0		1.6	12	57.76	152.47	15
71	7	25	6 134.3		0.3	7	61.56	149.64	250
71	7	25	115226.7		0.7	7	63.28	150.54	0
71	7	25	143638.8		0.1	4	62.25	151.20	75
71	7	25	153944.3		0.0	3	61.77	152.36	0
71	7	26	21420.4		1.7	7	63.05	151.13	150
71	7	26	23622.6		0.5	4	60.43	155.12	150
71	7	26	65753.9		0.4	12	59.92	151.38	15
71	7	26	82625.0		0.4	14	60.88	152.71	150
71	7	26	114230.6		0.5	7	64.35	156.29	200
71	7	26	125011.7		0.1	4	60.92	152.01	150
71	7	26	155351.6		0.0	3	61.60	149.22	0
71	7	26	161735.0		0.9	20	63.30	149.37	15
71	7	26	175513.5		0.0	4	61.85	149.28	250
71	7	26	2023 5.1		0.3	10	63.71	149.79	125
71	7	26	233552.4		2.7	11	62.30	148.69	200
71	7	27	42452.5		0.7	10	63.25	149.21	0
71	7	27	54853.2		0.3	14	62.01	151.18	200
71	7	27	650 9.6		0.0	4	62.16	151.46	40
71	7	27	951 5.4		0.3	6	57.14	156.77	15
71	7	27	1142 7.2		1.1	8	63.04	151.13	150
71	7	27	171013.9		0.0	3	61.29	149.93	0
71	7	28	042 4.6		0.3	5	61.37	150.20	40
71	7	28	04637.6		0.1	4	59.87	151.65	150
71	7	28	43013.2		0.9	11	63.84	148.86	75
71	7	28	44851.7		2.5	10	61.62	150.01	200
71	7	28	105254.6		0.4	8	60.70	151.13	40
71	7	28	125630.0		0.3	6	61.81	149.51	40

```
71  7 28 14 237.6 0.2  6  61.61 149.47 250
71  7 28 22 347.3 0.4  8  63.81 149.25 125
71  7 28 23 239.9 1.2 14  59.03 148.91  40
```

71	6	4	203746.0	0.4	7	61.65	150.88	64
71	6	5	133453.8	0.2	7	61.43	148.52	25
71	6	5	13718.6	0.4	10	61.60	150.91	65
71	6	5	63934.2	0.3	10	61.70	151.19	60
71	6	5	84543.5	0.0	5	61.58	151.46	50
71	6	5	811 4.7	0.2	8	62.02	150.51	24
71	6	6	16 159.9	0.2	9	61.08	147.96	14
71	6	6	121721.3	0.6	7	61.06	150.86	2
71	6	6	14 324.7	0.5	5	61.20	151.20	38
71	6	6	1620 1.6	0.4	9	61.56	149.57	49
71	6	7	18 140.4	0.4	8	61.99	149.39	46
71	6	7	62659.7	0.4	8	62.38	148.04	38
71	6	7	234750.0	0.4	9	62.38	149.62	37
71	6	7	74957.9	0.3	9	62.47	149.54	32
71	6	8	75256.7	0.2	6	61.06	149.55	37
71	6	8	144837.3	0.2	5	61.47	152.06	13
71	6	9	812 0.0	0.3	8	61.98	150.89	62
71	6	9	191015.0	0.3	6	62.03	149.31	37
71	6	9	2 935.7	0.3	7	62.39	150.02	37
71	6	10	16 2 3.3	0.4	7	61.49	149.79	37
71	6	10	1159 2.4	0.5	7	61.71	147.98	17
71	6	10	134436.7	0.3	7	61.79	149.80	46
71	6	10	164632.3	0.3	9	62.56	149.56	33
71	6	10	165517.4	0.2	9	62.52	151.25	67
71	6	11	17 815.6	0.2	6	61.39	150.64	54
71	6	11	1712 9.9	0.2	6	61.40	150.64	54
71	6	11	115426.8	0.3	6	61.71	149.15	27
71	6	12	194540.7	0.5	7	61.06	150.79	2
71	6	12	53959.2	0.5	8	61.42	146.16	3
71	6	12	2320 5.5	0.5	8	61.43	146.12	4
71	6	12	13 156.4	0.3	7	61.55	149.55	41
71	6	12	183610.6	0.3	5	61.65	149.70	40
71	6	12	95115.2	0.4	6	62.29	150.53	16
71	6	12	81626.5	0.2	9	62.79	151.14	118
71	6	13	327 7.8	0.2	6	61.83	149.53	54
71	6	14	3 222.8	0.5	7	60.98	147.13	5
71	6	14	454 7.4	0.5	7	61.20	150.68	0
71	6	14	21858.7	0.5	9	61.67	151.68	89
71	6	14	32752.3	0.3	5	61.71	149.80	44
71	6	14	7 631.1	0.2	5	61.90	149.58	46
71	6	14	213355.7	0.3	7	62.35	151.14	79
71	6	15	8 9 6.3	0.6	8	61.45	146.46	11
71	6	15	155233.7	0.3	6	61.91	150.00	47
71	6	15	44143.7	0.3	6	62.33	148.10	33
71	6	16	332 1.5	0.6	6	61.47	150.36	30
71	6	16	1041 6.6	0.6	8	61.53	149.87	35
71	6	16	1843 6.2	0.7	8	61.58	149.99	40
71	6	16	62354.2	1.3	8	61.53	151.36	33
71	6	16	162218.1	0.2	5	61.62	150.74	57
71	6	16	61634.8	0.6	7	61.82	149.62	33

71	6	16	22648.8	0.2	6	61.95	149.68	44
71	6	16	182120.5	0.2	8	62.54	152.26	8
71	6	16	1033 7.6	0.2	9	62.60	151.16	65
71	6	17	35817.7	0.4	8	61.13	151.93	92
71	6	17	84832.5	0.2	6	61.53	151.59	96
71	6	17	165140.3	0.2	7	61.65	149.82	51
71	6	17	21 040.6	0.4	9	61.75	149.77	48
71	6	17	33019.4	0.1	5	61.93	148.88	9
71	6	19	101227.6	0.4	8	61.35	148.72	27
71	6	19	22 139.7	0.3	8	61.41	147.76	10
71	6	19	151141.3	0.4	7	61.56	149.79	38
71	6	20	45411.4	0.2	6	61.07	146.98	13
71	6	20	153459.9	0.2	6	61.52	151.47	81
71	6	20	112545.1	0.5	6	61.74	149.11	24
71	6	21	536 4.7	0.2	6	61.94	150.66	53
71	6	21	55042.6	0.2	8	62.06	151.21	83
71	6	21	51249.8	0.3	5	65.43	146.33	33
71	6	22	214234.0	0.2	6	61.57	149.87	30
71	6	22	231425.5	0.4	6	61.64	150.33	46
71	6	25	42121.4	0.3	5	60.71	152.39	33
71	6	25	102335.1	1.1	7	61.02	146.86	33
71	6	25	5 852.6	0.4	7	61.52	149.94	39
71	6	25	55532.6	0.5	8	61.50	150.00	37
71	6	25	35422.7	0.5	6	61.66	149.62	38
71	6	25	21 0 5.6	0.3	9	62.37	151.26	88
71	6	26	222722.6	0.7	7	61.76	149.20	15
71	6	28	163913.0	3.0	7	61.40	149.14	20
71	6	28	193541.7	2.0	6	61.81	148.90	26
71	6	29	14138.7	0.4	5	61.35	149.22	21
71	6	29	52636.9	0.7	5	61.48	149.71	31
71	6	29	3 725.4	0.7	6	61.75	145.62	33
71	6	29	223012.4	0.4	6	61.77	149.95	38
71	6	30	54419.2	0.5	5	61.54	147.95	1
71	6	30	234627.9	0.1	7	62.54	149.11	33
71	7	1	162052.5	0.2	5	61.55	149.96	42
71	7	1	1532 5.3	0.3	7	61.95	150.80	62
71	7	1	83925.1	0.3	6	62.11	150.30	55
71	7	1	131946.2	0.5	7	62.22	149.51	48
71	7	1	104618.9	0.1	6	62.31	150.80	36
71	7	1	6 626.6	0.3	7	62.77	150.61	26
71	7	2	6 334.1	0.6	6	61.57	149.81	30
71	7	2	1258 9.5	0.9	8	61.62	150.78	16
71	7	2	111339.7	0.1	7	62.05	148.66	34
71	7	2	91222.7	0.4	7	62.52	149.51	70
71	7	2	1237 5.4	0.4	6	62.74	151.03	28
71	7	3	23 056.1	0.3	6	61.68	150.52	65
71	7	3	5 522.4	0.5	9	61.84	146.55	48
71	7	3	145746.8	1.2	5	61.67	147.29	33
71	7	4	215228.4	0.3	5	61.25	150.23	24
71	7	4	54321.0	1.0	6	61.37	146.90	33

71	7	4	82535.3	C.3	5	61.65	150.29	56
71	7	4	112013.6	0.5	7	61.35	147.28	52
71	7	4	201329.3	C.4	8	61.97	150.55	53
71	7	4	6 733.3	C.2	10	62.80	150.84	112
71	7	5	214729.9	0.5	9	61.27	146.94	2
71	7	5	75513.8	0.6	8	61.30	146.98	7
71	7	5	25049.0	0.4	10	61.34	147.62	19
71	7	5	19 4 1.9	C.9	9	61.45	150.11	31
71	7	5	153759.6	C.3	7	61.69	149.92	43
71	7	5	3 914.4	C.1	7	62.09	150.26	52
71	7	5	4 413.3	0.3	6	63.08	149.82	33
71	7	6	225817.5	0.3	6	61.14	150.99	39
71	7	6	1110 9.7	0.7	8	62.20	151.61	34
71	7	7	14 952.2	C.7	9	60.94	148.17	2
71	7	7	163835.1	0.5	9	61.43	147.31	16
71	7	7	124830.8	C.2	7	61.45	150.84	55
71	7	7	161425.9	C.2	7	61.59	150.02	49
71	7	7	C 959.9	0.3	6	62.18	149.29	39
71	7	7	1945 7.0	0.3	7	62.29	150.18	33
71	7	8	3 629.7	C.8	8	61.31	146.75	7
71	7	8	111214.5	0.3	6	61.96	150.81	39
71	7	8	832 5.3	C.3	8	62.18	151.01	52
71	7	8	153429.9	C.2	7	62.22	149.35	56
71	7	8	1442 8.5	0.1	6	62.40	150.85	100
71	7	8	32646.8	0.2	8	62.59	149.29	33
71	7	9	114720.7	0.5	7	62.00	148.06	15
71	7	9	192955.2	C.5	7	62.15	148.10	12
71	7	10	15 337.2	0.7	7	61.07	150.78	6
71	7	10	181022.9	C.5	8	61.20	146.65	2
71	7	10	232923.3	C.4	9	61.31	150.71	47
71	7	10	131531.0	C.5	9	61.30	150.37	15
71	7	11	35625.3	C.9	7	61.13	150.72	2
71	7	11	16 051.8	C.4	7	61.71	150.02	46
71	7	11	11056.3	0.5	11	61.80	150.37	14
71	7	11	1446 1.4	0.5	8	61.92	149.63	29
71	7	11	134018.1	C.2	5	62.74	150.35	73
71	7	12	14 142.0	0.4	7	61.54	149.94	42
71	7	12	10 954.9	C.2	7	61.55	151.42	79
71	7	12	34235.4	C.2	7	61.60	149.88	44
71	7	12	141049.8	0.3	7	61.66	149.91	43
71	7	12	05712.6	C.3	7	62.08	149.65	44
71	7	12	15 659.4	0.2	8	62.63	149.48	33
71	7	13	32621.9	C.4	8	61.49	151.80	101
71	7	14	1049 1.5	C.4	6	61.37	150.40	32
71	7	14	20 923.6	C.2	8	61.43	150.57	48
71	7	14	111343.3	0.1	9	62.28	151.10	75
71	7	15	15 654.5	1.3	6	60.73	147.60	27
71	7	15	113349.9	C.1	6	62.06	149.10	25
71	7	16	01434.1	C.5	9	62.08	148.73	23
71	7	17	51954.4	0.1	5	61.55	151.63	97

71	7	17	74234.0	C.8	5	62.45	148.53	146
71	7	18	133530.8	C.6	6	61.15	150.87	11
71	7	18	15 710.5	C.5	7	61.26	146.84	25
71	7	18	152730.9	C.1	5	61.51	150.94	38
71	7	18	522 4.6	C.7	5	61.68	146.28	10
71	7	18	173910.1	C.4	6	62.08	149.95	31
71	7	18	191740.5	C.2	7	62.11	148.81	55
71	7	19	195250.6	C.4	10	61.73	150.41	22
71	7	19	222755.3	C.3	7	61.97	150.57	18
71	7	19	225340.9	C.3	9	62.60	147.71	38
71	7	19	1129 8.4	C.4	7	62.90	150.79	33
71	7	20	101425.6	C.3	8	61.85	150.52	73
71	7	20	145056.7	C.4	7	62.60	150.83	29
71	7	21	184259.1	C.4	7	61.58	150.59	25
71	7	21	145636.3	C.5	7	62.18	150.38	37
71	7	21	2 525.9	C.7	5	62.15	150.70	33
71	7	22	17 438.4	C.3	5	61.40	148.00	32
71	7	22	1519 2.1	C.2	7	61.61	149.78	49
71	7	22	14 324.3	C.2	5	61.74	149.71	55
71	7	22	44551.9	C.3	6	61.93	148.07	31
71	7	23	753 5.1	C.5	8	61.00	150.77	0
71	7	23	174143.5	C.3	6	61.61	150.23	57
71	7	23	539 4.3	C.5	5	61.87	147.61	33
71	7	23	163045.6	C.4	6	61.94	148.37	28
71	7	23	113537.5	C.1	5	62.25	152.05	115
71	7	24	232135.5	C.3	10	61.34	150.68	53
71	7	24	231526.2	C.4	5	62.07	150.36	35
71	7	24	103920.6	C.4	9	62.91	150.98	38
71	7	24	12 344.8	C.1	9	62.91	150.98	118
71	7	25	6 248.7	C.2	7	61.60	149.69	38
71	7	26	233712.1	C.2	5	61.59	148.73	33
71	7	27	550 8.1	C.1	5	61.58	150.90	77
71	7	28	042 3.9	C.2	5	61.38	150.22	48
71	7	28	450 6.2	C.2	6	61.46	149.95	47
71	7	28	14 352.0	C.1	6	61.65	149.50	37
71	7	28	125629.4	C.2	6	61.82	149.56	46

72	1	2	63946.2	0.3	4	62.43	145.58	27
72	1	5	145243.4	0.1	4	65.36	150.05	27
72	1	8	151419.3	0.4	9	60.99	150.65	29
72	1	10	173334.3	0.7	4	61.49	146.98	5
72	1	10	21750.2	0.1	10	61.93	151.02	31
72	1	20	15 7 7.9	0.3	10	62.05	148.81	31
72	1	26	174757.6	0.8	10	63.59	150.96	29
72	1	27	0 754.4	0.4	7	61.90	147.94	69
72	1	31	223144.5	0.2	12	62.03	150.55	34
72	2	2	322 2.1	0.0	5	63.19	149.75	92
72	2	3	184345.7	0.2	7	63.03	150.64	114
72	2	7	1718 1.3	0.3	11	61.19	147.14	7
72	2	8	720 3.2	0.5	6	61.20	148.20	97
72	2	9	2 849.1	0.9	6	63.92	149.24	8
72	2	10	20 155.0	0.5	7	61.22	151.08	38
72	2	11	216 8.5	0.4	12	61.95	149.95	31
72	2	13	53758.1	0.5	12	64.07	150.13	18
72	2	13	165420.9	1.3	7	65.72	149.94	33
72	2	15	16 529.5	0.1	5	61.00	148.00	31
72	2	27	73726.8	0.5	10	61.58	146.20	8
72	2	27	9 830.0	0.2	10	63.23	150.70	144
72	2	28	203320.6	1.6	9	64.42	147.70	8
72	3	1	202850.3	0.5	12	60.86	150.75	65
72	3	6	4 026.6	0.1	7	62.36	147.72	60
72	3	6	6 020.6	0.2	7	62.38	149.67	76
72	3	6	62652.9	0.4	5	64.46	151.33	52
72	3	7	95330.2	0.1	5	61.39	147.43	22
72	3	9	1031 6.3	0.3	7	65.25	150.37	33
72	3	10	22915.7	0.2	7	62.96	146.90	4
72	3	12	15 024.0	0.3	14	61.52	147.66	29
72	3	16	202932.8	1.2	9	64.73	147.15	2
72	3	17	133213.6	0.6	9	64.68	147.56	7
72	3	18	4 028.8	0.2	10	63.13	150.41	122
72	3	20	05739.0	0.5	11	62.05	149.67	53
72	3	21	1757 2.7	0.6	6	65.18	146.85	4
72	3	26	20 8 1.7	0.2	15	60.92	147.35	10
72	3	26	185642.2	0.5	7	64.79	147.60	10
72	3	29	71216.4	0.5	7	61.36	148.74	100
72	3	29	43053.4	0.3	8	61.54	147.38	47
72	3	30	16 848.5	0.3	15	63.17	148.94	91
72	3	31	65413.1	0.2	8	65.74	154.65	24
72	4	2	21 4 2.5	1.3	10	64.75	147.72	1
72	4	3	19713.4	1.0	8	64.72	147.50	0
72	4	3	01020.8	0.2	11	64.80	146.79	8
72	4	4	45532.9	0.2	8	63.05	150.53	104
72	4	6	135515.9	0.2	11	63.36	148.69	67
72	4	9	18 557.3	0.2	11	64.02	151.00	34
72	4	11	11140.3	0.5	8	61.93	147.96	37
72	4	11	182135.3	0.5	15	61.99	150.46	18
72	4	11	23555.7	0.3	14	62.48	150.91	76

72	4	11	75158.1	1.2	10	64.69	147.58	1
72	4	12	730 6.8	0.6	8	64.77	147.54	4
72	4	13	1655 8.9	0.2	7	61.49	150.28	30
72	4	14	75820.0	0.9	11	64.03	147.11	2
72	4	15	144126.8	0.5	8	64.73	148.92	12
72	4	16	4 620.4	0.3	8	61.91	148.81	24
72	4	16	104518.9	0.5	7	64.85	147.76	9
72	4	17	135 5.7	0.3	9	63.49	147.59	3
72	4	19	124642.0	0.5	15	60.22	147.41	40
72	4	19	175337.2	0.4	10	61.24	147.27	27
72	4	19	212137.8	0.9	6	62.90	148.22	41
72	4	19	35841.9	0.1	10	63.00	151.21	140
72	4	20	165914.0	0.8	6	61.95	148.90	12
72	4	22	15 715.7	0.2	9	61.18	147.31	45
72	4	22	71943.2	0.4	15	62.36	151.00	101
72	4	25	8 336.5	0.4	11	60.92	147.00	0
72	4	25	133554.3	0.3	13	61.97	148.63	31
72	4	27	104459.3	0.3	15	62.66	149.61	84
72	4	27	101656.0	0.5	8	64.59	147.22	0
72	4	28	171314.9	0.4	16	61.35	146.87	29
72	4	28	19 515.6	0.2	16	63.61	149.78	135
72	4	29	25017.8	0.8	7	61.18	148.22	37
72	4	29	125518.7	0.2	11	62.03	150.81	126
72	4	29	73642.2	0.4	9	64.73	149.86	12
72	5	1	7 847.2	1.0	10	64.65	147.50	0
72	5	3	202930.6	0.2	8	64.06	147.39	0
72	5	3	10 230.0	0.1	6	65.41	151.91	29
72	5	5	144944.8	0.3	9	63.96	147.33	4
72	5	6	213636.9	0.3	10	62.96	147.34	1
72	5	8	161125.1	0.3	12	61.92	148.63	36
72	5	8	114257.9	0.1	4	65.45	151.91	27
72	5	9	43215.6	0.8	10	61.45	149.79	31
72	5	12	15731.4	0.4	9	61.74	147.85	30
72	5	13	23528.3	0.2	9	63.05	149.75	113
72	5	14	93955.3	0.3	15	61.86	150.26	32
72	5	14	42951.9	1.3	9	65.43	150.11	33
72	5	14	110 4.5	0.4	14	65.56	149.93	9
72	5	15	713 5.9	0.2	4	64.74	147.16	2
72	5	16	184510.8	0.5	16	61.95	147.11	49
72	5	16	164746.3	0.4	8	65.84	154.12	25
72	5	17	12 612.2	0.8	8	64.73	147.53	14
72	5	18	22642.4	0.6	7	64.16	150.02	0
72	5	23	173220.4	0.5	9	61.73	150.85	34
72	5	23	175643.2	0.1	4	63.21	148.99	38
72	5	24	639 1.0	1.8	4	61.75	148.62	67
72	5	25	19 913.9	0.4	6	65.41	150.13	35
72	5	28	12329.2	0.4	7	61.69	146.79	14
72	6	1	101126.3	0.2	7	65.54	149.96	8
72	6	6	184649.3	0.4	10	65.63	152.23	18
72	6	8	41855.4	0.4	13	61.53	146.62	36

72	6	8	44540.4	C.6	5	62.12	146.32	6
72	6	8	161229.5	C.2	5	62.35	147.91	10
72	6	16	11230.7	C.4	11	61.83	149.23	17
72	6	17	173327.2	C.1	12	63.07	150.40	74
72	6	18	43259.1	C.5	9	62.36	148.62	18
72	6	19	31354.0	C.2	7	61.94	148.54	4
72	6	22	115145.1	C.4	9	61.43	147.37	24
72	6	22	55734.1	C.2	14	61.41	147.57	24
72	6	22	144423.8	C.2	10	63.24	148.78	99
72	6	28	16 358.3	C.5	8	61.30	147.60	18
72	6	30	92540.9	C.4	12	59.23	151.90	69
72	6	30	133342.7	C.4	6	62.31	148.30	63
72	7	4	1233 4.6	C.2	13	63.80	149.14	122
72	7	7	52656.0	C.3	6	61.66	147.73	25
72	7	9	101959.5	C.3	10	63.82	147.30	3
72	7	10	234426.0	C.4	9	61.02	149.96	43
72	7	10	121259.3	C.5	9	61.35	147.66	3
72	7	11	202818.7	C.5	12	62.12	149.80	37
72	7	12	2020 8.5	C.8	11	59.07	145.42	37
72	7	12	144912.6	C.3	8	61.77	146.94	14
72	7	13	101523.5	C.6	7	61.41	150.04	2
72	7	13	102559.0	C.5	13	62.04	149.37	37
72	7	13	74122.3	C.5	14	62.84	149.34	39
72	7	21	16 111.3	C.8	6	61.96	149.07	14
72	7	22	155316.2	C.6	9	64.08	147.70	13
72	7	24	115529.6	1.0	9	65.29	150.05	1
72	7	27	235719.6	C.5	11	64.61	149.74	16
72	7	29	44121.0	C.4	12	61.59	146.55	0
72	8	3	0 955.4	C.2	14	61.88	150.52	22
72	8	3	163247.0	C.6	9	65.33	149.56	2
72	8	5	2 236.1	C.5	9	61.44	150.30	0
72	8	5	34820.3	C.6	7	62.50	149.58	106
72	8	5	232346.0	C.2	10	63.11	148.27	82
72	8	6	01123.5	C.2	9	61.49	147.63	12
72	8	9	164740.6	C.6	6	62.69	149.33	77
72	8	12	2 038.5	C.5	15	61.51	149.75	37
72	8	20	201659.5	C.3	12	61.51	146.25	32
72	8	20	23359.5	C.6	6	62.95	149.36	77
72	8	21	05758.9	C.3	14	62.50	151.25	89
72	8	27	45437.6	C.4	11	65.27	150.62	22
72	8	28	15310.1	C.4	13	63.41	150.43	25
72	8	31	153359.5	1.3	12	59.98	151.38	36
72	8	31	174221.9	C.C	6	61.74	148.49	37
72	9	1	32111.4	C.3	12	65.18	148.64	23
72	9	3	1128 6.0	C.6	14	60.47	147.26	2
72	9	3	102240.5	C.7	13	60.47	147.33	7
72	9	5	55210.2	C.4	8	61.07	149.36	19
72	9	7	171925.0	C.4	15	61.67	150.71	36
72	9	9	15 941.5	C.2	9	61.41	143.63	104
72	9	11	203649.5	C.4	17	62.23	150.08	28

72	9	19	193630.7	0.4	16	61.97	148.30	36
72	9	28	81335.3	0.8	5	61.95	149.55	4
72	10	4	161037.3	0.3	10	62.10	149.74	36
72	10	16	75329.4	0.4	12	61.27	151.00	38
72	10	19	552 4.5	0.5	11	61.57	150.59	29
72	10	25	15 332.5	0.8	11	61.28	150.62	15
72	11	7	9 341.8	0.2	9	65.78	150.13	22
72	11	9	165224.4	0.7	6	61.56	149.36	14
72	11	11	54647.5	0.4	14	60.38	150.36	2
72	11	15	1220 2.9	0.4	11	61.48	147.98	80
72	11	18	22342.1	0.3	19	63.17	149.47	91
72	11	21	2 418.0	0.4	18	62.23	149.68	34
72	11	25	61018.9	0.7	9	65.42	149.92	1
72	11	25	43154.4	0.5	15	65.46	149.96	2
72	12	19	919 5.8	0.3	17	61.10	151.18	38
72	12	29	184631.7	0.4	15	61.45	151.12	74
73	1	1	191720.5	0.2	11	64.73	148.70	17
73	1	9	162712.4	0.4	9	64.11	148.66	0
73	1	10	12731.2	0.4	15	62.30	149.08	80
73	1	17	9 939.6	0.0	4	64.74	147.49	14
73	1	22	133955.1	0.4	18	61.99	149.41	37
73	2	7	185223.4	0.3	9	61.25	150.46	52
73	2	8	15 049.4	0.4	14	61.79	150.10	29
73	2	22	224551.0	0.7	6	65.63	149.89	7
73	2	23	61040.4	0.5	14	61.42	150.75	66
73	2	28	19 348.4	0.4	8	65.60	149.93	3
73	3	5	83049.2	0.2	14	63.71	148.41	109
73	3	10	434 8.7	0.3	14	62.04	150.75	30
73	4	14	14 956.5	0.2	12	60.47	150.35	27
73	4	28	17 130.9	0.5	12	61.54	151.54	92
73	5	6	61214.9	0.6	9	61.29	149.45	41
73	5	8	102612.2	0.2	12	63.12	150.74	99
73	5	9	17 011.8	0.4	11	61.52	144.09	89
73	5	12	1447 9.8	0.4	12	62.11	149.66	32
73	5	12	143914.1	1.0	5	64.96	150.27	11
73	5	15	21 236.9	0.2	9	61.32	147.56	21
73	5	16	224513.1	0.5	9	61.71	149.81	31
73	5	18	183256.5	0.2	14	63.05	150.90	116
73	5	21	34956.7	0.4	9	61.15	151.00	64
73	5	21	53629.9	0.4	13	61.79	150.11	31
73	6	4	4 427.5	0.5	8	61.32	147.01	20
73	6	4	85315.8	0.5	5	64.37	148.63	0
73	6	16	75043.5	1.2	9	64.79	147.02	11
73	6	18	149 6.2	0.4	9	65.09	146.97	21
73	6	23	162332.9	0.2	11	63.29	150.27	121
73	6	26	04151.7	0.0	4	59.42	144.97	15
73	6	29	10 348.8	0.4	11	61.84	150.69	68
73	7	12	172443.8	0.4	9	61.13	151.26	72
73	7	24	31952.8	0.4	7	61.14	151.34	81
73	8	3	81939.3	0.4	8	62.36	151.32	68

73	8	14	152451.4	C.2	7	65.02	150.21	6
73	8	19	173452.0	C.2	14	63.23	150.42	118
73	9	1	10 248.5	C.3	13	61.03	147.19	C
73	9	3	13 3 3.9	C.2	13	60.44	148.68	C
73	9	8	22226.9	C.4	13	61.24	147.45	8
73	9	15	11 5 9.3	0.2	10	61.70	151.23	83
73	9	26	233958.0	C.5	10	61.22	146.57	21
73	9	26	132055.9	C.3	16	61.93	147.39	45
73	9	27	33336.8	C.2	14	63.03	151.04	141
73	9	27	54813.6	0.5	11	62.91	150.57	C
73	9	28	03446.2	C.3	12	61.36	151.42	98
73	9	28	95417.1	C.4	10	61.89	151.31	104
73	10	3	34358.8	C.6	16	63.59	150.73	8
73	10	10	151255.9	C.3	16	62.09	149.58	37
73	10	14	181114.1	C.1	6	64.85	148.99	21
73	10	16	55335.1	C.5	10	60.94	147.03	1
73	10	21	5 5 2.7	0.4	10	61.85	149.99	31
73	10	27	1649 4.3	C.3	7	61.93	149.30	44
73	10	28	04654.3	C.4	15	61.72	147.00	38
73	10	30	74132.4	C.7	14	63.51	151.15	7
73	11	1	165022.6	C.3	17	61.99	150.59	37
73	11	3	55645.5	C.2	7	61.75	150.16	64
73	11	6	115954.4	C.3	11	61.91	152.04	150
73	11	9	213523.3	0.3	12	61.87	150.54	61
73	11	11	21550.2	C.3	10	61.18	146.77	20
73	11	17	151736.2	C.5	11	61.33	150.69	26
73	11	17	163430.6	C.8	10	61.42	150.89	34
73	11	20	4 258.1	C.3	14	62.12	149.11	13
73	11	30	143036.6	C.5	16	64.95	152.58	26
73	12	4	753 1.2	C.5	15	61.79	149.89	31
73	12	5	93621.9	C.7	5	60.12	148.82	99
73	12	13	92639.9	C.2	10	61.71	147.52	30
73	12	16	14941.7	C.3	16	62.57	148.21	35
73	12	17	154324.7	C.4	14	61.43	146.37	32
73	12	22	101949.5	C.1	4	63.29	148.60	42
73	12	26	1021 8.7	C.2	9	64.14	148.48	1

APPENDIX II

Appendix II consists of descriptions of several computer programs witten in the course of this work. All of the programs are written in FORTRAN (IV) and were designed to run on the University of Alaska IBM 360/40.

HYPLOT. This program reads a deck of cards which contains sets of hypocenter parameters, selects hypocenters which meet specified location and other constraints and writes a plot tape which will direct a Calcomp plotter to plot hypocenter cross sections. The projection geometry used for these cross sections is given in Figure 3-6.

The user specifies an origin, an azimuth, a thickness, and the number of cross sections to be plotted. The program finds geometrical vectors in the horizontal plane in the specified azimuthal direction and perpendicular to this direction with length equal to the thickness and the length, respectively, of the projection volume. It then finds vectors to all of the epicenters with respect to the specified origin and computes dot products of these vectors with the geometrical vectors. Using these dot products the program decides whether a given epicenter is inside the specified projection volume or not. Note that it is assumed that the depth never exceeds 300 km. The volume is 600 km long (in the direction perpendicular to the azimuth), 300 km deep and as thick as specified (in the

azimuthal direction). If a hypocenter is within the projection volume, the program computes coordinates in the plane perpendicular to the projection azimuth and scales these to the appropriate number of inches for the plotter and calls a plot subroutine which writes on tape instructions for plotting the projection of this hypocenter. After all of the hypocenters have been tested for a given projection volume, new unit vectors for the next adjacent projection volume in the specified azimuth are created and all of the hypocenters are tested for this volume. This process is repeated for the number of cross sections specified. Plot subroutines are called to mark and label coordinate boxes for each cross section and to plot the associated projection parameters: The origin in degrees of lattitude and longitude, the limiting origin (the tip of a vector in the specified azimuth from the origin with length equal to the thickness of the volume, also the origin for the next projection volume) in degrees of lattitude and longitude, the projection azimuth, the number of events plotted, the number sorted, and the thickness of the projection volume in kilometers. For an example see Figure 3-7. Following is a step-by-step explanation of the program (a copy of which follows this explanation):

```
      REAL L
      [illegible] ABC/'ABC'/,BLANK/'   '/
      DIMENSION HT0(49),HT15(49),HT40(49),HT50(49),HT75(49),HT100(49),HT
     *125(49),HT150(49),HT200(49),HT250(49),HT300(49),ISTN(50),STNLAT(50
     *),STNLON(50),STX(50),STY(50),STZ(50)
  910 FORMAT(A3,2F10.3)
  920 FORMAT(12F6.2)
  930 FORMAT(I2,3I3,I2,F4.1,F4.1,I3,F8.3,F7.3,I3)
  940 FORMAT(A3,10X,2I2,F3.1)
  945 FORMAT(' ISTA  RES  LAT       LON    DEP YRMODY HRMN SEC  SD  NO
     *     Y       Y'/)
  950 FORMAT(1X,A3,F5.1,F7.3,F9.3,I4,I3,2I2,I3,I2,F5.1,F4.1,I3,11X,F9.3,
     *F7.3)
  960 FORMAT('******',A3,' NOT IN STATION COORDINATE LIST******')
      C=180/3.14159
      READ(1,920) HT0,HT15,HT40,HT50,HT75,HT100,HT125,HT150,HT200,HT250,
     *HT300
      I=1
   50 READ(1,910) ISTN(I),STNLAT(I),STNLON(I)
      IF(ISTN(I).EQ.ABC) GO TO 90
      STAD=(90.-STNLAT(I))/C
      STAL=-STNLON(I)/C
      STX(I)=SIN(STAD)*COS(STAL)
      STY(I)=SIN(STAD)*SIN(STAL)
      STZ(I)=COS(STAD)
      I=I+1
      GO TO 50
   90 IMAX=I-1
      WRITE(3,945)
  100 READ(1,930,END=200) YR,MO,DY,HR,MN,SEC,SD,NO,ELAT,ELON,DEPTH
   99 READ(1,940) ISTA,IHR,IMN,SEK
      IF(ISTA.EQ.BLANK) GO TO 100
      DO 101 I=1,IMAX
      IF(ISTA.EQ.ISTN(I)) GO TO 102
  101 CONTINUE
      WRITE(3,960) ISTA
      GO TO 99
  102 ORTIME=HR*3600+MN*60+SEC
      ARTIME=IHR*3600+IMN*60+SEK
      IF(ARTIME.LT.ORTIME) GO TO 99
      T=ARTIME-ORTIME
      R=6371-DEPTH
      O=(90.-ELAT)/C
      L=-ELON/C
      SO=SIN(O)
      DELTA=ARCOS(STX(I)*SO*COS(L)+STY(I)*SO*SIN(L)+STZ(I)*COS(O))*C
      K=DELTA*2.
      EK=K
      DK=2.*(DELTA-EK/2.)
      K=K+1
      KR=(6396.-R)/25.
      GO TO (1,2,3,4,5,6,7,7,8,8,9,9,10),KR
    1 IF(DEPTH.GT.15) GO TO 13
      TH1L=HT0(K)
      TH2L=HT15(K)
      TH1=TH1L+(HT0(K+1)-TH1L)*DK
      TH2=TH2L+(HT15(K+1)-TH2L)*DK
      CRES=TH1+(TH2-TH1)*(6371.-R)/15.-T
      GO TO 20
   13 TH1L=HT15(K)
      TH2L=HT40(K)
      TH1=TH1L+(HT15(K+1)-TH1L)*DK
      TH2=TH2L+(HT40(K+1)-TH2L)*DK
      CRES=TH1+(TH2-TH1)*(6356.-R)/25.-T
      GO TO 20
    2 IF(DEPTH.LT.40) GO TO 13
      TH1L=HT40(K)
      TH2L=HT50(K)
      TH1=TH1L+(HT40(K+1)-TH1L)*DK
      TH2=TH2L+(HT50(K+1)-TH2L)*DK
      CRES=TH1+(TH2-TH1)*(6331.-R)/10.-T
      GO TO 20
    3 TH1L=HT50(K)
      TH1U=HT50(K+1)
      TH2L=HT75(K)
      TH2U=HT75(K+1)
      R1=6321.
      GO TO 11
    4 TH1L=HT75(K)
      TH1U=HT75(K+1)
      TH2L=HT100(K)
```

```
0067              Y=-6*II
0068              CALL SYMBOL(-3.,Y,.14,13,90.,-1)
0069           43 CONTINUE
0070              CALL SYMBOL(-4.25,-4.75,.21,'DEPTH IN KILOMETERS',90.,19)
0071              CALL SYMBOL(-3.67,-1.1,.21,'50',0.,2)
0072              CALL SYMBOL(-3.,-1.,.14,13,90.,-1)
0073              CALL SYMBOL(-3.13,.25,.21,'-100',0.,4)
0074              CALL SYMBOL(-2.13,.25,.21,'-200',0.,4)
0075              CALL SYMBOL(-1.,0.,.14,13,0.,-1)
0076              CALL SYMBOL(-1.13,.25,.21,'-100',0.,4)
0077              CALL SYMBOL(-4.,-4.75,.21,'PROJECTED EPICENTRAL DISTANCE IN KILOMETERS',0.,4
0078             *5*,0.,63)
0079              LAJ=LAI
0080              PAJ=PAI
0081              T=I*5/R
0082              L1I=LAI-ARSIN(SIN(A)*SIN(T))*C
0083              LI=L1I/C
0084              P=ACOS((COS(T)-SIN(L1I*SIN(LI))/COS(L1I/COS(LI))*C
0085              IF (180-A*A) 51,52,52
0086           51 PAI=PAI+P
0087              GO TO 53
0088           52 PAI=PAI-P
0089           53 PI=PAI/C
0090              AJX=SIX
0091              AJY=AIY
0092              AJZ=AIZ
0093              AIX=R*COS(LI)*COS(PI)
0094              AIY=R*COS(LI)*SIN(PI)
0095              AIZ=R*SIN(LI)
0096              UX=AIX-AJX
0097              UY=AIY-AJY
0098              UZ=AIZ-AJZ
0099              VX=(UZ*AJY-UY*AJZ)/R
0100              VY=(UX*AJZ-UZ*AJX)/R
0101              VZ=(UY*AJX-UX*AJY)/R
0102              0=0
0103              READ(0 7
0104              DO 14 L=1,K
0105              READ(7) FX,FY,FZ,YM
0106              DX=FX-AJX
0107              DY=FY-AJY
0108              DZ=FZ-AJZ
0109              DCTV=(DX*UX+DY*UY+DZ*UZ)/SI
0110              IF (DCTV-SI) 10,10,13
0111           10 IF (DCTV) 13,11,11
0112           11 DCTV=(DX*VX+DY*VY+DZ*VZ)/SI
0113              IF (SW*SW-DCTV*DCTV) 14,12,12
0114           12 X=DCTV/100
0115              IF(YM) 63,61,60
0116           61 Y=0
0117              GO TO 62
0118           63 Y=-YM/50
0119           62 CALL SYMBOL(X,Y,.14,4,0.,-1)
0120              0=0+1
0121           14 CONTINUE
0122              OK=K
0123              CALL NUMBER(.42,-6.75,.21,LAJ,0.,2)
0124              CALL NUMBER(1.63,-6.75,.21,PAJ,0.,2)
0125              CALL NUMBER(1.63,-7.25,.21,PAI,0.,2)
0126              CALL NUMBER(.42,-7.25,.21,LAI,0.,2)
0127              CALL NUMBER(1.32,-7.75,.21,47.,0.,-1)
0128              CALL NUMBER(1.75,-8.25,.21,0.,0.,-1)
0129              CALL NUMBER(3.01,-8.25,.21,OK,0.,-1)
0130              CALL PLOT(9.,0.,-3)
0131           19 CONTINUE
0132              CALL EXIT
0133              END
```

Step	Explanation
1 and 2	Specify the types of the variables.
3	Input format for hypocenter parameters. Same as equivalent portion of EPICENTER-II output format.
4 and 5	Initialize plot subroutines.
6 - 10	User specified initial conditions: LA1 and PA1, lattitude and longitude of origin (degrees); AZA, azimuth of projection with respect to north (degrees); N, number of cross sections desired; SI, thickness of projection.
11 - 21	Program specified initial conditions: SW, half length of projection volume; R, radius of the earth; C, radian to degree conversion factor; AIX, AIY, AIZ, rectangular coordinates of the origin; K, count of events read.
22 - 32	Read hypocentral parameters, test quality constraints, if o.k., compute rectangular coordinates of hypocenter and write them on disk: DEV, rms deviation of arrival time residuals; LH, PH, YH, lattitude, longitude, and depth of hypocenter; MAG, magnitude of event.

33	Set final count of number of events.
34 - 37	Find azimuth in radians.
38	Initialize do loop for number of cross sections.
39 - 78	Draw and label coordinate axis for plot of cross section.
79 - 101	Find limiting origin (next origin) and geometrical vectors in rectangular coordinates: AJX, AJY, AJZ, and AIX, AIY, AIZ, coordinates of origin and limiting origin, respectively; UX, UY, UZ and VX, VY, VZ, coordinates of azimuthal and perpendicular geometrical vectors, respectively.
102	Initialize count of events plotted in present cross section.
103	Prepare to search list of hypocenters.
104 - 121	Read hypocenter from disk list, compute coordinates (DX, DY, DZ) with respect to origin, form dot product with azimuthal (DCTU) and perpendicular (DCTV) vectors and decide if epicenter is within projection volume. If so, scale projection plane coordinates of hypocenter to inches and write them on the plot tape.

122	Redefine number of events read.
123 - 131	Finish annotating plot of cross section.
132 -133	Fini.

The following list gives the program sequence for control, program, and data cards for HYPLOT:

```
* $$ JOB HYPLOT
// PAUSE SET UP FOR JOB HYPLOT SCRATCH=181
// JOB HYPLOT, (billing no.), (name), C=D, T=5
// MT^ REW, SYSOOG
// EXEC $ WRIDGE
// OPTION LINK
// EXEC FFORTRAN
program HYPLOT (steps 1-133)
/*
// EXEC $FLINKEDT
// EXEC
data (EPICENTR-II output format)
99.0 (col. 27-30)
/*
/&
* $$ EOJ HYPLOT
```

STARES: Given observed station arrival times and the origin time and location of an earthquake, this program computes the Herin arrival time residual and the coordinate of the epicenter in inches about lattitude 62.5°N and longitude 149.5°W. These coordinates give a lambert conformal mapping about this point at a scale of 1 to 1 million. The output may be used as input to PLOTRES which will generate a plot tape to control the Cal Comp 30" plotter. The result is a plot of residual arrival times to a given station plotted at the epicenter of the event used.

The following list is a step-by-step explanation of the program (a copy of which follows this list):

Step	Explanation
1-3	Define variable types
4	Input format for station names and location
5	Input format for Herin travel time table.
6	Input format for event origin time and location (same as EPICENTR-II output)
7	Input format for observed arrival time at stations (same as EPICENTR-II input)
8	Heading format for STARES printed output
9	Output format for STARES (printed and punched)

10	Output message if an arrival-time card is read for a station not in the station coordinate list (see steps 4 and 14)
11	Radian to degree conversion
12	Read Herin travel time tables: HT0 is for zero km depth, HT15 for 15, HT40 for 40, etc.
13-23	Read station coordinate list. Dummy station ABC must be last card in the list. IMAX = number of stations in the list; STX (I), etc. are rectangular coordinates for these stations.
24	Write heading for printed output.
25	Read an event card.
26-30	Read associated set of reading cards.
31-32	If a reading card is read for a station not in list, write message.
33-46	Compute observed travel time and distance to station from event origin: T = travel time, DELTA = distance.
47-110	Find Herin travel time based on distance and depth. Four values are found which surround the desired value which is found by interpolation between these values in the next program segment.

111-120	Interpolate as above and compute residual arrival time, RES.
121-130	Compute coordinates of epicenter in inches about lattitude 62.5°N and longitude 149.5°W. These coordinates, X and Y, give a Lambert conformal mapping about this point at a scale of 1-1 million.
131	Write results on disk for later sorting by station.
132	Repeat for all input data (event plus reading cards).
133-139	Read results off disk, arrange by station and write printed list and punched card list.
140-142	Fini.

```
0001          IMPLICIT REAL*4 (A-Z)
0002          INTEGER I,J,K,L,M,N,II,N1
0003       90 FORMAT(11X,F3.1,9X,F6.1,2X,F5.1,2X,F3.0,7X,F3.1)
0004          CALL PLOTST
0005          CALL PLOT(6.,9.,23)
0006          LA1=40.75
0007          PA1=149.0
0008          AZA=0.0
0009          N=4
0010          S1=69.4
0011          SW=300
0012          R=6371
0013          C=180/3.1415927
0014          LA1=LA1
0015          PA1=PA1
0016          LT=LA1/C
0017          P1=PA1/C
0018          A1X=R*COS(LT)*COS(P1)
0019          A1Y=R*COS(LT)*SIN(P1)
0020          A1Z=R*SIN(LT)
0021          K=1
0022       31 READ(1,90) DEV,LH,PH,YH,MAG
0023          IF(LH.GE.99) GO TO 33
0024          IF(DEV.GT.2.0) GO TO 31
0025          TE=LH/C
0026          PE=PH/C
0027          EX=R*COS(TE)*COS(PE)
0028          EY=R*COS(TE)*SIN(PE)
0029          EZ=R*SIN(TE)
0030          WRITE(7) EX,EY,EZ,YH
0031          K=K+1
0032          GO TO 31
0033       33 K=K-1
0034          IF (180-AZA) 1,2,2
0035        1 A=(270-AZA)/C
0036          GO TO 3
0037        2 A=(AZA-90)/C
0038        3 DO 19 I=1,N
0039          CALL PLOT(3.,0.,2)
0040          CALL PLOT(3.,-6.,2)
0041          CALL PLOT(-3.,-6.,2)
0042          CALL PLOT(-3.,0.,2)
0043          CALL PLOT(0.,0.,2)
0044          CALL SYMBOL(0.,0.,.14,13.0,.,-1)
0045          CALL SYMBOL(-.35,.25,.21,112,0.,-1)
0046          CALL SYMBOL(.7a,.25,.21,'100',0.,3)
0047          CALL SYMBOL(1.,0.,.14,13.0,.,-1)
0048          CALL SYMBOL(2.,.),.14,13.0,.,-1)
0049          CALL SYMBOL(1.7a,.25,.21,'200',0.,3)
0050          CALL SYMBOL(2.7a,.25,.21,'300',0.,3)
0051          DO 41 II=1,5
0052          Y=-II
0053          CALL SYMBOL(3.,Y,.14,13,90.,-1)
0054       41 CONTINUE
0055          DO 42 II=1,5
0056          X=3-II
0057          CALL SYMBOL(X,-6.,.14,13.0,.,-1)
0058       42 CONTINUE
0059          CALL SYMBOL(-3.,-6.75,.21,'PROJECTION ORIGIN        N      W',0.,33)
             *3)
0060          CALL SYMBOL(-3.,-7.25,.21,'LIMITING ORIGIN          N      W',0.,33)
             *3)
0061          CALL SYMBOL(-3.,-7.75,.21,'AZIMUTH OF PROJ PLANE        DEGREES',0.,35)
             *,35)
0062          CALL SYMBOL(-3.,-8.25,.21,'NUMBER OF EVENTS PLOTTED       OF',0.,3
             *3)
0063          DO 43 II=1,4
0064          Y=-6.1*II
0065          AL=300-II*50
0066          CALL NUMBER(-3.93,Y,.21,AL,0.,-1)
```

```
0077                  TH2=HT100(K+1)
0078                  RT=6296.
0079                  GO TO 11
0080               5  TH1=HT100(K)
0081                  TH1=HT100(K+1)
0082                  TH2=HT125(K)
0083                  TH2=HT125(K+1)
0084                  RT=7271.
0085                  GO TO 11
0086               6  TH1=HT125(K)
0087                  TH1=HT125(K+1)
0088                  TH2=HT150(K)
0089                  TH2=HT150(K+1)
0090                  RT=6246.
0091                  GO TO 11
0092               7  TH1=HT150(K)
0093                  TH1=HT150(K+1)
0094                  TH2=HT200(K)
0095                  TH2=HT200(K+1)
0096                  RT=6221.
0097                  GO TO 12
0098               8  TH1=HT200(K)
0099                  TH1=HT200(K+1)
0100                  TH2=HT300(K)
0101                  TH2=HT300(K+1)
0102                  RT=6171.
0103                  GO TO 12
0104               9  TH1=HT300(K)
0105                  TH1=HT300(K+1)
0106                  TH2=HT400(K)
0107                  TH2=HT400(K+1)
0108                  RT=6121.
0109                  GO TO 12
0110              10  TH1=HT400(K)
0111                  DES=TH1+(HT400(K+1)-TH1)*DK-T
0112                  GO TO 20
0113              11  TH1=TH1+(TH1H-TH1L)*DK
0114                  TH2=TH2+(TH2H-TH2L)*DK
0115                  DES=TH1+(TH2-TH1)*(RT-R)/25.-T
0116                  GO TO 20
0117              12  TH1=TH1L+(TH1H-TH1L)*DK
0118                  TH2=TH2L+(TH2H-TH2L)*DK
0119                  DES=TH1+(TH2-TH1)*(RT-R)/50.-T
0120              20  DES=DES
0121                  AKM=0.+150.13-1.7264*FLAT
0122                  Y=(FLON-149.5)*AKM*69.
0123                  IF(Y.GT.0.) GO TO 110
0124                  THETA=ATAN(-Y/2990.)
0125                  GO TO 120
0126             110  THETA=ATAN(Y/2990.)
0127             120  DIST=SQRT(Y*Y+8610333.)-2990.)*COS(THETA)
0128                  Y=(FLAT-62.5)*111.47*COS(TH
0129                  X=X.2994
0130                  Y=Y.2994
0131                  WRITE(71 ISTA,RES,FLAT,FLON,DEPTH,YR,MO,DY,HR,MN,SEC,SD,NO,X,Y
0132                  GO TO 99
0133             700  DO 710 I=1,1***
0134                  READ 7
0135             705  READ(7,END=7131 ISTA,RES,FLAT,FLON,DEPTH,YR,MO,DY,HR,MN,SEC,SD,NO,
                    *X,Y
0136                  IF(ISTA.NE.ISTN(I)) GO TO 705
0137                  WRITE(2,753)ISTA,RES,FLAT,FLON,DEPTH,YR,MO,DY,HR,MN,SEC,SD,NO,X,Y
0138                  WRITE(3,753)ISTA,RES,FLAT,FLON,DEPTH,YR,MO,DY,HR,MN,SEC,SD,NO,X,Y
0139                  GO TO 705
0140             710  CONTINUE
0141                  CALL EXIT
0142                  END
```

The following list gives the program sequence for control, program and data cards for STARES:

```
*  $$ JOB STARES
// JOB STARES, (billing no.), (name), C=D, T=30
// EXEC $WRIDGE
// OPTION LINK
// EXEC FFORTRAN
program STARES (steps 1-142)
/*
// EXEC $FLNKEDT
// EXEC
data - Herin travel time tables
data - station coordinate list (must end with ABC)
data - sets of event card followed by reading
       cards for that event followed by a blank card.
/*
/&
* $$ EOJ STARES
```

APPENDIX III

CALIBRATION: Calculation of Harmonic System Magnification

Introduction

Since the data used in this study were obtained from several different seismograph systems which have been variously calibrated (some not at all) it is desirable to use a uniform method for calculating magnifications for each of the systems used. This calculation requires knowledge of the characteristics of each component in the seismograph system: Seismometer, amplifier, telemetry system and recorder. To the extent possible an attempt has been made to calibrate each of these components separately except for the seismometers whose response has been calculated theoretically since no shake table was available. Additionally these calibrations and calculations were compared to other available calibrations to check their reliability.

The harmonic system magnification, M(f), is given by the equation

$$M(f) = S(f)\ A(f)\ T(f)\ R(f) \qquad \text{(A3-1)}$$

where S(f) is the seismometer sensitivity in V/mm

A(f) is the amplifier gain in V/V

T(f) is the telemetry system gain in V/V

R(f) is the recorder-display sensitivity in mm/V

Calibration calculations for each of these components are given in the following sections.

Seismometer sensitivity

For a theoretical discussion of seismometry see Heiland, 1951. Eaton (1973) gives the following equation for the sensitivity of a seismometer as seen at the amplifier input:

$$S(f) = \frac{2\pi f^3 G_e}{[(f_o^2 - f^2)^2 + 4\lambda^2 f_o^2 f^2]^{1/2}} \qquad \text{(A3-2)}$$

where f is frequency in Hz,

G_e is the effective main coil generator constant in V/mm/s,

f_o is the natural frequency of seismometer in Hz,

λ is the damping factor

with $$G_e = G \frac{R_x}{R_c + R_x} \qquad \text{(A3-3)}$$

where G = main coil generator constant, V/mm/s

R_x = external damping resistance, Ω

R_c = effective main coil resistance, Ω

Equation A3-2 was tested by using it to calculate the response of a Geotech 18300 seismometer whose instrumental parameters and observed sensitivity are given in Figure 12, page 36 of the "Preliminary Operation and Maintenance Manual/Portable Short-Period Seismometer, Model 18300" published on 8 April 1965 by the Geotechnical Corporation, 3401 Shiloh Road, Garland, Texas. Table A3-1 compares the theoretical and observed sensitivities for this seismometer. The instrumental parameters and the

Table A3-1

Theoretical response of the Geotech 18300 seismometer compared to observed sensitivity in volts/millimeter.

Instrumental parameters: f_o = 0.8s, λ= .67, M = 5.0kg, R_c = 160Ω, R_x = 410Ω, R_{cd} = 381Ω

f	0.4	0.6	0.8	1.0	2.0	4.0	5.0	6.0	7.0	8.0	10.	15.	20.	30.
S(f)	.062	.192	.372	.552	1.25	2.50	3.13	3.75	4.37	5.00	6.24	9.36	12.5	18.7
Obs.	.048	.185	.377	.545	1.14	2.37	3.00	3.58	4.10	4.86	6.00	8.90	11.5	18.1
Ratio	(1.29)	1.04	1.01	1.01	1.10	1.05	1.04	1.05	1.07	1.03	1.04	1.05	1.09	1.03

Average Ratio = 1.05 (excluding 1.29)

observed sensitivity taken from the above manual are given in the first and fourth lines, respectively, of the table. The theoretical sensitivity, S(f), given in line three was calculated from equations A3-2 and A3-3. The main coil generator constant, G in V/mm/s, was determined using the relation given on page 22 of the above manual:

$$G = (4\pi f_o M R_{cd})^{1/2} \qquad \text{(A3-4)}$$

where f_o is the natural frequency of the seismometer in Hz,

M is the mass of the inertial mass in kg and

R_{cd} is the critical damping resistance in ohms,

which holds if the open circuit damping is negligible. The ratio of the largest to the smallest of the theoretical and observed sensitivities is given on line five of the table and the average of these ratios (excluding the ratio for 0.4 Hz which had a percentage difference almost five times the average) is given on line six. This table shows that, on the average, the theoretical sensitivity is within five percent of the observed. Since this corresponds to an error of two-hundredths of a magnitude, one can conclude that equation A3-2 is satisfactory for determining the sensitivity of a Geotech 18300 seismometer.

The sensitivity, S(f), of the Geotech Ranger SD-215 seismometer was calculated in the same manner as was the 18300 and is given in column two of Table A3-2. The instrumental parameters were obtained from page 26 of the "Unattended Seismological Observatory

Table A3-2

Theoretical response of the Geotech Ranger SD-215 seismometer compared to observed sensitivity in volts/millimeter

Freq.	S(f)	$O_1(f)$	$O_2(f)$	$O_3(f)$	$O_4(f)$	$\overline{O}(f)$	$\frac{\overline{O}(f)}{S(f)}$
Hz	V/mm	V/mm	V/mm	V/mm	V/mm	V/mm	
0.10	.00078	.00174	.00079	.00030	.00104	.00097	1.24
0.15	.00265	.00298	.00278			.00288	1.09
0.20	.00628	.00602	.00646	.00913	.00723	.00721	1.14
0.30	.0211	.0185	.0209			.0197	.934
0.40	.0498		.0564	.0562		.0563	1.13
0.50	.0958	.0827	.111	.109		.101	1.05
0.60	.161	-----	.186		.184	.185	1.14
0.70	.244	.222	.281			.252	1.03
0.80	.341	-----	.393			.393	1.15
1.00	.561	.569	.672	.556	.648	.611	1.09
1.50	1.08	1.10	1.21			1.16	1.07
2.00	1.53	1.62	1.74	1.55	1.69	1.65	1.08
3.00	2.35	2.41	2.66			2.54	1.08
4.00	3.13	3.02	3.45			3.24	1.04
5.00	3.93	3.55	3.98	4.12	3.92	3.89	.99
6.00	4.72	4.03	4.60			4.32	.92
7.00	5.50	4.66	5.08			4.87	.89
8.00	6.28	4.67	5.43			5.05	.80
10.0	7.85	4.31	5.49	5.78	5.42	5.25	67
15.0	11.8						
20.0	15.7						
30.0	23.5						

<1.08>

(Development Report)" (USO), SC-M-67-613A, published in November 1968 by the Optical and Detection Division 9213 of Sandia Laboratories, Albuquerque, New Mexico. They are as follows: f_o=1.0, λ=0.7, R_c=2000Ω, R_x=2700Ω, and G_e=125V/m/S. It should be noted that the natural frequency of the SD-215 is adjusted by means of six small rod magnets and that these magnets also provide some of the damping. The USO system is designed so that when operating into the 2700Ω input impedance of the amplifier, the seismometer is .7 critically damped. The calculation of S(f) is compared to four observed sensitivities which are given in columns three through six. The first observed sensitivity, $0_1(f)$, was determined from a cal-coil test run by Ron Rasmussen and the author on 15 May 1973. A block diagram of the equipment configuration for this test is shown in Figure A3-1 and the reduced data are given in Table A3-3.

The sensitivity, $0_2(f)$, given in column four was derived by dividing the combined seismometer-amplifier response from Figure 9, page 29, of the USO report by the Sandia amplifier response given in Table A3-6. The sensitivities, $0_3(f)$ and $0_4(f)$ given in columns 5 and 6 were obtained, respectively, from the Fairbanks 2 August, 1967 and Vernal 16 August, 1967 USO field reports on file at the Seismology Laboratory, University of Alaska, Fairbanks. The average observed sensitivity $\overline{0}(f)$ is given in column seven and is compared to the theoretical sensitivity by means of the

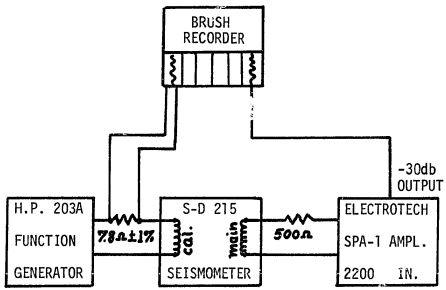

2700 EXTERNAL RESISTANCE YIELDS .7 CRITICAL DAMPING

LOW PASS FILTER CUTOFF: 5HZ. ATTEN.: -48-30 = -78db

Figure A3-1. SD-215 seismometer calibration.

Table A3-3
Calibration of the Ranger SD-215 seismometer S/N 106
15 May 1973 Ron Rasmussen and John Davies

f	A_r	G_r	A_a	G_a	i	V_a	G(-78)	V_s	Y	S
Hz	div	mv/div	div	mv/div	ma	volts	V/V	mv	µm	V/mm
.100	36.7	1.00	16.6	5.00	4.68	.0830	6.93	11.98	8424	.00174
.150	36.5	"	31.1	5.00	"	.1555	17.1	9.09	3744	.00298
.200	36.6	"	30.0	10.0	"	.3000	29.0	10.34	2106	.00602
.300	36.6	"	36.8	20.0	"	.7360	52.2	14.09	936.0	.0185
.500	36.4	"	37.2	50.0	"	1.860	81.9	22.71	337.0	.0827
.700	36.6	"	29.9	100	"	2.990	96.1	31.11	171.9	.222
1.00	36.6	"	40.9	100	"	4.090	104.7	39.06	84.24	.569
1.50	36.4	"	38.9	100	"	3.890	115.7	33.62	37.44	1.10
2.00	36.6	"	31.1	100	"	3.110	111.9	27.79	21.06	1.62
3.00	36.4	"	20.5	100	"	2.050	111.9	18.32	9.360	2.41
4.00	36.5	"	28.0	50.0	"	1.400	108.1	12.95	5.265	3.02
5.00	36.3	"	18.2	50.0	"	.910	93.3	9.75	3.370	3.55
6.00	36.4	"	27.3	80.0	"	.546	70.8	7.71	2.340	4.04
7.00	18.2	2.00	32.3	10.0	4.66	.323	49.6	6.51	1.712	4.66
8.00	18.2	"	17.9	10.0	"	.179	35.7	5.01	1.311	4.69
10.0	18.3	"	11.1	5.00	"	.0555	18.8	2.95	.8388	4.31
15.0	18.0	"	(3.7)	2.00	"	(.00740)	----	----	-----	----
15.0	32.2	10.0	(6.1)	5.00	41.2	.0350	5.72	6.12	3.296	(2.28)
20.0	32.2	10.0	(5.1)	5.00	41.2	.0255	2.57	10.76	1.554	(7.11)
30.0	31.9	10.0	(3.9)	5.00	41.2	.0195	.711	27.43	.8240	(40.7)

Column Headings:

f, frequency
A_r, p-p amplitude resistor voltage
G_r, Brush recorder sensitivity for A_r
A_a, p-p amplitude amplifier output
G_a, Brush recorder sensitivity for A_a
i, current = $A_r G_r / 7.82$
V_a, amplifier output voltage = $A_a G_a$
G(-78), SPA-1 amplifier response with 78 db attenuation = G(-48) : 31.62
V_s, seismometer output voltage = $V_a / G(-78)$
Y, equivalent ground motion = C_1 / f^2 where $C = .018$ m/A·s^2
S, seismometer sensitivity = V_s / Y

ratio $\overline{O}(f)/S(f)$ given in the last column. A weighted average of this ratio for f=0.15 to f=4.0 is given in brackets at the bottom of this column. The weighting factor was simply the number of values averaged to obtain $\overline{O}(f)$. The ratio for f=0.10 was excluded because it indicated a percent variation of three times the weighted average, probably representing the increasing significance of noise in the measurement of O(f) at low voltage levels. It is remarked in the USO field notes referenced above that the expected linear increase in sensitivity of a seismometer when measured in a cal-coil test begins to fall off at higher frequencies due to a transformer-like interaction of the coils. The systematic decline of the observed values relative to the theoretical values at f greater than 4Hz is attributed to this effect and is the reason for excluding the $\overline{O}(f)/S(f)$ ratios in this range. The weighted average ratio of 1.08 indicates that the observed sensitivities were on the average eight percent higher than the theoretical values (which would imply an error in magnitude determination of three hundredths of a magnitude). However, during a 1Hz shake test described on page 33 of the USO report sensitivities of .566 and .574 V/mm were obtained which average only two percent higher than the S(1)=.561 value, and cal-coil tests of the same seismometers yielded 1Hz sensitivities of .534 and .533 V/mm which average five percent less. The theoretical sensitivity appears to be within plus or minus eight

per cent of the measured sensitivity and is therefore an adequate estimate of the response of the Geotech Ranger SD-215 seismometer.

Amplifier gain

The amplifier response, A(f), includes the filter response and any attenuation due to gain settings, dividers, or limiters which is introduced between the amplifier and the telemetry system. An Electro-Tech SPA-1 and a Sanda USO amplifier were calibrated by Ron Rasmussen and the author on 15 May 1973 (the raw data is on file at the Seismology Laboratory, Geophysical Institute, University of Alaska, Fairbanks). The equipment configuration is shown in Figure A3-2 and the reduced data is given in Tables A3-4 and A3-5. Column headings for these tables are: A_i and A_o, the function generator and amplifier outputs, respectively as measured on the six channel Brush recorder in divisions; G_b, the Brush sensitivity in millivolts per division; $V_i = A_i \times G_b \times 10^{-3}$; $V_o = A_o \times G_b \times 10^{-3}$; $G_{-12} = 2.94 \times 10^3 \times$ Vo/Vi, the amplifier gain with 12db of attenuation switched in; $G_o(db) = G_{-12}(db) + 12$, the amplifier gain with zero attenuation given in db; $G_o(kV/V) = G_{-12}(kV/V) \times 3.981$, the amplifier gain with zero attenuation given in kilovolts per volt.

The SPA-1 calibration is compared in Table A3-6 to values scaled from Figure 1-2, page 1-4 of the "Operators Manual/Short Period Amplifier Systems", No. L4-32A published by Electro-Technical Labs. Division, Mandrel Industries, Inc., P. O. Box

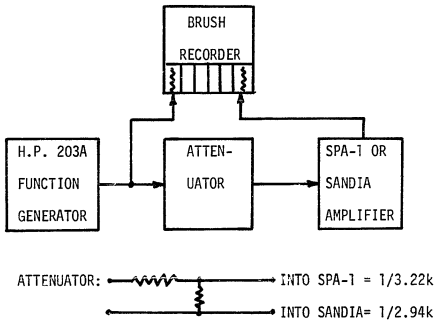

Figure A3-2. Amplifier calibration.

Table A3-4

Calibration of the SPA-1 amplifier S/N 196
Cutoff frequency: 5Hz Attenuation: 48db (-18 and -30 output)
Ron Rasmussen and John Davies, 15 May 1973

f	A_i	A_o	G_b	V_1	V_o	G_{-48}	G_o
Hz	div	div	mv/div	volts	volts	kV/V	db
.05	21.8	5.6	2	1.09	.0112	.033	78.4
.10	21.8	37.0	2	1.09	.0740	.219	94.8
.15	21.6	36.3	5	1.08	.182	.542	102.7
.20	21.7	31.0	10	1.09	.310	.916	107.2
.30	21.5	27.7	20	1.08	.554	1.65	112.3
.40						2.16	
.50	21.8	43.8	20	1.09	.876	2.59	116.3
.60						2.90	
.70	21.6	20.4	50	1.08	1.02	3.04	117.7
.80						3.20	
1.0	21.8	22.3	50	1.09	1.12	3.31	118.4
1.5	21.8	24.7	50	1.09	1.24	3.66	119.3
2.0	21.8	24.0	50	1.09	1.20	3.54	119.0
3.0	21.7	24.0	50	1.09	1.20	3.54	119.0
4.0	21.7	23.2	50	1.09	1.16	3.42	118.7
5.0	21.7	20.0	50	1.09	1.00	2.95	117.4
6.0	21.6	15.0	50	1.08	.750	2.24	115.0
7.0	21.6	26.4	20	1.08	.528	1.57	111.9
8.0	21.6	18.9	20	1.08	.378	1.13	109.1
10.0	21.5	19.9	10	1.08	.199	.593	103.5
15.0	21.4	12.0	5	1.07	.060	.181	93.2
20.0	21.3	12.5	2	1.07	.025	.0752	85.5
30.0	21.2	7.4	1	1.06	.0074	.0225	75.0
50.0	21.0	2.5	1	1.05	.0025	.00767	65.7

Table A3-5

Calibration of the Sandia USO amplifier S/N R5415 at -12db
Ron Rasmussen and John Davies, 15 May 1973

f	A_i	A_o	G_b	V_i	V_o	G_{-12}	G_o	G_o
Hz	div.	div.	mv/div	volts	volts	kV/V	db	kV/V
.05	28.5	25.1	100	1.43	2.51	5.16	86.3	20.54
.10	28.5	32.0	200	1.43	6.40	13.2	94.4	52.55
.20	28.5	19.3	500	1.43	9.65	19.8	97.9	78.83
.30	28.5	21.1	500	1.43	10.55	21.7	98.7	86.39
.40								90.15
.50	28.3	22.2	500	1.42	11.10	23.0	99.2	91.56
.60								93.33
.70	28.1	22.5	500	1.41	11.25	23.5	99.4	93.56
1.0	28.1	22.5	500	1.41	11.25	23.5	99.4	93.56
1.5	28.1	22.3	500	1.41	11.15	23.2	99.3	92.36
2.0	28.1	22.1	500	1.41	11.05	23.0	99.2	91.56
3.0	28.5	21.5	500	1.43	10.75	22.1	98.9	87.96
4.0	28.4	20.2	500	1.42	10.10	20.9	98.4	83.20
5.0	28.3	18.8	500	1.42	9.40	19.5	97.8	77.63
6.0	28.4	43.2	200	1.42	8.64	17.9	97.1	71.26
7.0	28.3	39.9	200	1.42	7.98	16.5	96.3	65.69
8.0	28.3	36.1	200	1.42	7.22	14.9	95.4	59.32
10.0	28.2	30.1	200	1.41	6.02	12.6	94.0	50.16
15.0	28.3	18.8	200	1.42	3.76	7.78	89.8	30.97
20.0	28.2	25.0	100	1.41	2.50	5.21	86.3	20.74
30.0	28.0	12.1	100	1.40	1.21	2.54	80.1	10.11
50.0	27.5	21.9	20	1.38	.438	.933	71.4	3.71

Table A3-6

Comparison of SPA-1 amplifier calibration to manual

f	f5	f7	f10	Test	Ratio
0.40	.540M	.540M	.540M		<.08>
0.60	.719	.719	.719		
0.80	.815	.815	.815		
1.00	.876	.876	.876	.832M	.950
2.00	.948	.975	.975	.891	.940
4.00	.792	.941	1.00	.861	1.09
5.00	.674	.874	1.00	.741	1.10
6.00	.511	.786	.961	.562	1.10
7.00	.341	.694	.920	.394	1.16
8.00	.259	.580	.860	.285	1.10
10.0	.143	.345	.719	.150	1.05
15.0	.0511	.143	.350	.0457	.894
20.0	.0191	.0569	.146	.0188	.984
30.0	(.00566)	.0168	.0475	.00562	.993

35306, Houston, Texas 77036. The column headings for this table are: f, frequency in Hertz; F5, F7 and F10, SPA-1 response in millions of volts per volt with low-pass filter cut off frequency of 5, 7 and 10 Hertz, respectively; Test, G_o from Table A3-4 in millions of volts per volt; Ratio, Test/F5 with the average percent variation given in brackets at the top of the column. The average variation is eight per cent which is satisfactory agreement.

There is no frequency response for the Sandia amplifier given in the USO report; however, there is a sensitivity curve given on page 29 for the combined response of the Ranger SD-215 seismometer and the Sandia USO amplifier. In Table A3-7 values scaled from this curve are compared to the product of the individual seismometer and amplifier responses given in Tables A3-2 and A3-5 respectively. Row headings for Table A3-7 are: Freq., frequency in Hertz; SA(f), combined seismometer-amplifier sensitivity from page 29 of the USO report in kilovolts per millimeter; S(f)A(f), product of the seismometer and amplifier responses given in Tables A3-2 and A3-5 respectively (kV/mm); Ratio, SA(f)/S(f) A(f). The average of the percent variations given in the Ratio row is 15% corresponding to an error in magnitude determination of six hundredths of a magnitude. Although this comparison gives an average variation twice that of the previous checks, it still indicates satisfactory agreement. It should be noted that there are twice as many sources of error in this comparison.

Table A3-7

Combined SD-215 seismometer - Sandia USO amplifier sensitivity in kilovolts per millimeter.

f	0.10	0.15	0.20	0.30	0.40	0.50	0.60	0.70	0.80	1.00	1.50	2.00	3.00	4.00	5.00	6.00	7.00	8.00	10.0
SA(f)	.0416	.186	.509	1.81	5.09	10.2	17.4	26.3	36.8	62.9	112.	160.	234.	287.	309.	328.	334.	322.	276
S(f)A(f)	.0916	.199	.475	1.60	----	7.57	----	20.8	----	53.3	102.	148.	212.	251.	275.	288.	306.	278.	216
Ratio	.454	.935	1.07	1.13	----	1.35	----	1.26	----	1.18	1.10	1.08	1.10	1.14	1.12	1.14	1.09	1.16	1.28

Telemetry system

The seismograph systems used in this study employed three modes of connecting the amplifier output to the recording devices: (1) direct connection, (2) phone lines and (3) VHF telemetry. For all three cases the gain of the telemetry link was one. In the first case this is obvious. In the second and third cases the amplifier output drives a voltage-controlled-oscillator (VCO) and the signal is transmitted in an FM mode to a discriminator which feeds the recording device. In these cases the VCO-discriminator pairs are always adjusted to a gain of one. Therefore T(f) in equation A3-1 is always taken to be unity. This factor is, however, a possible source of error because VCO's and discriminators do drift somewhat.

Recorder-display system

Both the Seismology Laboratory at the University of Alaska and the Palmer Observatory record their seismic data on a Geotech Develocorder and display the analog trace on a Geotech Film Viewer. The Palmer Observatory employs automatic calibration units which daily feed one Hertz sinusoidal signals into the seismic amplifiers and hence calibrate the entire amplifier-telemetry-recorder-viewer system. For these stations the magnification given by Palmer is used.

For the University of Alaska stations a calibration of the recorder display system was made by Ron Rasmussen and Doug

VanWormer on 20 April 1971. The equipment configuration for this test is shown in Figure A3-3 and the reduced data is given in Table A3-8. As is shown in the figure the calibration signal was fed in ahead of the fixed-value resistive attenuator and the output was measured on the FilmViewer. The sensitivities given in the table are in millimeters per volt. Note that for most of the stations the low gain trace originated in the -30db amplifier output, but for some the discriminator output was fed into two develocorder channels, one of which had roughly 10 times more attenuation ahead of it than the other.

For the Skwentna temporary stations the recorder-display system was calibrated using the ten Hertz time-code carrier signal as shown in Figure A3-4. This signal which was recorded on one channel of the tape recorder was fed into all of the channels of the Sanborn chart recorder. The calibration data for this test are given in the top part to Table A3-9. Row headings for this portion of the table are: $A_5(10)$, trace amplitude in divisions with an attenuation of 500 times (A500); $R_5(10) = A_5(10) \div 3.20$, reponse at ten Hertz with A500 in divisions per volt; $R_5(10)$, response at ten Hertz and A500 in millimeters per volt; $R_2(10)$, response at ten Hertz and A200 in millimeters per volt.

The above calculation gives the response at one frequency and assumes that the tape recorder channels all respond identically.

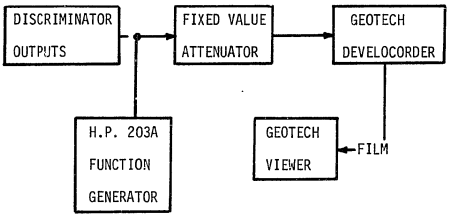

Figure A3-3. Develocorder-Viewer calibration.

Table A3-8
Develocorder Calibration 20 April 1971 Ron Rasmussen and Doug VanWormer
Sensitivity given in millimeters per volt

Galvanometer number and seismic data designator code

Freq.	A-PAX	B-SVW-H	1-SVW-L	2-MIN	3-TNN	4-MCB-H	5-MCB-L	6-BIG	7-GLM-H	8-GLM-L
.4	106.2	107.1	112.0	85.7	95.2	100.0	8.8	102.5	102.5	9.5
.6	106.2	"	109.5	"	"	"	"	99.0	"	"
.8	105.7	"	"	88.1	"	"	"	97.5	"	"
1.0	104.8	105.7	112.0	"	"	"	"	95.0	"	9.3
2.0	106.2	108.6	109.5	"	"	99.0	"	"	"	"
4.0	106.2	110.5	112.0	"	"	100.0	"	"	"	9.5
5.0	106.2	"	113.1	88.5	96.4	"	8.6	96.2	"	"
6.0	106.2	"	114.3	89.0	97.6	"	8.8	97.5	"	"
7.0	110.5	112.4	"	89.7	98.2	"	"	98.7	103.0	"
8.0	114.8	114.3	"	90.5	100.0	"	"	100.0	103.5	"
10.0	114.8	"	"	"	"	"	"	"	"	"
15.0	101.0	95.2	100.0	81.0	88.1	81.0	7.4	85.0	90.0	8.3
20.0	71.4	64.3	66.7	57.1	61.9	61.0	5.0	62.5	60.0	5.9
30.0	34.3	31.0	33.3	23.8	27.6	23.8	2.4	29.5	29.0	2.6

Galvanometer number and seismic data designator code

Freq.	9-Time	10-PJD-H	11-PJD-L	12-BRH	13-SCM-H	14-SCM-L	15-HPP	16-BLR-H	C-BLR-L	D-NCK-L
.4	3.60	97.5	8.8	95.0	85.0	90.0	107.5	91.0	67.5	11.5
.6	3.60	"	"	"	82.5	"	"	90.0	64.0	"
.8	3.56	"	"	"	"	"	"	89.0	65.0	"
1.0	3.58	98.0	"	92.5	"	87.5	"	82.5	61.5	11.3
2.0	3.60	97.5	"	"	80.0	90.0	"	85.0	"	"
4.0	3.62	"	"	"	"	"	"	87.5	56.0	11.4
5.0	3.64	98.2	8.9	93.7	81.2	"	"	"	53.0	11.6
6.0	3.64	99.0	9.0	95.0	82.5	"	"	"	50.0	11.9
7.0	3.67	100.7	9.1	"	"	"	108.7	89.5	47.5	12.1
8.0	3.70	102.5	9.3	"	"	"	110.0	91.5	45.0	12.4
10.0	3.60	"	"	"	80.0	"	"	92.5	37.5	12.9
15.0	3.00	97.5	8.4	77.5	65.0	75.0	95.0	86.0	25.0	11.9
20.0	2.00	65.0	6.0	55.0	42.5	55.0	63.5	60.0	17.5	8.0
30.0	1.00	28.5	2.6	24.5	20.0	25.0	27.5	25.0	10.0	3.0

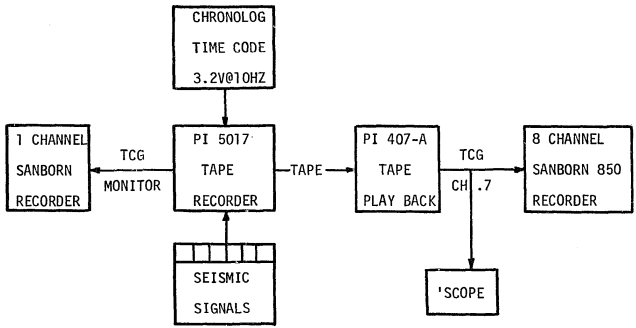

Figure A3-4. Skwentna recorder-display system calibration.

Table A3-9

Calibration Data for Skwentna Tape Recorder-Playback-Display System

Sanborn Ch. Data Code	2 SKN	3 SKE	4 SKV	5 SNL	6 KCH	8 TLN
A_5(10) div	18.0	17.0	17.5	17.0	15.0	13.5
R_5^2(10) div/V	5.63	5.31	5.47	5.31	4.69	4.22
R_5^2(10) mm/V	4.47	4.22	4.34	4.22	3.72	3.35
R_2^2(10) mm/V	11.1	10.6	10.9	10.6	9.30	8.38

Sanborn frequency response in cm at A200 with 6.2 Vp-p sinusoidal input

5Hz	2.45	2.55	2.45	2.55	2.50	2.45
10	2.38	2.55	2.40	2.52	2.40	2.40
20	2.30	2.50	2.30	2.50	2.32	2.20
30	2.30	2.45	2.30	2.50	2.25	2.10
40	2.35	2.48	2.32	2.55	2.30	2.05
50	2.45	2.50	2.40	2.55	2.35	2.05
60	2.60	2.55	2.46	2.60	2.35	2.10
70	2.75	2.60	2.60	2.70	2.40	2.12
80	2.75	2.55	2.53	2.55	2.05	2.20
90	2.50	2.20	2.23	2.10	1.95	2.20
100	2.30	1.80	1.90	1.80	1.55	2.00

In the following it is further assumed that the tape recorder and playback have a flat response over the frequency range .5 to 10Hz. The eight channel Sanborn recorder was calibrated at several frequencies in this range and this data is given in the lower part of Table A3-9. Note that the playback into the Sanborn recorder was made at ten times real time so that the Sanborn was calibrated at 5,10,20,30,...,100Hz corresponding to .5,1.0,2.0,3.0,...10.Hz in terms of the seismic data. The Sanborn frequency response data given in the lower part of Table A3-9 were normalized to the recorder-display system sensitivity at ten Hertz given in the upper part of the table and the resultant tape recorder-playback-display system response is given in Table A3-10.

Magnification

A summary of the seismometer and amplifier response data presented in preceeding sections is given in Table A3-11. The seismometer responses are calculated using equation A3-2 and the instrument parameters given at the bottom of Table A3-12. The first two sensitivities are for Geotech 18300 seismometers and the third is for the SD-215. The first two amplifier responses are for the Electro-Tech SPA-1 with 5 and 10 Hertz cutoff frequencies respectively. The first (5Hz) response is taken from the calibration data given in Table A3-4 and the second (10Hz) from data in the Electro-Tech manual referenced above and given in Table A3-6.

Table A3-10

Skwentna Tape Recorder-Playback-Display System

Sensitivity in Millimeters per Volt

f Hz	CH.2 SKN	CH.3 SKE	CH.4 SKV	CH.5 SNL	CH.6 KCH	CH.8 TLN
0.5	11.8	15.0	14.1	15.0	15.0	10.3
1.0	11.5	15.0	13.8	14.8	14.4	10.1
2.0	11.1	14.7	13.2	14.7	13.9	9.22
3.0	11.1	14.4	13.2	14.7	13.5	8.80
4.0	11.3	14.6	13.3	15.0	13.8	8.59
5.0	11.8	14.7	13.8	15.0	14.1	8.59
6.0	12.5	15.0	14.1	15.3	14.1	8.80
7.0	13.3	15.3	14.9	15.9	14.4	8.88
8.0	13.3	15.0	14.5	15.0	12.3	9.22
9.0	12.0	13.0	12.8	12.4	11.7	9.22
10.	11.1	10.6	10.9	10.6	9.30	8.38

Table A3-11

Summary of Seismometer and Amplifier Responses

f	$S_1(f)$	$S_2(f)$	$S_3(f)$	$A_1(f)$	$A_2(f)$	$A_3(f)$
Hz	V/mm	V/mm	V/mm	kV/V	kV/V	kV/V
.10	.000469	.000414	.00078	55.0	-----	52.6
.20	.00374	.00331	.00628	230.	-----	78.8
.30	.0126	.0111	.0211	414.	-----	86.4
.40	.0298	.0263	.0498	542.	540.	90.2
.50	.0571	.0506	.0958	650.	620.	91.6
.60	.0957	.0846	.161	728.	719.	93.3
.70	.146	.129	.244	763.	765.	93.6
.80	.205	.181	.341	804.	815.	93.6
1.0	.335	.296	.561	831.	876.	93.6
1.5	.648	.573	1.08	919.	-----	92.4
2.0	.915	.809	1.53	889.	975.	91.6
3.0	1.40	1.23	2.35	889.	-----	88.0
4.0	1.87	1.65	3.13	859.	1000.	83.2
5.0	2.34	2.08	3.93	741.	1000.	77.6
6.0	2.81	2.48	4.72	563.	961.	71.3
7.0	3.28	2.91	5.50	394.	920.	65.7
8.0	3.75	3.31	6.28	284.	860.	59.3
10.	4.69	4.14	7.85	149.	719.	50.2
15.	7.04	6.22	11.8	45.5	350.	31.0
20.	9.40	8.31	15.7	18.9	146.	20.7
30.	14.1	12.5	23.5	5.65	47.5	10.1
50.	23.5	20.8	39.3	1.93	-----	3.71

Table A3-12

Seismograph System Harmonic Magnification
for Five University of Alaska Stations

Station	BIG	BLR	GLM	PJD	SCM
Seismometer	18300[1]	18300[2]	SD-215[3]	18300[1]	18300[1]
Amplifier	SPA-1	SPA-1	Sandia	SPA-1	SPA-1
Attenuation	F5-30db10:1	F5-12db5:1	-12db	F5-12db10:1	F5-24db10:1
Recorder	Dev.-View.	Dev.-View.	Dev.-View	Dev.-View.	Dev.-View.
Hz	mm/μ	m/μ	m/μ	m/μ	m/μ
0.40	5.22	0.649	.115	.0395	.00866
0.60	21.5	.275	.386	.171	.0360
0.80	52.4	.679	.821	.402	.0878
1.00	88.2	1.07	1.35	.686	.153
2.00	251.	3.27	3.61	1.99	.458
4.00	444.	5.75	6.71	3.94	.947
5.00	479.	6.17	7.86	4.28	1.20
6.00	444.	5.58	8.66	3.92	1.41
7.00	350.	4.45	9.35	3.27	1.57
8.00	307	3.94	9.68	2.74	1.69
10.0	212.	2.75	10.2	1.80	1.71
15.0	96.9	1.37	8.27	.782	.869
20.0	35.5	.478	4.91	.289	.359
30.0	7.45	.0888	1.73	.0570	.0826

1) f_o = 1.0 Hz, λ = 0.7 critical, R_c = 160Ω, R_x = 216Ω, G = 130 V/m/s
2) f_o = 1.0 Hz, λ = 0.7 critical, R_c = 97.0Ω, R_x = 160Ω, G = 106 V/m/s
3) f_o = 1.0 Hz, λ = 0.7 critical, R_c = 2000Ω, R_x = 2700Ω, G = 218 V/m/s

The third amplifier response is for the Sandia USO amplifier whose calibration data are given in Table A3-5.

The harmonic magnifications for five University of Alaska seismograph stations are given in Table A3-12. These magnifications are calculated using equation A3-1 and the data given in Tables A3-8 and A3-11 with T(f)=1. The magnifications for five Skwentna stations given in Table A3-13 were calculated in the same manner using Tables A3-10 and A3-11. Three of the magnification calculations from Table A3-12 are compared in Table A3-14 to calibration-coil driven frequency response tests of the entire system which were made by Ron Rasmussen, Doug VanWormer, and the author in September 1971. These tests are described in detail in an in-house report on file at the seismology laboratory of the University of Alaska. They consisted of driving the seismometer (in situ) with a known sinusoidal current through its calibration coil and measuring the peak-to-peak output on the FilmViewer. This output was divided by the equivalent earth motion calculated from the calibration coil current to obtain the system magnification. Table A3-14 shows that at one Hertz this test gave magnifications which were consistently higher than the calculations given in Table A3-12. This discrepancy averages 27 per cent which corresponds to an error in magnitude determination of about one tenth.

Table A3-13

Seismograph System Harmonic Magnification
for Five Skwentna Stations

Station*	KCH	SHL	SKV & YNL	TLN
Attenuation	-18db	-24db	-42db	-18db
Hz	m/μ	m/μ	mm/μ	m/μ
.5	.0701	.0351	4.15	.0481
1.0	.507	.260	30.5	.355
2.0	1.42	.755	85.3	.945
3.0	2.12	1.15	130	1.38
4.0	2.79	1.52	170	1.73
5.0	3.08	1.64	190	1.88
6.0	2.81	1.53	177	1.75
7.0	2.34	1.30	155	1.44
8.0	1.65	1.01	122	1.23
10.	.820	.467	60.3	.739

*All stations consisted of type 1 (see Table A3-12) Geotech 18300 seismometers and Electrotech SPA-1 amplifiers with a five Hertz cutoff, and were recorded on the tape system whose sensitivity is given in Table A3-10.

Table A3-14

Comparison of Measured to Calculated Magnifications

Station	BIG	BLR	SCM	
$M_m(1)$	106.K	1.42M	198K	
$M_{cu}(1)$	88.2K	1.07M	153K	
Ratio	1.20	1.33	1.29	<1.27>

LITERATURE CITED

Atwater, T., Implications of Plate Tectonics for the Cenozoic Tectonic Evolution of West. N. America, Geol. Soc. Am., 81, 3513-3536, 1970.

Atwater, T. and P. Molnar, Relative Motion of the Pacific and North American Plates Deduced from Sea-Floor Spreading in the Atlantic, Indian and South Pacific Oceans, in Proceedings of the Conference on Tectonic Problems of the San Andreas Fault System, eds. R. L. Kovach and A. Nur, Stanford U. Pub., 1973.

Barazanzi, M. and J. Dorman, World Seismicity Maps Compiled from ESSA, C&GS, Epic. Data 1961-1967, Bull. Seis. Soc. Am., 59, 369-380, 1969.

Barnes, D. F., Four Preliminary Gravity Maps of Parts of Alaska, U. S. Geol. Survey, open file report, 1967.

Benioff, H., Orogenesis and deep crustal structure - additional evidence from seismology, Geol. Soc. Am., 65, 385-400, 1954.

Berg, E., Crustal Structure in Alaska - a brief summary, Geophys. Inst. Sci. Rept., 1967.

Berg, E., N. Sperlich and W. Feetham, Large Aperture Seismic Telemetering System for Central Alaska, Geophys. Inst. Sci. Rept., 1967.

Berg, E., S. Kubota and J. Kienle, Preliminary Determination of Crustal Structure in the Katmai National Monument, Alaska, Bull. Seism. Soc. Am., 57, 1367-1392, 1967.

Berg, Eduard, Ronald Rasmussen, The Effect of Barometric Pressure Variation on the "U.S.O." Long-Period Seismometer, Geophy. Inst., Univ. of Alaska Technical Report, AFSOR contract nos. F-99620-68-C-0066, F-44620-70-C-0031, 1970.

Berg, Eduard, Crustal Deformation Release Failure and Tilts in Alaska, Geophys. Inst., Univ. of Alaska Final Report, AFOSR Contract F-44620-70-C-0031, 1971.

Berg, Eduard, Crustal Structure in Alaska, Tectonophysics, 20, 164-182, 1973.

Berg, Eduard, George H. Sutton, Dynamic Interaction of Seismic and Volcanic Activity of the Nazca Plate Edges, preprint, 1974.

Biswas, N. N., P-Wave Travel Time Anomalies: Aleutian-Alaska Region, Tectonophysics, 19, 361-367, 1973.

Burk, C. A., Geology of the Alaska Peninsula - Island Arc and Continental Margin (Part 1 - Text, Part 2 - Geologic Map in Two Sections, Part 3 - Tectonic Map), Geol. Soc. Am., Memoir 99, 250 pp., 1965.

Burke, Kevin, W. S. E. Kidd, J. Tuzowilson, Relative and Latitudinal Motion of Atlantic Hot Spots, Nature, 245, 133, 1973.

Butler, H. H., Palmer Seismological Observatory, Earthquake Notes, 42(1) 15-36, 1971.

Carder, D. S., D. Tocher, C. Bufe, S. W. Stewart, J. Eisler, and E. Berg, Seismic Wave Arrivals from Longshot, 0° - 27°, Bull. Seism. Soc. Am., 57, 573-590, 1967.

Coats, R. R., Magma Type and Crustal Structure in the Aleutian Arc, AGU Geophys. Mono., 6, 92-109, 1962.

Davies, J. and E. Berg, Crustal Morphology and Plate Tectonics in South Central Alaska, Bull. Seism. Soc. Am., 63, 673-677, 1973.

Davies, Geoffrey F., and James N. Brune, Regional and Global Fault Slip Rates from Seismicity, Nature Phys. Sci., 229, 101-107, 1971.

Davis, T. N. and C. Echols, A Table of Alaska Earthquakes, 1788-1961, Geophys. Res. Rep. UAG R-131, Geophys. Inst., Univ. of Alaska, 1962.

Dewey, J. F. and J. M. Bird, Mountain Belts and the new Global Tectonics, J. Geophys. Res., 75, 2625-2647, 1970.

Eaton, J. P., HYPOLAYR, a Computer Program for Determining Hypocenters of Local Earthquakes in an Earth Consisting of Uniform Flat Layers over a Half Space, U. S. Geol. Survey, open file report, 1970.

Engdahl, E. R., Relocation of intermediate depth earthquakes in the central Aleutians by seismic ray tracing, Nature, Phys. Sci. Lett., 245, 23-25, 1973.

Gedney, L., C. Matteson and R. B. Forbes, Seismic Refraction Profiles of the Ash Flow in the Valley of Ten Thousand Smokes, Katmai National Monument, Alaska, J. Geophys. Res., 75, 2619-2624, 1970.

Gedney, L., L. Shapiro, D. VanWormer and F. Weber, Earthquake Epicenters in Interior Alaska, and their Correlation with Mapped Faults, Geophys. Inst. Sci. Rep. UAG R-218, Geophys. Inst., Univ. of Alaska, March, 1972.

Grow, J. A., Crustal and Upper Mantle Structure of the Central Aleutian Arc, Scripps Inst. Oceanogr., preprint, 1972 (reproduced as Figure 82, p. 237 in Le Pichon, Francheteau and Bonnin, 1973).

Grow, J. A. and T. Atwater, Mid Tertiary Tectonic Transition in the Aleutian Arc, Geol. Soc. Am., 81, 3715-3722, 1970.

Gutenberg, B. and C. F. Richter, Seismicity of the Earth and Associated Phenomena, Princeton Univ. Press, Princeton, New Jersey, 1954.

Hales, A. L. and T. Asada, Crustal Structure in Coastal Alaska, in The Earth Beneath the Continents, Am. Geophys. U. Geophysical Mono., 10, eds. J. S. Steinhart and T. J. Smith, 420-432, 1966.

Hamilton, W. and W. B. Myers, Cenozoic Tectonics of the Western United States, Rev. Geophys., 4, 509-549, 1966.

Hanson, K., E. Berg, and L. Gedney, A Seismic Refraction Profile and Crustal Structure in Central Interior Alaska, Bull. Seism. Soc. Am., 58, 1657-1665, 1968.

Heiland, C. A., Geophysical Exploration, fourth printing, Prentice-Hall, Inc., New York, pp. 580-597, 1951.

Hein, J. R., Increasing Rate of Movement with Time between California and the Pacific Plate: from Delgada Submarine Fan Source Areas, J. Geophys. Res., 78, 7752-7762, 1973.

Herrin, E., Seismological Tables for P, Bull. Seism. Soc. Am., 58, 1196-1219, 1968.

Honda, H., On the mechanism of deep earthquakes and the stress in the deep layer of the earth crust, Geophys. Mag. Japan. Met. Agency, 8, 179-185, 1934.

Isacks, B., J. Oliver and L. R. Sykes, Seismology and the New Global Tectonics, J. Geophys. Res., 73, 5855-5899, 1968.

Ishida, M., Seismicity and travel time anomaly in and around Japan, Bull. Eq. Res. Inst., 48, 1023- 1051, 1970.

Jacob, K. H., Global Tectonic Implication of Anomalous Seismic P Traveltimes from the Nuclear Explosion Longshot, J. Geophys. Res., 77, 2556-2573, 1972.

Jacob, K. H., Three Dimensional Seismic Ray Tracing in a Laterally Heterogeneous Spherical Earth, J. Geophys. Res., 75, 6675-6689, 1970.

Jeffreys, Harold, and K. E. Bullen, Seismological Tables, British Assoc. for the Advancement of Science, London, 1958.

Kanamori, H., Seismological Evidence for a Lithospheric Normal Faulting--The Sanriku Earthquake of 1933, Phys. Earth Planet. Interiors, 4, 289-300, 1971.

King, P. B., Tectonic Map of North America, U. S. Geol. Survey Map, 1969.

Lahr, J. C., R. A. Page and J. A. Thomas, Catalog of Earthquakes in South Central Alaska, April-June, 1972, U. S. Geol. Survey, open file report, 1974.

Lee, W. H. K., J. C. Lahr, HYPO71: a Computer Program for Determining Hypocenter, Magnitude and First Motion Pattern of Local Earthquakes, U. S. Geol. Survey, open file report, 1972.

LePichon, X., Sea-Floor Spreading and Continental Drift, J. Geophys. Res., 73, 3661-3697, 1968.

LePichon, Xavier, Jean Francheteau and Jean Bonnin, Developments in Geotechtonics 6/Plate Tectonics, Elsevier Sci. Pub. Co., New York, 1973.

Matumoto, T. and R. A. Page, Microaftershocks Following the Alaska Earthquake of March 28, 1964: Determination of Hypocenters and CrustalVelocities in the Kenai Peninsula - Prince William Sound Area, in the Prince William Sound, Alaska Earthquake of 1964 and Aftershocks, IIB, 157-173, 1969.

Mauk, F. J., J. Kienle, Microearthquakes at St. Augustine Volcano, Alaska, Triggered by Earth Tides, Science, 182, 386-389, 1973.

McElhinny, M. W., Mantle Plumes, Paleomagnetism and Polar Wandering, Nature, 241 523-524, 1973.

Menard, H. W., Transitional Types of Crust under Small Ocean Basins, J. Geophys. Res., 72, 3061-3073, 1967.

Minster, J. B., T. H. Jordan, P. Molnar, E. Haines, Numerican Modelling of Instantaneous Plate Tectonics, Geophys. J. R. Astr. Soc., 36, 541-576, 1974.

Morgan, W. J., Rises, Trenches, Great Faults, and Crustal Blocks, J. Geophys. Res., 73, 1959- 1982, 1968.

Peter, G., D. Elvers and M. Yellin, Geological Structure of the Aleutian Trench Southwest of Kodiak Island, J. Geophys. Res., 70, 353-366, 1965.

Peters, D. C. and R. S. Crosson, Application of Prediction Analysis to Hypocenter Determination Using a Local Array, Bull. Seism. Soc. Am., 62, 775-788, 1972.

Pitman, W. C., and D. E. Hayes, Sea-Floor Spreading in the Gulf of Alaska, J. Geophys. Res., 73, 6571-6579, 1968.

Plafker, G., Tectonics of the March 27, 1964 Alaska Earthquake, U. S. Geol. Survey Prof. Paper 5431, I1-I74, 1969.

Richter, C., Elementary Seismology, W. H. Freeman and Co., San Francisco, 1958.

Rittman, A. (translated by E. A. Vincent), Volcanoes and Their Activity, John Wiley and Sons, New York, 1962.

Sherburne, R. W., S. T. Algermissen and S. T. Harding, The Hypocenter, Origin Time, and Magnitude of the Prince William Sound Earthquake, March 28, 1964, in The Prince William Sound, Alaska, Earthquake of 1964 and Aftershocks, Vol. IIB, 49-50, U. S. Dept. of Commerce, ESSA, 1969.

Shor, G. G., Structure of the Bering Sea and the Aleutian Ridge, Marine Geol., 1, 213-219, 1964.

Shor, G. G., Seismic Refraction Studies off the Coast of Alaska: 1956-57, Bull. Seism. Soc. Am., 52, 37-57, 1962.

Stauder, W., Mechanism of the Rat Island Earthquake Sequence of February 4, 1965, with Relation to Island Arcs and Sea Floor Spreading, J. Geophys. Res., 73, 3847- 3858, 1968.

Stauder, W., Tensional Character of Earthquake Foci beneath the Aleutian Trench with Relation to Sea Floor Spreading, J. Geophys. Res., 73, 7693-7701, 1968.

Stone, D. B., Geophysics in the Bering Sea and Surrounding Areas: A Review, Tectonophysics, 6, 433-460, 1968.

Stone, D. B., and D. R. Packer, Plate Motions, Hot Spots, Paleomagnetism and the Tectonics of Western North America and Alaska, Preprint, 1974.

Sugimura, A. and S. Uyeda, Island Arcs - Japan and its Environs, Developments in Geotectonics, 3, Elsevier Scientific Pub. Co., Amsterdam-London-New York, 1973.

Sykes, L. R., B. L. Isacks and J. Oliver, Spatial Distribution of Deep and Shallow Earthquakes of Small Magnitude in the Fiji-Tonga Region, Bull. Seism., Soc. Am., 59, 1093-1113, 1969.

Tarr, A. C., New Maps of Polar Seismicity, Bull. Seism. Soc. Am., 60, 1745-1747, 1970.

Tatel, H. E., and M. A. Tuve, The Earth's Crust: Seismic Studies, Carnegie Inst., Wash. Year Book, 55, 81-85, 1956.

Tobin, D. G. and L. R. Sykes, Relationship of Hypocenters of Earthquakes to the Geology of Alaska, J. Geophys. Res., 71, 1659-1667, 1966.

Tobin, D. G. and L. R. Sykes, Seismicity and Tectonics of N. E. Pacific, J. Geophys. Res., 73, 3821-3845, 1968.

Tosimatu, T. and P. L. Ward, Microearthquake Study of Mount Katmai and Vicinity, Alaska, J. Geophys. Res., 72, 2557-2568, 1967.

VanWormer, J. D., J. Davies and L. Gedney, Seismicity and Plate Tectonics in South Central Alaska, Bull. Seism. Soc. Am., 64, in press, 1974.

Wadati, K., On the Activity of deep-focus earthquakes in the Japan Islands and neighbourhoods, Geophys. Mag. Japan Met. Agency, 8, 305-325, 1935.

Willis, D. E., G. D. George, K. G. Poetzl, C. E. Saltzer, A. F. Shakal, R. D. Torfin, T. L. Woodzich and C. Wolosin, Seismological Aspects of the Cannikin Nuclear Explosion, Bull. Seism. Soc. Am., 62 1377-1395, 1972.

Woollard, G. P. and W. E. Strange, Gravity Anomalies and the Crust of the Earth in the Pacific Basin, in the Crust of the Pacific Basin, American Geophys. Union Geophys. Monogr. #6, 60-80, Eds. G. A. MacDonald and H. Kuno, 1962.

Woollard, G. P., N. A. Ostenso, E. Thiel and W. E. Bonini, Gravity Anomalies, Crustal Structure and Geology in Alaska, J. Geophys. Res., 65, 1021, 1037, 1960.

Zeitz, I., G. E. Andreasen and A. Grantz, An Aeromagnetic Study of the Cook Inlet Area, Alaska (abstract), Geophysics, 23, 1059-1060, 1958.